UNIVERSITÀ
degli STUDI
di CATANIA

PhD programme in Ingegneria dei Sistemi, Energetica, Informatica e delle Telecomunicazioni

---

Ruben Crispino

Development of smart multi-sensor solutions for the Active Aging and Well Being

---

PhD thesis

Supervisor:
Chiar.mo Prof. B. Andò

---

academic year XXXIII

Contents

List of Figures

Chapter 1

Introduction

An Active and Healthy Ageing (AHA) society would be a resource from which everyone can benefits. The development of AHA scenario is gaining more and more interest all over the world. The European Union (EU) only, with its conglomerate of more than 500 million people, posses around 19.2% (approximately 100 million) of older adults [1]. Europeans are now living longer than ever before and the age profile of the entire society is rapidly changing.

Population ageing is a long-term development that has been evident for several decades in Europe. This process is being driven by historically low fertility rates, increasing life expectancy and, in some cases, migratory patterns. Projections suggest that the ageing of the EU's population will quicken in the coming decades, with a rapid expansion in the number and share of older people.

The total population of the EU is projected to increase from 512 million in 2018 to peak at 525 million by 2044, before falling marginally through to 2050. The population of older people (those aged 65 years or more) will increase significantly, rising from 101 million at the start of 2018 to reach 149 million by 2050. During this period, the number of people in the EU aged 75-84 years is projected to expand by 60.5%, while the number aged 65-74 years is projected to increase by 17.6%. In contrast, the latest projections suggest that there will be 9.6% fewer people aged less than 55 years living in the EU by 2050 [2].

Such developments are likely to have profound implications, not only

for individuals, but also for governments, business and civil society, impacting more than ever the health and social care systems.

These findings highlight several questions from both an individual and public perspective. Who will take care of the current generation as we become older? What types of health and social organisations should we develop to preserve the quality of life of an ageing population and sustain our health care systems over the medium and long term? The growing number of older people has been perceived by many as a threat to Europe's economy and competitiveness, in particular when it comes to the sustainability of its healthcare systems.

Supporting an Active and Healthy Ageing is one answer to these questions. Maintaining a healthy ageing population may lower the demands for health care services while being supportive to their fellow generation.

To face this challenging situation, the EU Commission has launched several initiatives to promote active ageing across Europe.

These initiatives, such as the European Innovation Partnership on Active and Healthy Ageing (EIP-AHA), the Active and Assisted Living Joint Programme (AAL JP) as well as the Knowledge and Innovation Community (KIC) on Health and Active Ageing, aim to ensure that this generation of elderly can benefit from healthier lives, receive appropriate care as well as live independently.

The topics involved are vast and multidisciplinary but, from a technical perspective, what can be done? Which are the main issue that can be addressed?

Focusing on health-related problems, a primary threat is represented by the progressive impairment in performing Activities of Daily Living (ADL), representing a measure of functional decline associated with frailty [3, 4]. Frailty is often linked to the loss of autonomy in performing ADLs as well as health-related problems requiring an institutionalisation, and/or hospitalisation, with direct influences on the quality of life.

From a public health perspective, frailty is a multidimensional issue resulting from changes in physical and mental health and functional status as well as lack of social and economic resources. Functional decline is associated with lower psychosocial status, namely social isolation, malnutrition, and comorbidity, which are all determinants of frailty. Among the indicators of frailty, falls and precursive behaviours, such as postural

instabilities, are major contributors. They both contribute in a substantial way to the limitation of mobility and premature hospitalization. Statistical analysis prove that one-third of people over the age of 65 who live in the community fall each year and this proportion increases to 50% of those aged 80 years and older. Those residing in care or nursing settings have an even greater risk of falls and fractures. Approximately 30% of falls require medical treatment, often resulting in emergency department visits and subsequent hospitalisations [5]. Annually there are more than 30.000 fall related deaths amongst people aged 65 years and older within the EU region [6]. Falls are far more common than strokes or heart attacks, and can be just as serious in their consequences. Even falls without injury can lead to post-fall anxiety, fear and subsequent dependency on family carers or even admittance into nursing care facilities.

Elderly are not the only players being affected by falls and postural instabilities. People suffering from neurodegenerative diseases, such as the Parkinson's disease, also suffer from postural instabilities and consequent falls within one year from the onset of the disease.

A range of falls prevention interventions have been developed within both research and practice. These include clinical assessment and treatment of fall risk factors such as exercise programs that focus on balance and muscle strength, medication management and vision checking. Although big progresses have been made through the years, falls are still a serious issued nowadays. How can technology play a central role in this context?

A possible way is to provide solutions aiming at the prevention, or early detection, of falls and falls precursors.

Those points are the baseline of many European, national and regional strategies.

It is therefore clear how the development of technologies for improving the quality of life does play a fundamental role both at national and European level.

For this reason, this Ph.D. thesis aims at providing a deeper understanding of aging-related issues with a specific focus on falls, postural instabilities, and the effect of the user's habits in prevention; moreover, rigorous methodologies for the detection and classification of these phenomena will be presented.

Concerning falls detection and classification, event-driven approaches (i.e. based on advanced template matching techniques) exploiting different methods to evaluate the similarity between pre-defined templates and unknown events (cross-correlation and Dynamic Time Warping), as well as different classification strategies specifically designed for their implementation in power-limited devices, are proposed. Main novelties introduced may summarized as follow:

- event-driven approach: makes the methodology robust against undesired dynamics;
- pattern normalization: makes the method robust against users' characteristics;
- similarity measurement: based on cross correlation and Dynamic Time Warping (DTW);
- event-driven classification: the classifier uses values defined upon similarity rather than amplitude;
- use of ROC curves for optimal threshold identification.

Regarding postural instabilities, the following activities have been addressed: the validation of a low-cost wearable device for real-time classification of postural status and a classification strategy using time-frequency features built upon the Wavelet transform. In particular, the wearable device is fully validated through a thorough comparison with a Gold Standard while, the method based on time-frequency features, uses the Discrete Wavelet transform (DWT) exploiting a K-Nearest Neighbour classifier. Main novelties introduced by this activity are summarized in the following:

- development of a postural classification methodology using inertial systems;
- device validation by means of a Gold Standard;
- assessment of the classification strategy;

- definition of a performance index rating the reliability of the classification outcome;
- use of the Wavelet theory for the postural classification task.

In the context of user's habits monitoring, a system based on a Radio Frequency Identification (RFID) technology is introduced to monitor the right intake of nutrient, in terms of both nutrition and hydration, as well as the user's interaction with home appliances, exploitation of indoor environments and activity rate. The solution has been developed in the context of an Interreg project called NATIFLife [7]. The project aims at developing an innovative framework of assistive home automation systems which could improve elderly autonomy. The development of an integrated platform of assistive technology, which is open to the integration of traditional and innovative solutions, can produce an improvement of the quality of life of elderly and people with mobility impairments. In detail, the project aims at the assessment of the user's habits, activity rate, nutrition and hydration, as well as the use of home appliances. The RFID system aims at integrating, in the NATIFLife platform, functionalities such as food/beverage monitoring as well as a unique identification of the user living the environment. Advantages of the adopted solution as respect to others, are related to its low invasiveness, good flexibility in terms of tags distribution, re-allocation and quantity, ease of use and installation. All the above-mentioned features are mandatory while addressing effective assistive devices.

Within each application, the assessment and reliability of the solutions have a cardinal role. When dealing with solutions of assistive technology, it must be pointed out that the final goal is the adoption of these technologies by end-users. For the solutions to be fully accepted, they must strictly adhere to the requirements of reliability and robustness. To this end, the assessment procedures proposed in the thesis are used to verify the usability of the solutions for the addressed applications, as well as validating the reliability of the decision-making processes.

Although not strictly related to the activity carried on during the PhD, two important aspects have to be taken into account while dealing with the development of Assistive Technology: the User Centered Design (UCD) approach and the assessment by end-users. Regarding the fall

detection activity, the dangerous nature of the events did not allow the involvement of end-users for the assessment. That is why a public available dataset has been used for this task. Regarding the UCD approach, event though a first trails has been done on integrating the fall detection methodology in hardware, the latter was just meant to verify the feasibility of the embedded implementation and hence any optimization on the basis of real users' requirements has been done.

Similar conclusion in case of postural monitoring; since the dataset has been acquired by healthy users simulating postural instabilities (simulation validated by neurologists), the development of the hardware did not require the UCD approach. In this particular case, end-users could not be involved based on the regulations of the laboratory ethics committee (the solution still had to be validated). Future efforts will be focused to the study of the user' acceptability by means of real end-users during their daily activities.

The development of the RFID solution, conversely to the others, was primarily meant to design and validate the requirements' conformity dictated by the NATIFLife project.

Main novelties of this thesis compared with the state of the art may be summarized in:

- development of methodologies for pattern identification and classification easily implementable into low power embedded device;
- search for the optimal combination between features, similarity measures and classification techniques;
- analysis of the models ability to generalize to an independent dataset (Cross Validation)
- introduction of reliability measures.

The remaining of the thesis is divides as follow, in Section 2 are given basic theoretical concepts which are used in the development of the methodologies, Section 3 provides a review of the state of the art for fall detection along with the proposed methodology, Section 4 deal with the fall detection strategy assessment, in Section 5 is given a review of the

state of the art for postural analysis along with the two proposed methodologies, Section 6 presents the RFID research results developed within the NATIFLife project while Section 7 provides a synthesis of the solutions addressed in this thesis along with some final remarks.

Chapter 2

Theoretical Tools

2.1 Correlation

One of the most common ways of quantitatively comparing two functions is through the use of the correlation operator. Correlation attempt to quantify how much one function is like another. The linear correlation between two functions or signals can be obtained using the Pearson correlation coefficient defined as:

$$r_{xy} = \frac{1}{(N-1)\sigma_x\sigma_y}\sum_{n=1}^{N}(x_n - \bar{x})(y_n - \bar{y}) \tag{2.1}$$

where r_{xy} represents the correlation between the signal x and the reference function y; $\bar{x}$ and $\bar{y}$ the mean values of signals x and y, and σ_x σ_y the standard deviations of x and y respectively. In this form, the equation scales the correlation coefficient r_{xy} to be between [-1,1]. In case the $\bar{x}$ and $\bar{y}$ are equal to zero, and we are not concerned with the scale a simpler equation can be used:

$$r^*_{xy} = \frac{1}{N}\sum_{n=1}^{N} x[n]y[n] \tag{2.2}$$

where r^*_{xy} represent the unscaled correlation between the signal x and the reference function y. If continuous functions are involved, the summation becomes an integral and the discrete functions $x[n]$ and $y[n]$ become

continuous functions $x(t)$ and $y(t)$:

$$r^*_{xy} = \frac{1}{T}\int_0^T x(t)y(t)dt \tag{2.3}$$

The integration (or summation) and scaling simply takes the average of the product over its range. Both Equations 2.2 and 2.3, will not range between ± 1, but they do give relative values that are proportional to the linear correlation. The correlation have the largest possible positive value when the two functions are identical and the largest negative value when the two functions are opposites. In case Equations 2.2 and 2.3 should be normalized between $[-1, 1]$ it is enough to divide by the product of the standard deviations:

$$r_{xy} = \frac{r_{xy}}{\sigma_x \sigma_y} \tag{2.4}$$

Mathematical correlation does a pretty good job in evaluating the similarity but, in some circumstances, signals that are very much alike may have a mathematical correlation of zero. This issue can be easily reproduced considering the correlation of two sequences $x = sin(\omega t + 0°)$ and $y = sin(\omega t + 90°)$ as shown in Figure 2.1. Sine and cosine have zero

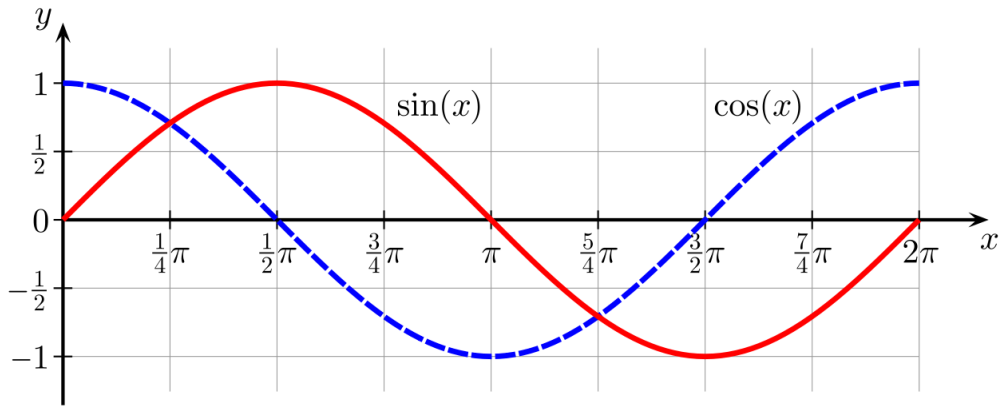

Figure 2.1: The figure shows two identical temporal sequences phase shifted. *The correlation is equal to* 0

correlation even though they describe the same signal but phase-shifted. Intuitively this is explained considering that any positive correlation between them, over one portion of a cycle, is canceled by a negative correla-

tion over the rest of the cycle. This shows that correlation does not always measure general similarity.

Cross-Correlation provides a solution in this sense.

2.1.1 Cross-Correlation

The mathematical dissimilarity between identical but time/phase shifted sequences, represent a real problem when trying to determine similarity between signals. To get around this problem, an efficient solution is that of performing the correlation for many different time/phase shifts. The equation for cross-correlation is derived from Equation 2.2 by introducing a variable shift into one of the two functions. Regardless which function is shifted with respect to the other, the result does not change. The cross-correlation operation is then a series of correlations over different time shifts k:

$$r_{xy}[k] = \frac{1}{N}\sum_{n=1}^{N} x[n]y[n+k] \quad k = 0, 1, 2, ...K \tag{2.5}$$

where k is the shift, or lag, and specifies the number of shifted samples for a given correlation. The K value depends on how the end points are treated. The value of K may be as long as the length of the signal but, more often, length is extended with zeros to enable correlations at all possible shift positions: positive and negative. In such cases, K would be the combined length of the two signals minus one. Extending a signal with zeros is called "zero padding".

For continuous functions, the time shifting is continuous and the correlation becomes a continuous function of a continuous time shift:

$$r_{xy}(\tau) = \frac{1}{T}\int_{0}^{T} x(t)y(t+\tau)dt \tag{2.6}$$

where variable τ is a continuous variable of time that specifies the time shift of $x(t)$ with respect to $y(t)$. The variable τ is analogous to the lag variable k.

An example of cross-correlation between two functions is given in Figure 2.2.

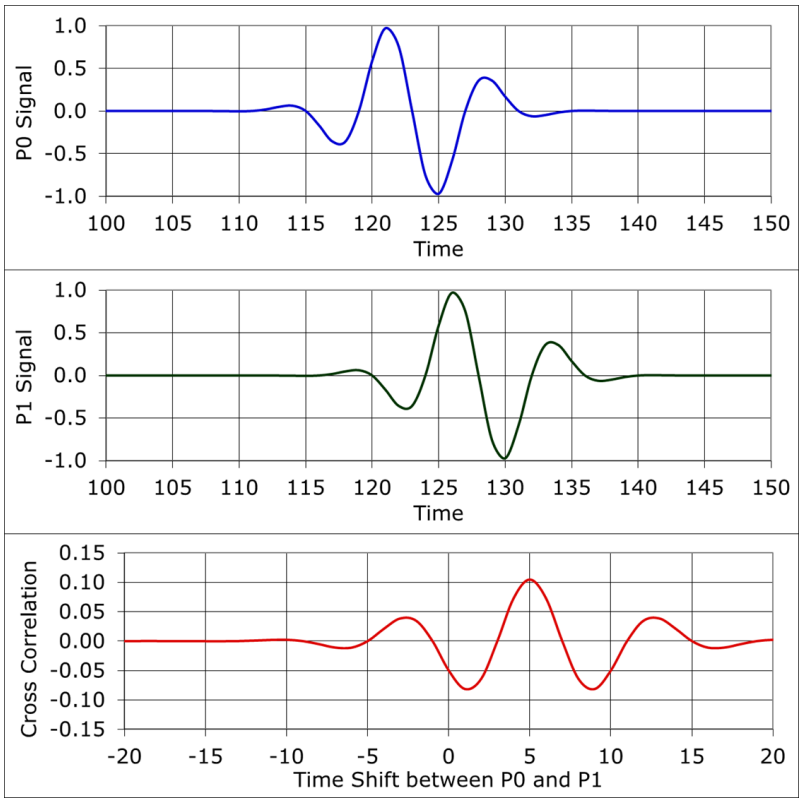

Figure 2.2: An example of cross-correlation between 2 identical time shifted sequences (blue and black curves). The cross-correlation (red curve) succeed in providing a measure of similarity between the two sequences.

2.1.1.1 Sequences Alignment

The cross-correlation tool provides an interesting property when dealing with sequence alignment. Since every time shift (or lag in case of discrete signals) is addressed when computing the cross-correlation, the time instant, corresponding to the highest value, match to the time lag ϕ between the two sequences. To clarify it, let us consider Figure 2.2. The P_0 signal is 5 units of time ahead of P_1 signal. Looking at the time shift corresponding to the highest cross-correlation value (red one), this information is clearly

available. In mathematical terms this is translated into:

$$\phi = \max_{\tau} r_{xy}(\tau) = \max_{\tau} \frac{1}{T} \int_0^T x(t)y(t+\tau)dt \tag{2.7}$$

in case of continuous signals, and in

$$\phi = \max_{k} r_{xy}[k] = \max_{k} \frac{1}{N} \sum_{n=1}^{N} x[n]y[n+k] \quad k = 0, 1, 2, ...K \tag{2.8}$$

in case of discrete signals.

This property opens to automatic algorithm for signal alignment.

2.1.2 Complexity

In computer science, the time complexity describes the amount of time required by an algorithm to run. Time complexity is commonly estimated by counting the number of elementary operations performed by the algorithm, supposing that each elementary operation takes a fixed amount of time to perform. Thus, the amount of time taken and the number of elementary operations performed by the algorithm are taken to differ by at most a constant factor.

Since an algorithm's running time may vary among different inputs of the same size, one commonly considers the worst-case time complexity, which is the maximum amount of time required for inputs of a given size. The time complexity is generally expressed as a function of the size of the input. Since this function is generally difficult to compute exactly, and the running time for small inputs is usually not consequential, one commonly focuses on the behavior of the complexity when the input size increases—that is, the asymptotic behavior of the complexity. Therefore, the time complexity is commonly expressed using big O notation, typically $O(n)$, where n is the input size in units of bits needed to represent the input.

Algorithmic complexities are classified according to the type of function appearing in the big O notation. For example, an algorithm with time complexity $O(n)$ is a linear time algorithm and an algorithm with time complexity $O(n\alpha)$ for some constant $\alpha > 1$ is a polynomial time algorithm.

In case of simple correlation and sequence length N the time complexity is $O(N)$.

In case of cross-correlation with k number of lags (or time shift) and sequence length N the time complexity is $O(kN)$.

2.2 Dynamic Time Warping

DTW algorithm has earned its popularity as the time-series similarity measure minimizing the effects of shifting and distortion in time by allowing non-linear warping of time series in order to detect similar shapes with different phases.

The objective of DTW is to compare two (time-dependent) sequences $X := (x_1, x_2, ..., x_N)$ of length $N \in \mathbb{N}$, and $Y := (y_1, y_2, ..., y_M)$ of length $M \in \mathbb{N}$. These sequences may be discrete signals (time-series) or, more generally, feature sequences sampled at equidistant points in time. The latter is the only constrain imposed to the sequences (this problem can be simply overturned by re-sampling).

Given a feature space Φ, then $x_n, y_m \in \Phi$ for $n \in [1 : N]$ and $m \in [1 : M]$. In order to compare two different features $x, y \in \Phi$, a local distance measure must be defined:

$$c : \Phi \times \Phi \to \mathbb{R} \geq 0 \tag{2.9}$$

Intuitively $c(x, y)$ has a small value when sequences are similar and large value if they are different. In some text the distance function may be referred as "local cost function". Evaluating the local cost function for each pair of elements of the sequences X and Y, one obtains the *cost matrix* $C \in \mathbb{R}^{N \times M}$ defined by $c(n, m) := c(x_n, y_m)$ representing all pairwise distances between X and Y: It is defined as:

$$C \in \mathbb{R}^{M \times N} : c(n, m) = ||x_n - y_m||, n \in [1 : N], m \in [1 : M] \tag{2.10}$$

Once the local cost matrix is built (an example is provided in Figure 2.3), the algorithm finds the alignment path which runs through its low-cost areas (Figure 2.4). This produce an alignment having minimal overall cost.

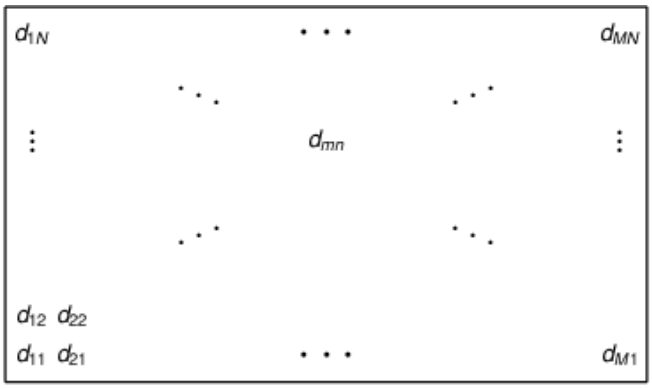

Figure 2.3: Example of construction of a **local cost matrix.**

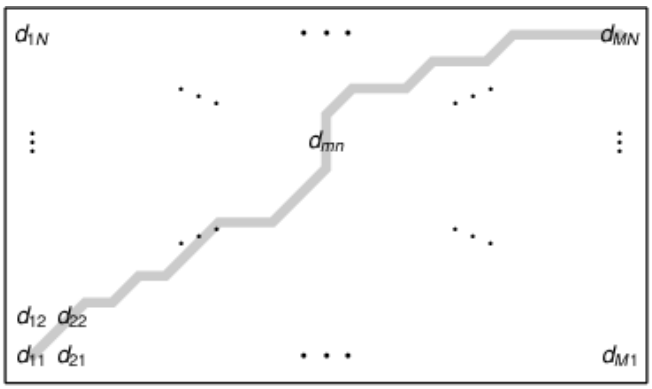

Figure 2.4: Example of a possible low-cost path in the **local cost matrix.**

An alignment path (or warping path) is defined as follow:

An (N, M)-warping path is a sequence of points $s = (s_1, s_2, ..., s_L)$ with $s_l = (n_l, m_l) \in [1 : N] \times [1 : M]$ for $l \in [1 : L]$ satisfying the following criteria.

- **Boundary condition:** $s_1 = (1, 1)$ and $s_P = (N, M)$. The boundary condition enforces that the first elements of X and Y as well as the last elements of X and Y are aligned to each other. In other words, the alignment refers to the entire sequences X and Y.
- **Monotonicity condition:** $n_1 \leq n_2 \leq ... \leq n_K$ and $m_1 \leq m_2 \leq ... \leq m_K$. The monotonicity condition reflects the requirement of faithful

timing: if an element in X precedes a second one this should also hold for the corresponding elements in Y, and vice versa.

- **Step size condition:** $s_{p+1} - s_p \in \{(1,1),(1,0),(0,1)\}$ .This criteria constrain the alignment path from long jumps while aligning the two temporal sequences expressing a kind of continuity condition: no element in X and Y can be omitted and there are no replications in the alignment.

Note that the step size condition implies the monotonicity condition. Figure 2.5 illustrates the three criteria.

The total cost function $c_p(X,Y)$ of a warping path p between X and Y with the respect to the local cost measure c is defined as:

$$c_p(X,Y) = \sum_{l=1}^{L} c(x_{n_l}, y_{m_l}) \tag{2.11}$$

Finally, an *optimal warping path*, p^* between X and Y is a warping path having minimal total cost among all possible warping paths.The DTW distance $DTW(X,Y)$ between X and Y is then defined as the total cost of p^*:

$$\begin{aligned} DTW(X,Y) &= c_{p^*}(X,Y) \\ &= min(c_p(X,Y) \quad | \quad p \text{ is an } (N,M)\text{-warping path}) \end{aligned} \tag{2.12}$$

To find the optimal warping-path p^*, a possible way is to test every possible path between X and Y. Such a procedure, however, leads to a computational complexity that is exponential the length of N and M. An algorithm, whose time complexity equals to $O(NM)$, is now introduced. Its primary aim is to avoid an exponential dependency on N and M size. Let us start defining sequences $X(1:n) := (x_1, x_2, ..., x_n)$ for $n \in [1:N]$ and $Y(1:m) := (y_1, y_2, ..., y_m)$ for $m \in [1:M]$ and set:

$$D(n,m) := DTW(X(1:n), Y(1:m)) \tag{2.13}$$

The values $D(n,m)$ define a $N \times M$ matrix D, which is also called *accumulated cost matrix*. In the following, each matrix entry, whether for the cost matrix C or for the accumulated cost matrix D, will be referred to

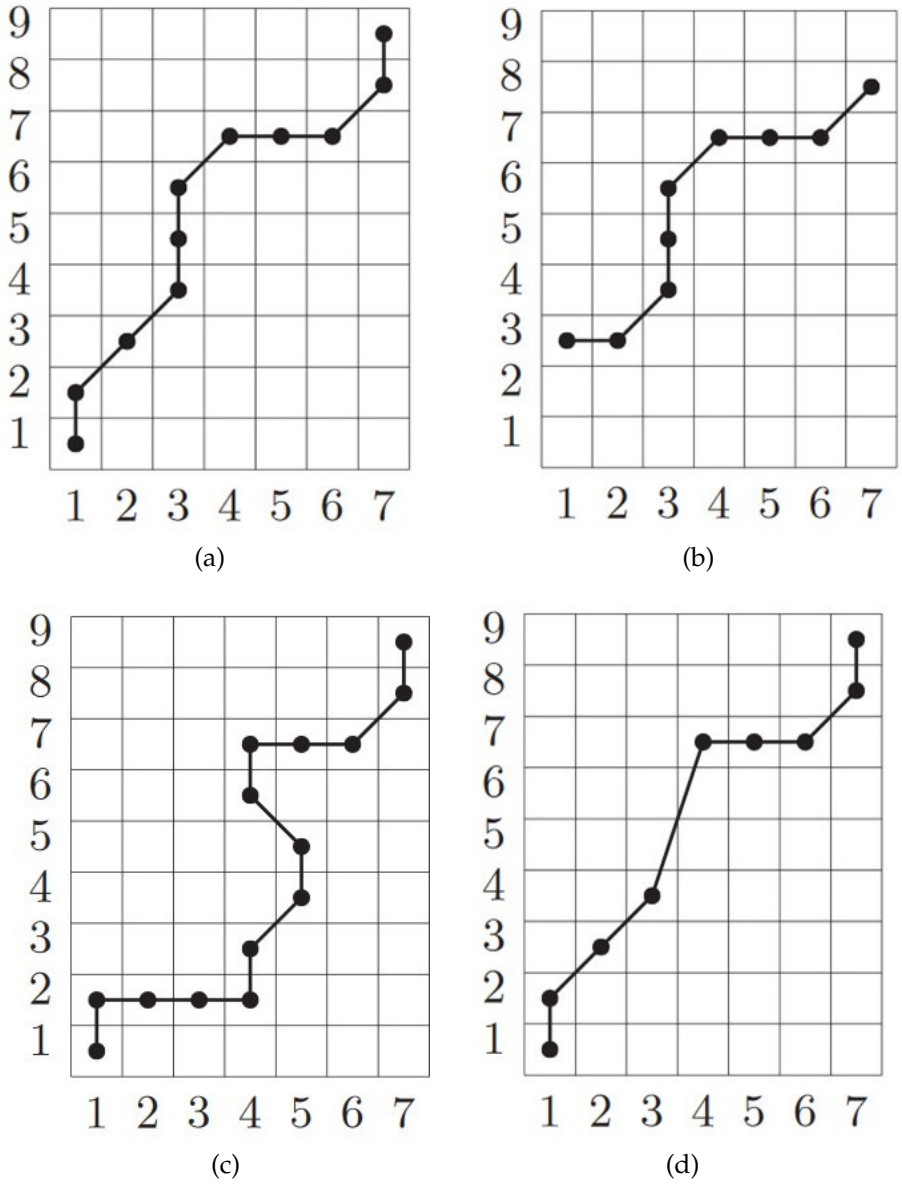

Figure 2.5: Example of path for some sequence X of length $N = 9$ and some sequence Y of length $M = 7$. (a)Warping path satisfying every criteria. (b)Boundary condition is violated. (c) Monotonicity condition is violated. (d)Step size condition is violated.

as a cell. An efficient computation for the D matrix is provided in the following theorem:

The accumulated cost matrix D satisfies the following identities: $D(n,1) = \sum_{k=1}^{n} c(x_k, y_1)$ for $n \in [1:N]$, $D(1,m) = \sum_{k=1}^{m} c(x_1, y_k)$ for $m \in [1:M]$, and

$$D(n,m) = min\{D(n-1,m-1), D(n-1,m), D(n,m-1)\} + c(x_n, y_m) \tag{2.14}$$

for $1 < n < N$ and $1 < m < M$. In particular, $DTW(X,Y) = D(N,M)$ can be computed with $O(NM)$ operations.

The proof is left to dedicated textbook.

The provided theorem makes easier a recursive computation of the matrix D. The initialization can be simplified by extending the matrix D with an additional row and column and formally setting $D(n,0) = \infty$ for $n \in [1:N]$, $D(0,m) = \infty$ for $m \in [1:M]$, and $D(0,0) = 0$. Then the recursion of Equation 2.14 holds for $n \in [1:N]$ and $m \in [1:M]$. Furthermore, note that D can be computed in a column-wise fashion, where the computation of the $m-$th column only requires the values of the $(m-1)-$th column. This implies that if one is only interested in the value $DTW(X,Y) = D(N,M)$, the storage requirement is $O(N)$. Similarly, one can proceed in a row-wise fashion, leading to $O(M)$. However, note that the running time is $O(NM)$ in either case. Furthermore, to compute an optimal warping path p^*, the entire $(N \times M)-$matrix D is needed.

Various modifications have been proposed in order to speed up DTW computations as well as to better control the possible routes of the warping paths. These and other aspects are left to dedicated textbooks.

2.2.1 Complexity

Given $X = (x_1, x_2, ...x_N)$ with $N \in \mathbb{N}$, and $Y = (y_1, y_2, ...y_M)$ with $M \in \mathbb{N}$, the algorithm has a complexity, in the worst case, of $O(MN)$.

2.3 Receiver Operating Characteristic (ROC)

A ROC graph is a technique for visualizing, organizing and selecting classifiers based on their performance. It has been widely used in signal detection theory, to depict the tradeoff between hit rates and false alarm rates of classifiers, and for use in visualizing and analyzing the behavior of diagnostic systems. This is why, the medical community has an extensive literature on the use of ROC graphs for diagnostic purposes.

Recently, ROC graphs have been adopted by the machine learning community, due in part to the realization that simple classification accuracy is often a poor metric for measuring performance.

ROC graphs are conceptually simple, but there are some non-obvious complexities that arise when they are used in research. Since the ROC theory has been around for a long time and extensive literature has been published since then, in the following sections only a brief overview of main properties will be addressed with specific attention to aspects needed in the remaining of the thesis.

2.3.1 Classifier performance

Let us start with a very simple classification problem using only two classes where, an instance I, is mapped to one element of the set $\{p, n\}$ of positive and negative class labels.

A classification model is a function mapping instances to predicted classes. Some classification models produce a continuous output, others produce a discrete class label indicating only the predicted class of the instance. To differentiate actual and the predicted class, the set $\{Y, N\}$ is used for the class prediction produced by a model.

Given a classifier and an instance, there are four possible outcomes. If the instance is positive and it is classified as positive, it is counted as a TP (true positive); if it is classified as negative, it is counted as a FN (false negative). If the instance is negative and it is classified as negative, it is counted as a TN (true negative); if it is classified as positive, it is counted as a FP (false positive). Given a classifier and a set of instances (the test set), a two-by-two confusion matrix (shown in Figure 2.6) can be constructed representing the dispositions of the set of instances. The

numbers along the major diagonal represent the correct decisions made, and the numbers of the other diagonal represent the errors between the various classes. Using this matrix, different metrics can be defined, such

		Predicted class: Positive	Predicted class: Negative
Actual class	Positive	TP	FN
	Negative	FP	TN

Figure 2.6: Confusion matrix.

as the true positive rate (TPR - also called hit rate, recall or **sensitivity**):

$$TPR = \frac{TP}{TP + FN} \tag{2.15}$$

the false positive rate (FPR - or false alarm rate):

$$FPR = \frac{FP}{FP + TN} \tag{2.16}$$

the specificity:

$$S_p = \frac{TN}{TN + FP} = 1 - FPR \tag{2.17}$$

precision:

$$Precision = \frac{TP}{TP + FP} \tag{2.18}$$

accuracy:

$$Acc = \frac{TP + TN}{TP + FN + FP + TN} \tag{2.19}$$

and F_1:

$$F_1 = \frac{TP}{TP + \frac{1}{2}(FP + FN)} \tag{2.20}$$

Each of these metrics, can be used to quantify a classifiers' performances.

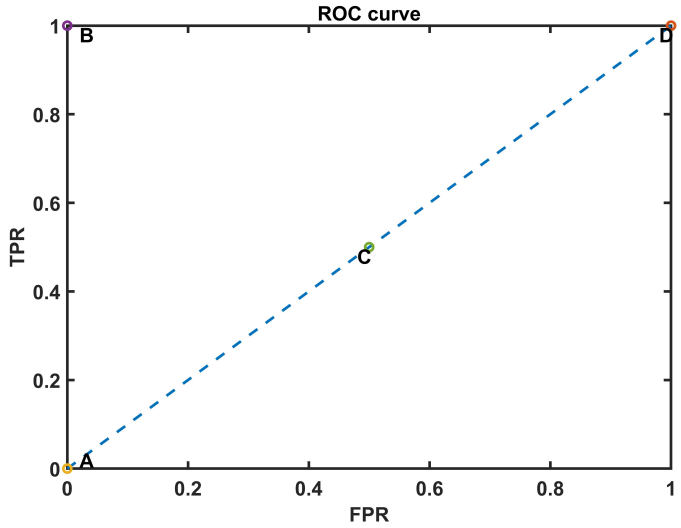

Figure 2.7: Example of a ROC graph showing 4 discrete classifiers.

2.3.2 ROC space

ROC curves are two-dimensional curves in which TPR is plotted in the y axis and the FPR on the x axis. In essence, a ROC curve depicts relative tradeoffs between benefits (TPR) and cost (FPR).

A discrete classifier is one that outputs only a class label. Each discrete classifier produces an FPR-TPR pair corresponding to a single point in the ROC space (points A, B, C and D in Figure 2.7 are an example).

Some of these possible points have specific meaning. The point with coordinate (0,0) (point A in Figure 2.7), represents a classifier that never issue a positive classification and consequently no FP errors. The point with coordinate (1,1) (point D in Figure 2.7), represents a classifier issuing always positive classification with a consequent increase in the FP errors. The upper left corner, coordinate (0,1), represents the perfect classification (point B in Figure 2.7). In a practical way, one point in the ROC curve is better than another if more Northwest than the first.

The diagonal line $y = x$ represents a classifier randomly guessing a class (point C in Figure 2.7). A random classifier will produce a ROC point that "slides" back and forth on the diagonal based on the frequency with which it guesses the positive class.

Although any point has been shown in the lower right triangle of the graph, actually, if a classifier performs even worse than random guessing, a point on that area may appear.

2.3.3 Considerations on the Classifier's Output

Some consideration must be done on the output of a classifier. Basically, a classifier can have a discrete or a continuous valued output. The nature of the output have a direct effect on what is shown in the ROC graph.

2.3.3.1 Binary vs Non-Binary Classifiers

Many classifiers, such as decision trees or rule sets, are designed to produce only a class decision, i.e., a Y or N on each instance. When such a discrete classifier is applied to a test set, it yields a single confusion matrix, which in turn corresponds to one ROC point. Thus, a discrete classifier produces only a single point in ROC space. Some others classifiers, such as a logistic regression or neural network, produces probability or score, a numeric value that represents the degree to which an instance is a member of a class. Such a ranking or scoring classifier may be used with a threshold to produce a binary classifier: if the score is above the threshold, the classifier produces a Y, else a N.

2.3.3.2 ROC Curves

As previously stated, in case a classifier outputs a continuous-valued score, a threshold can be used to force a binary classifiers. Varying the threshold within a given range, a ROC curve can be build in the ROC space. An example of a possible ROC curve is provided in Figure 2.8. Specifically, moving from the left most point to the right most one, thresholds values are the lowest and highest respectively.

The shape of the curve can be smooth in case the number of addressed instances is big, or can looks like a step function in the opposite case.

Although ROC curves are primary used to compare classifiers' performances, the possibility to evaluate all the metrics introduced so far for

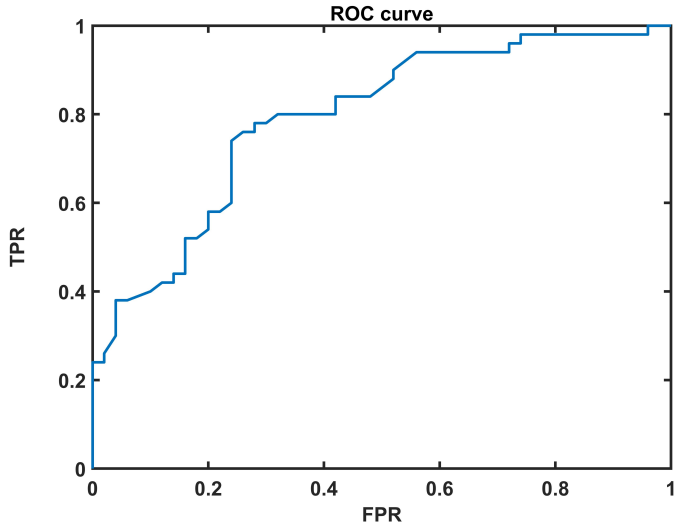

Figure 2.8: Example of a ROC curve where each point has been computed for a given threshold value.

different threshold values allows to find an optimal threshold maximizing a specific metric.

2.3.4 Using ROC Theory for Optimal Threshold Identification

ROC graphs can be successfully used for the identification of threshold maximizing a given metric. For each threshold value, TP, FP, TN, FN indexes are computed to obtain the TPR and FPR metrics needed for the curve. However, same indexes can be used to calculate all other metrics defined in Section 2.3.1.

Different methods can be adopted for the identification of the optimal thresholds and some of them will be introduced.

2.3.4.1 Method 1

A first technique is based on the Youden Index (YI), which represents the vertical distance between the 45° line and the point on the ROC curve.

The formula for the Youden index is:

$$YI = S_e + S_p - 1 \tag{2.21}$$

where higher values are better than lower.

To find the optimal threshold, we can look for the higher obtainable YI value.

2.3.4.2 Method 2

This second method is based on the distance to corner. The distance to the top-left corner of the ROC curve for each threshold value is given by:

$$d = \sqrt{(1 - S_e)^2 + (1 - S_p)^2} \tag{2.22}$$

where lower distances to the corner are better than higher distances.

To find the optimal threshold, we can look for the lower obtainable distance value.

This method has been used in Section 5.2.4.

2.3.4.3 Method 3

This method is based on the positive likelihood ratio. It is basically the ratio of the true positive rate (S_e) to the false positive rate ($1 - S_p$). This likelihood ratio statistic measures the value of the test for increasing certainty about a positive diagnosis and it is defined as:

$$PLR = \frac{TPR}{FPR} \tag{2.23}$$

where higher values are better than lower.

To find the optimal threshold, we can look for the lower obtainable PLR value.

2.3.4.4 Method 4

This method is based on the maximization of both S_e and S_p.

For the optimal threshold determination, the intersection between the S_e and S_p is used. An example of a curve built using this two metrics, for

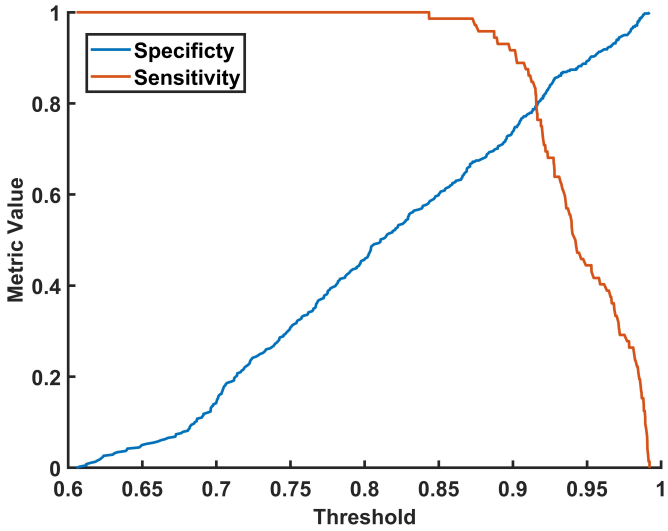

Figure 2.9: S_e VS S_p metrics for different threshold values.

different threshold values, is shown in Figure 2.9. For this given example, the optimal threshold (according to the specific requirement) is 0.92.

This method has been used in Section 3.2.5.1.

Chapter 3

A Fall Detection Strategy for The Assistive Technology Context

The fall detection algorithms belong to the general class of Event Detection strategies. The term Event Detection (ED) refers to a vast class of strategies aiming at the detection of the occurrences of specific events and categorize them. Solutions may drastically differ as a function of the nature of the event under analysis. Are we dealing with audio signals, video streams or inertial data? Which is the frequency range? What about the variability of the event? Does it suffer from time warping and/or translation? If dealing with pictures, which are the resolution involved? Should the method be translation or rotation invariant? Which power constrain does the application have?

It is evident that a unique detection strategy cannot be realized but rather this must be strictly defined according to the specific nature of the addressed events. For this reason, in the remainder of this thesis, we will only refer to events that are common in the context of Assistive Technology (AT), such as the ones coming from falls, postural instabilities, and related.

3.1 On the Implementation of a Fall Detection System

Before introducing the work, it is worth to deepen the knowledge on the general solutions provided in the literature. This is a mandatory step devoted to properly justify and understand the methodologies covered in this thesis.

As for falls and ADLs detection systems, interesting solutions have been widely proposed and described by the scientific community. Those solutions cover both the hardware and algorithm implementation.

To provide a clear analysis, during this brief review, the classification structure provided in [8] will be adopted. In particular, falls event detectors are divided into wearables, non-wearables (ambient sensors, vision sensors, and radio-frequency sensors), and hybrid systems.

3.1.1 Wearable Solutions

Different approaches have been proposed for falls and ADLs detection in the Active Assisted Living contexts using wearable solutions. Two primary category are addressed: customized devices [9, 10, 11, 12] and smartphone-based platforms [13, 14, 15, 16, 17].

3.1.1.1 Customized Systems

As for customized systems, inertial-based solutions have been widely preferred by researchers and scientist as a practical and non-intrusive way to monitor people's activities, while preserving their privacy. Such systems show good performances in detecting and classifying falls, ADLs, and physiological parameters. Focusing on falls detection systems, some examples are presented in the following.

In [9] the authors introduce an algorithm for fall detection. The system adopts a triaxial accelerometer and a supervised clustering approach, implemented through a one-class support vector machine classifier. Results show that the approach is invariant to age, weight, height of people, and to the relative positioning area of the measurement system thus allowing to overpower typical drawbacks arising from threshold-based

methodologies such as the need to adjust several parameters depending on the user's characteristics. Although preliminary results are encouraging, the inclusion of an FPGA suggests that the algorithm may require a significant computational power. Moreover, tests have been done using a relatively small dataset.

In [18] a multisensor data fusion approach is investigated for the sake of falls and human activities classification with particular regard on elders and people with neurological diseases. The working principle consists of an advanced signal processing technique carried out on data acquired using an accelerometer and a gyroscope. Specifically, the presented system can recognize critical events such as falls or prolonged inactivity, to monitor the user posture, and to notify alerts to caregivers. A major outcome of this work relies on the information provided by the system, which can be useful to monitor the evolution of the user's pathology with a particular interest in rehabilitation tasks. The mean value of the sensitivity index computed across different classes of falls and ADLs considered through the paper is 0.81%, while the average value of the specificity index is 0.98%.

In [19] a system based on an automatically adjustable threshold value for a pre-impact fall detection system is presented. Several experiments have been conducted evaluating performance such as sensitivity, specificity, and accuracy. The method can differentiate pre-impact fall from normal activities of daily living with 99.48% sensitivity, 95.31% specificity, and 97.40% accuracy with 365.12 ms of lead time.

A fall detection system, based on an instrumented insole is presented in [20]. Since high-acceleration activities are the one with a higher risk for falls, four low-acceleration activities, four high-acceleration activities, and eight types of high-acceleration falls have been investigated. A Support Vector Machine with a Leave-One-Out cross-validation provides a fall detection sensitivity of 99.6%, specificity of 100%, and accuracy of 99.9%. The classification results are comparable to other fall detection models in the State-of-the-art, while also including high-acceleration ADLs to challenge the classification model.

In [21], the authors propose a fall detection methodology based on a non-linear classification feature and a Kalman filter with a periodicity detector to reduce the false-positive rate. The methodology requires a

sampling rate of only 25 Hz, it does not require large computations or memory and it is robust among devices. The system has been tested using the SisFall dataset achieving 99.4% of accuracy.

3.1.1.2 Smartphone-Based Solutions

Although different surveys seem to reveal that smartphone-based assistive devices are not fully accepted by elderly, due to apparent request of technological skills, it must be considered that the monitoring of falls and human activities do not require any action by the user, thus habilitating fully smartphone-based solutions as a convenient way to perform such tasks [22].

A first example is the one shown in [23]. It exploits a two-step algorithm to monitor and detect fall events using the embedded accelerometer. The proposed solution uses techniques to properly detect fall-like events (such as lying on a bed or sudden stop after running) based on a multiple kernel learning support vector machine along with a threshold-based strategy. Experimental results reveal that the system detects falls with high accuracy (97.8% and 91.7%), sensitivity (99.5% and 95.8%), and specificity (95.2% and 88.0%) when placed around the waist and thigh, respectively. The system also achieves a false alarm rate of 1 alarm per 59 hours of usage.

In [24] the authors propose a fall detection algorithm made up of a feature extraction and recognition processing. Six features were analyzed where, four of them, were related to the gravity vector extracted from accelerometer data. During the testing phase, a set of six features was clustered by a support vector machine. The main feature contains the vertical directional information and provides a distinct pattern of fall-related activity. This feature acts as a trigger-key in recognition processing to avoid false alarms which leads to excessive computation. The results show that the algorithm achieve a sensitivity of 96.67% and specificity of 95%.

Another interesting work is the one discussed in [25]. The paper proposes a fall classification strategy consisting of different approaches (detection of inactivity, detection of falls by thresholds analysis, detection of falls by device orientation analysis and detection of falls with decision trees algorithm) merged, in order, to improve the efficiency and accuracy

of the fall detection process. Through the databases Mobifall, Mobifall2 and a custom database, tests performed with the proposed methodology showed 87.65% of specificity and 95.45% of sensitivity, with maximum detection delay of 3 seconds.

3.1.2 Non-Wearable Solutions

These types of systems try to propose a different perspective on the fall detection issue. In this area, camera-based systems are the most adopted approaches. Nowadays, cameras are becoming increasingly common among consumers and can be employed in many different contexts, such as the active assisted living ones and for security. A major advantage of these systems rely on their capability to monitor more complex behaviors with respect to wearable solutions.

Although analyzing visual streams from cameras to automatically detect users' behavior is a challenging task [26], since it implies the need to differentiate users from the environment where the users operate, human activities and falls analysis has anyway attracted considerable attention in the computer vision and image processing communities [27, 28, 29, 30].

As an example, in [27], Messing et al. have used a particular technique for daily activity recognition, based on the velocity histories of tracked key points. The solution exploits a generative mixture model for video sequences, which shows similar performance compared to local spatio-temporal features on the KTH activity recognition dataset (a dataset provided by KTH Royal Institute of Technology in Stockholm).

In [28] the authors discuss a solution based on the use of an RGB-D (Kinect-style) cameras for fine-grained recognition of kitchen activities. The system developed combines depth (shape) and color (appearance) to solve several perception problems fundamental for smart space applications: locating hands, identifying objects and their functionalities, recognizing actions and tracking object state changes through actions. The system can robustly track and recognize different activities of daily living.

A key challenge in the computer vision context deals with the detection and classification of falls based on variations in human silhouette shape. In order to face this problem, the study presented in [31] pro-

poses a multivariate exponentially weighted moving average (MEWMA) monitoring scheme, which is effective in detecting falls since sensitive to small changes. In order to distinguish real falls from some fall-like gestures, a classification stage based on a support vector machine (SVM) is applied to detected sequences. The methodology has been validated using the University of Rzeszow fall detection dataset (URFD) and the fall detection dataset (FDD). The results of the MEWMA-based SVM are compared with three other classifiers: neural network (NN), naïve Bayes and K-nearest neighbor (KNN). Results show the capability of the developed strategy to distinguish fall events.

In [32] a vision-based solution using Convolutional Neural Networks to detect falls in a sequence of frames is proposed. To model the video motion, and to make the system independent on the considered scenario, an optical flow images as input to the networks followed by a novel three-step training phase is introduced. The method has been evaluated in three public datasets achieving state-of-the-art results.

3.1.3 Hybrid System

In many application scenarios, there is a need to differentiate activities characterized by similar motions or gestures but corresponding to different behaviors. Typically, these situations can arise from actions like carrying a glass of water or carrying a pillbox, or when an object is used or simply carried around.

A solution for the aforementioned problems is discussed in [33], where an approach based on direct motion measurements with inertial sensors and detection of object interaction with RF-ID for high-level activity recognition is proposed. The system uses a sensor fusion strategy based on different levels of abstraction for simultaneously integrating many channels of heterogeneous sensor data. This approach was evaluated with one Activity of Daily Living (ADL) breakfast scenario and one home care scenario where the proposed approach reached an accuracy of 97% and 85% respectively.

A paper discussing the performance limitations of using individual wearable sensors instead of hybrid solutions, especially for the classification of similar activities, is presented in [34]. This is mainly based

on a data fusion strategy of features extracted from experimental data collected by different sensors: a tri-axial accelerometer, a micro-Doppler radar, and a depth camera. Preliminary results show that combining information from heterogeneous sensors improves the overall performance of the system. The classification accuracy attained using this fusion approach improves by 11.2% compared to radar-only use, and by 16.9% compared to the accelerometer. Furthermore, adding features extracted from an RGB-D Kinect sensor, the overall classification accuracy increases up to 91.3%.

3.1.4 Discussion

The cited solutions highlight the huge number of alternatives when dealing with falls and ADLs detectors.

The choice of one or another solution is usually driven by the application, performance requirements, user skills, invasivity, computational power requirements, and many more. But focusing on elderly people or people with neurological disease, solutions based on wearable devices prove to be the most effective. Although, in general, better performances can be achieved using different approaches, none of them can guarantee all the specifications defining a reliable, robust and user-centered system. Wearable systems, and especially the one based on inertial devices, if appropriately designed, can guarantee continuous monitoring, no matter where, can run the algorithms in standalone mode, avoiding blind spot in the detection phase and preserve, natively, their privacy. Of course, all these advantages come with a cost: resource-hungry algorithms cannot be easily embeddable in such low power devices. For this reason, a specific effort has been made to develop an efficient and reliable algorithm whose integration into a wearable low power device could have been feasible.

These conclusions are at the base of every choice and considerations throughout the entire thesis.

3.2 Event-Driven Methodology for Fall Detection and Classification

The proposed methodology for falls and ADLs detection exploits an event-driven approach that is able to guarantee high robustness against exogenous dynamics and a normalization phase improving the system robustness against users' characteristics. These results are obtained through a cautious design of the entire pre-processing chain.

3.2.1 The Event-Driven Classification Methodology

The detection methodology, schematized in Figure 3.1, is based on an event-driven template matching technique where "template", called "Signature" from now on, represents the core of the entire event detection technique. It is based on the consideration that ADLs and falls are both characterized by a typical shape in the time evolution of the events [35]. It is straightforward to deduce that different events have slightly different signatures. Signatures may be built using different mathematical models starting from the raw inertial measurements, and the two adopted ones will be introduced in Section 3.2.2.2.

The evaluation of how close an event is to a given signature (template) is demanded to a function measuring their similarity employing either a cross-correlation or a Dynamic Time Warping (DTW) technique. Cross-correlation is known to be one of the most powerful, yet computationally manageable, methods for similarity measurements thanks to the invariance to the translations and the robustness to the additive noise of the signal. DTW instead is one of the algorithms for measuring similarity between two temporal sequences, which may vary in speed. For instance, similarities in walking could be detected using DTW, even if one person walks faster than the other, or in presence of accelerations and decelerations during an observation. One of the advantages of the DTW technique relies on the possibility to adopt the same signatures in different inertial systems, where quantities, such as the sampling frequency, may slightly change the shape in time of two identical time series.

Finally, two classifiers will be investigated for the sake of fall detection.

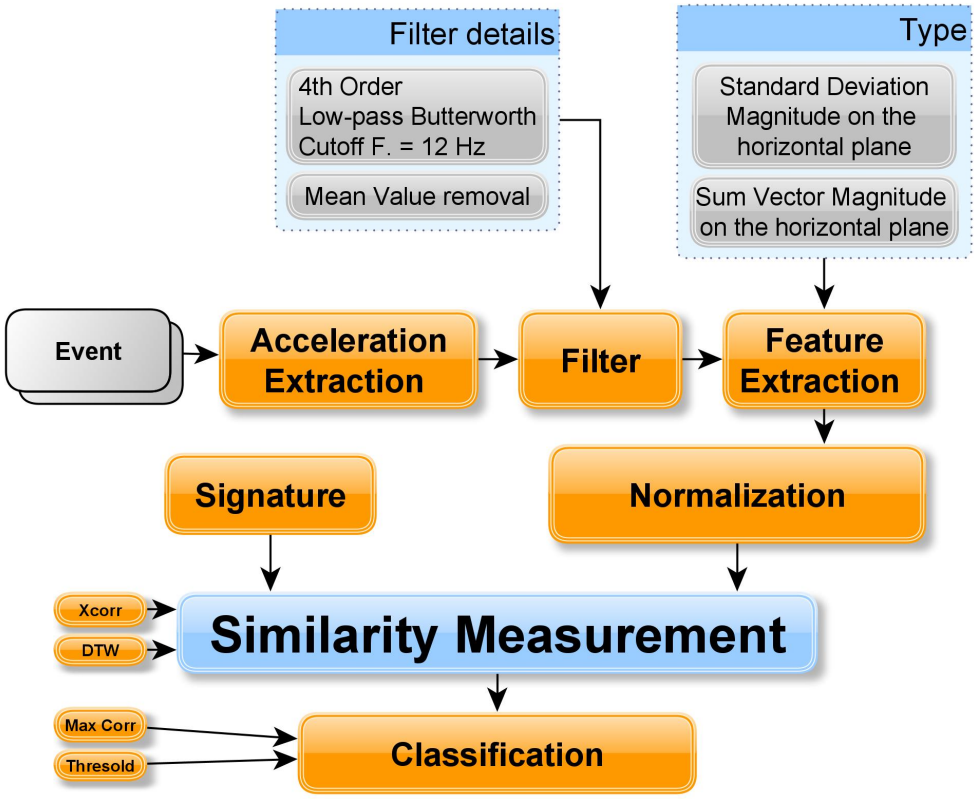

Figure 3.1: The Event-Driven Classification Methodology

In total, 8 different combinations of features, similarity measurements and classifiers will be investigated.

3.2.2 Pre-processing

The pre-processing step prepares the raw measurements for optimal use inside the method. A carefully designed pre-processing is mandatory for optimal extraction of useful information from the data. From now on when referring to "inertial data" or "raw data" will we indicate only the acceleration components of any of the possible inertial quantities that can be acquired using an inertial system. The reason behind that relies on a reduced complexity of the method itself, since dealing with a reduced number of quantities, and, in the meantime, reduce the amount of infor-

mation that should be processed by an embedded device.

In the following sections, the details of each of the steps involved in the pre-processing phase will be presented along with examples of the related output.

3.2.2.1 Filtering Stage

Many variables must be taken into account when designing a proper filter (Figure 3.2). One of these is the frequency range.

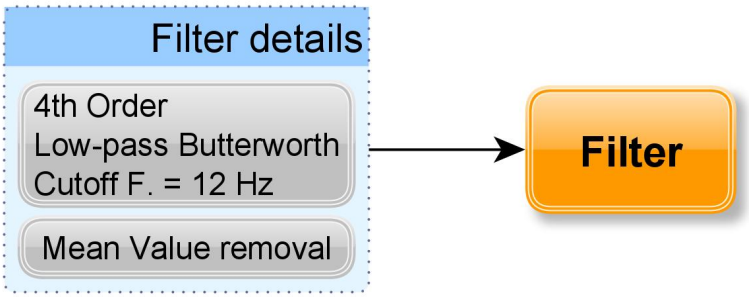

Figure 3.2: Filtering stage properties.

The human motion frequency range belongs to the range [0, 12] Hz [36, 37, 38]. According to this, a low-pass filter with a cut-off frequency f_c of 12 Hz is required to remove both electronic noises, arising at a higher frequency, and unwanted variation due to phenomenons which are not directly associated with human motion. In particular, a 4^{th} order Butterworth filter has been selected due to its simplicity, as it present similar results than more elaborated IIR and FIR filters. An interesting property of this kind of filter relies on its maximal band flatness (no ripples) at the expense of a wide transition band. A reduction of the transition band can be achieved by increasing the filter order which in turn introduces an excessive ripple in the passband and a higher delay in the filtered signal.

An example of a 4^{th} order Butterworth filter with a cut-off frequency, f_c, of 12 Hz and a sampling frequency, f_s, of 200 Hz is given in Figure 3.3. The normalized frequency, f_n, given in Figure 3.3 is related to f_s and f_c according to equations from 3.1 to 3.5.

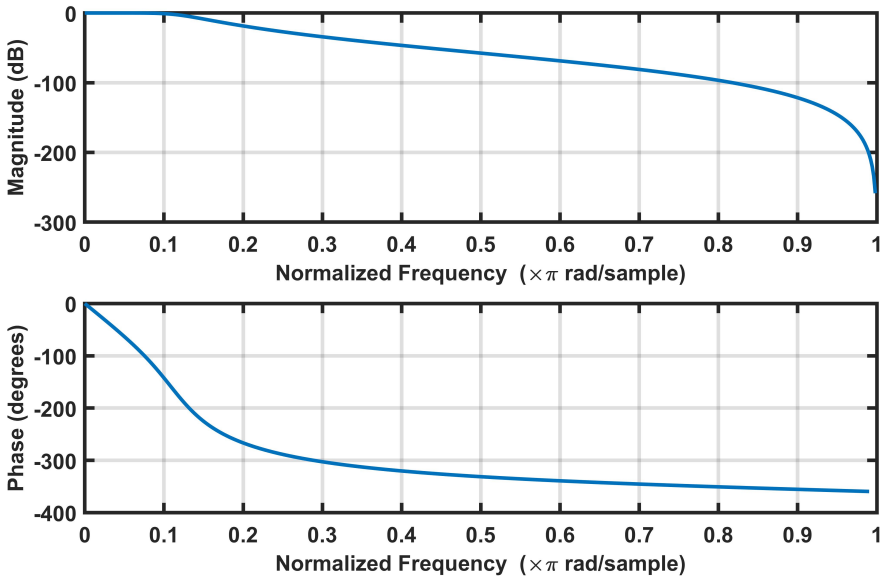

Figure 3.3: Bode plot of a 4^{th} order Butterworth filter.

$$f_n = \frac{f_c}{f_s} \tag{3.1}$$

Equation (3.1) is a number (no units) showing how many sampling periods with frequency f_s are in the sampled signal f_c. However, according to Nyquist-Shannon theorem, the sampling frequency is always at least two times the frequency f_c. Thus (3.1) is never larger than $1/2$. To have f_n in the range [0, 1], we multiply (3.1) with a factor 2 (3.2):

$$f_n = 2\frac{f_c}{f_s} \tag{3.2}$$

and hence:

$$f_c = \frac{\omega_c}{2\pi} \tag{3.3}$$

$$f_n = 2\frac{f_c}{f_s} = \frac{\frac{\omega_c}{\pi}}{f_s} \tag{3.4}$$

multiplying both side of (3.4) by π:

$$\pi f_n = \frac{\omega_c}{f_s} \frac{\text{rad}}{\text{sample}} \tag{3.5}$$

f_n as a unit equal to $[\pi \frac{\text{rad}}{\text{sample}}]$ as shown in Figure 3.3.

Since the procedure is based on signatures, which represents the "time" evolution of an event, the DC components can be removed by subtracting the mean value from each axes.

An output of this stage is shown in Figure 3.4 where are given respectively the raw acceleration in the three axes, the output of the Butterworth filter and the same signal with mean value removed.

3.2.2.2 Feature Extraction

Several features have been used by the scientific community for fall detection experiments. A detailed list is given in [39] where it emerges that features like mean, standard deviation, sum vector magnitude and tilt angles, due to its simplicity, yet informative, are commonly used features in existing fall detection experiments. This is explained considering that generic equations such as mean, standard deviation and variance can be applied to any motion sensors.

The choice of the specific feature extraction tools has been done according to [40] where a deep features comparison is provided using the SisFall dataset. The adopted features are:

$$SVM_c[K] = \sqrt{a_x^2[k] + a_y^2[k] + a_z^2[k]} \tag{3.6}$$

$$SDM_c[K] = \sqrt{\sigma_x^2[k] + \sigma_y^2[k] + \sigma_z^2[k]}; \quad \text{with} \quad \sigma_i = std(\widetilde{a}_i[k]) \tag{3.7}$$

where SVM stands for Sum Vector Magnitude while SDM stands for Standard Deviation Magnitude; the subscript c stands for "complete" indicating the use of all the acceleration components.

Here, one sample of acceleration in the three axis is defined as the vector $\overrightarrow{a} = [a_x, a_y, a_z]^T \in \mathbb{R}$, the sliding window used for computing the dynamic features is denoted with $\widetilde{a}[k] = [\overrightarrow{a}^T[k - N_v + 1], ..., \overrightarrow{a}^T[k]]^T \in$

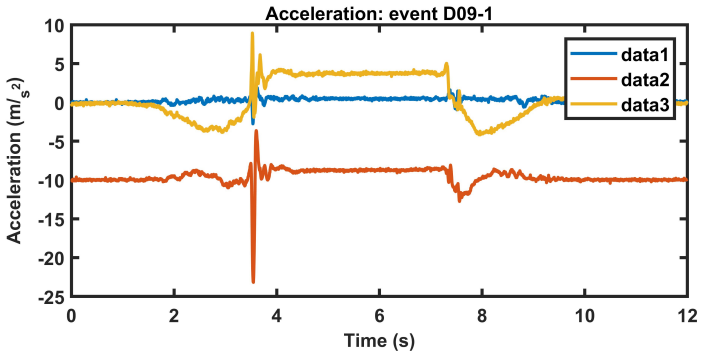

(a)

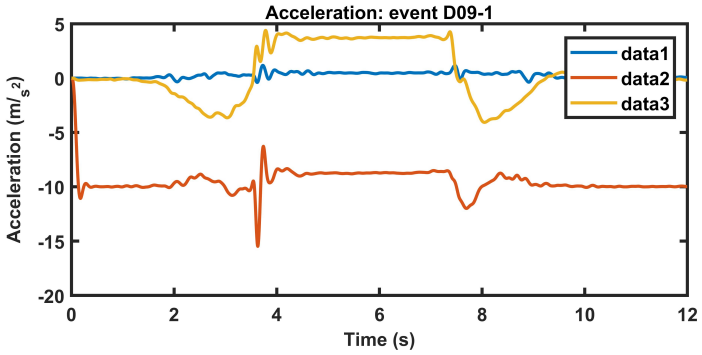

(b)

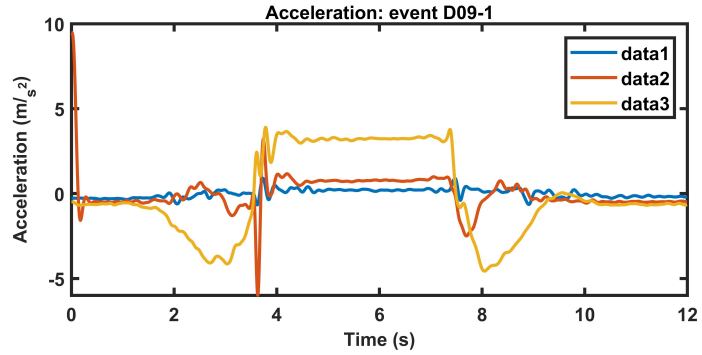

(c)

Figure 3.4: Steps involved in the filtering process of a test event: (**a**) Raw acceleration; (**b**) Butterworth filter output; (**c**) Filtered output with mean value removed. Data 1 to data 3 represent respectively the x, y and z axes.

$\mathbb{R}^{N_v x 3}$ at time sample k, where N_v is the number of samples in the selected window. The standard deviation operator is defined as $\sigma(\cdot)$.

If the measurements system (i.e the wearable system) is placed in the center of mass of the body (Figure 3.5), the acceleration vertical axis can be neglected from the computation of both features. This helps reduce the number of false positives caused by the high accelerations achieved in the vertical axis with many ADLs [39]. The equations becomes:

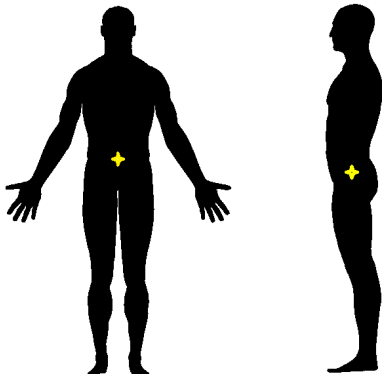

Figure 3.5: Position of the center of mass of human body (indicated in yellow).

$$SVM[K] = \sqrt{a_x^2[k] + a_y^2[k]} \tag{3.8}$$

$$SDM[K] = \sqrt{\sigma_x^2[k] + \sigma_y^2[k]}; \quad \text{with} \quad \sigma_i = std(\widetilde{a}_i[k]) \tag{3.9}$$

if a_z is the vertical axis.

As it will be proved in Section 4.2.3, the SDM produces a signature better representing the whole classes of fall which has been proved to be more effective in the class discrimination phase.

For the sake of clarity, two examples of features, one built with the SVM and another with the SDM are presented in Figure 3.6 and 3.7. Both are computed using the same test event.

3.2.2.3 Normalization

As previously introduced, we are interested in the time evolution of an event rather than its amplitude. This is a first reason behind the normal-

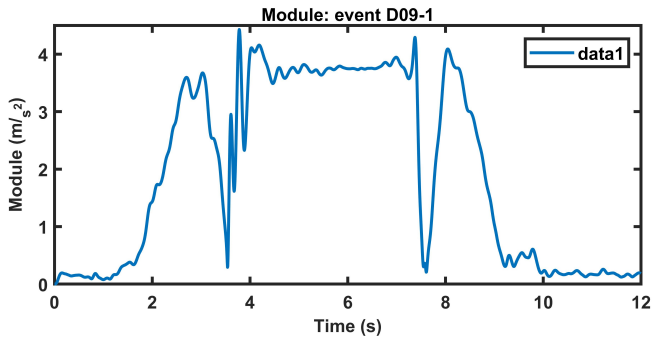

Figure 3.6: SVM feature built on a test event.

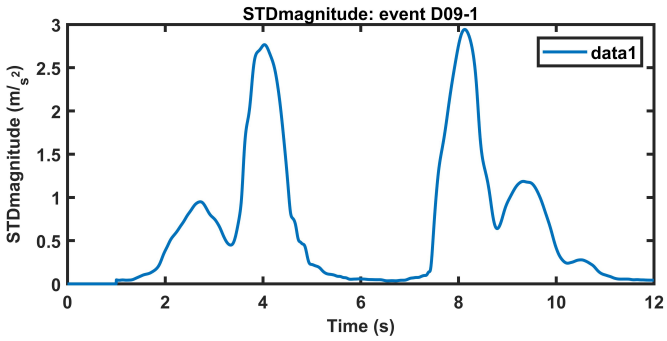

Figure 3.7: SDM feature built on a test event.

ization phase. Another reason is based on the well know physic relation relating body mass and its acceleration. The acceleration module of a falling body may change consistently as a function of weight and height. For this reason, since the methodology should be as much as possible independent from these quantities, a normalization is then suggested. Those two reasons underlie the need for normalizing.

The normalization procedure constrains signals in the range $[0,1]$, thus preserving the signal's dynamics, while assuring the generalization of the classification strategy.

Figure 3.8 shows the obtained output, after the normalization phase, for one of the features presented in Section 3.2.2.2.

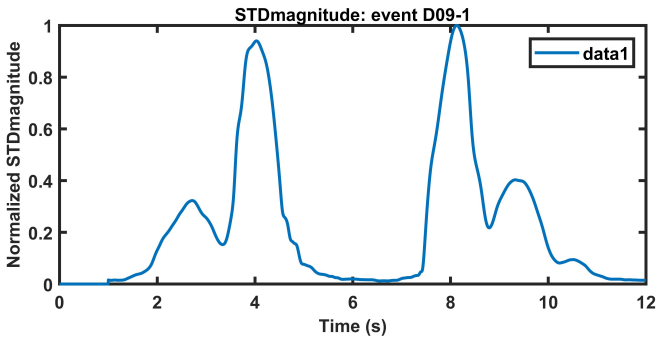

Figure 3.8: Normalized SDM test feature.

3.2.3 Signature: Definition and Building Process

A signature is defined as a typical time evolution of an inertial event uniquely describing a specific event. As it will be clarified in the following, to build a reliable set of signatures (one per each addressed class of events), a high-quality dataset, including several observations for each class of falls and ADL is required.

The signatures building process (Figure 3.9) shares the same pre-processing, described in Section 3.2.2, along with two more phases: 1) features alignment and 2) averaging.

The signals alignment is based on the time delay between patterns, estimated by computing the cross-correlation between signals (more details on this theoretical tool are given in Section 2.1).

Given the aligned features $x_1, x_2, ..., x_n$, with n number of events in the adopted dataset, the signature X at instant k, obtained by averaging, is computed as shown in Equation 3.10.

$$X[k] = \frac{1}{n} \sum_{i=1}^{n} x_i[k] \tag{3.10}$$

The alignment phase and relative averaging are shown in Figure 3.10.

Since the process is based on the averaging of the aligned features, the dataset choice plays a decisive role. A dataset with a reduced number of events, both in terms of observations and type, can results in an overfitted template not fully representing the class of interest. The danger of such an outcome is related to the deceiving results of any performance evalu-

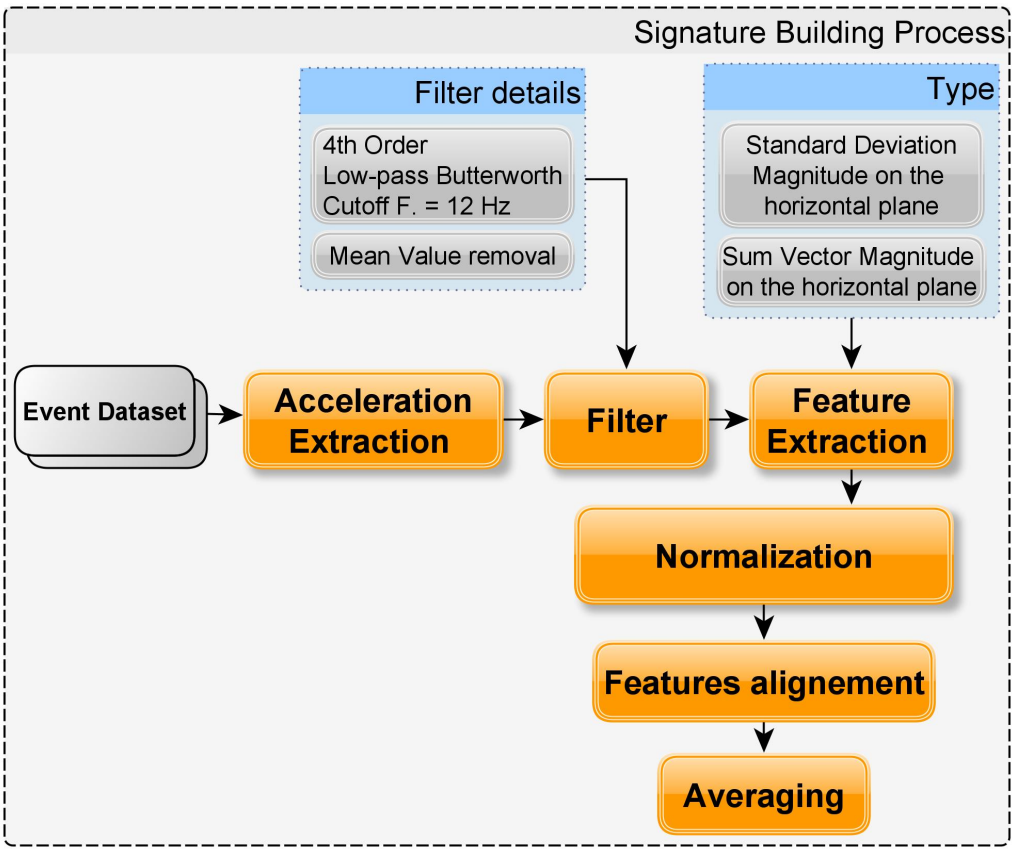

Figure 3.9: Signature building process.

ation of detectors based on these templates. The actual performances of the method can result to be much lower when tested with dataset with a bigger data variance (in terms of subjects involved, number of observations, type of events, and so on.)

It must be specified that the signatures building process is only required once and need to be performed offline employing a dedicated algorithm. Once built, signatures are not subjected to any changes. This is a relevant advantage when addressing a method integration in low power hardware.

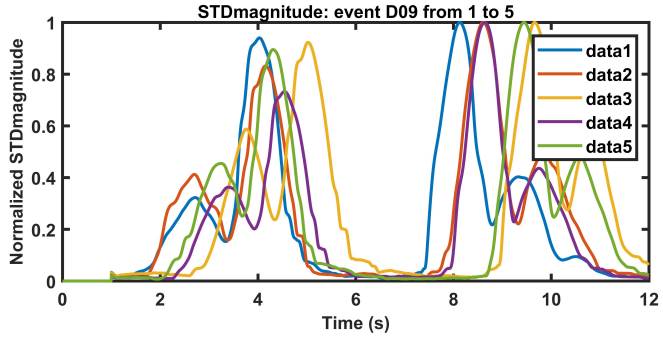

(a)

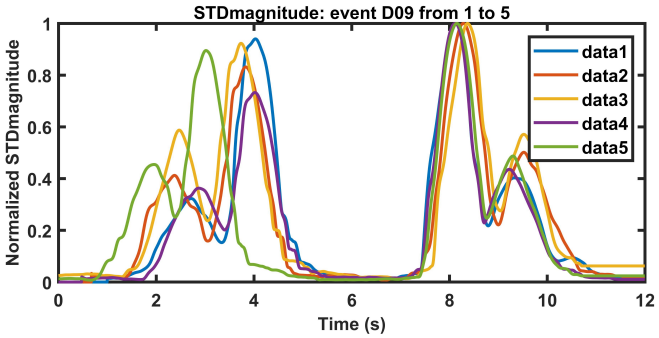

(b)

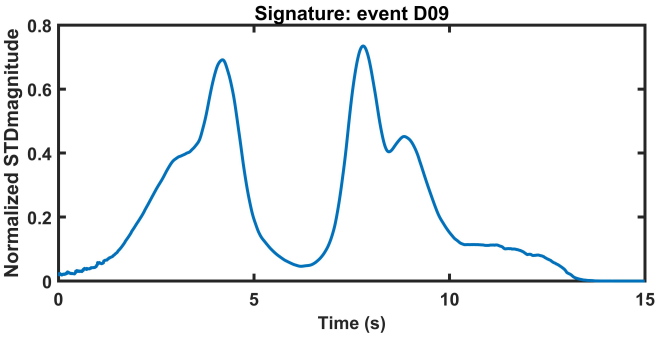

(c)

Figure 3.10: Signature building process. (**a**) Non aligned SDM test features; (**b**) aligned SDM test features; (**c**) signature obtained by averaging the aligned test features. Data 1 to data 5 represent 5 different features computed using 5 different observations.

3.2.4 Similarity Measurement

The similarity measurement is the procedure giving rise to the scores vector which is afterward passed to the classification block.

In statistics and related fields, a similarity measure (or similarity function) is a real-valued function that quantifies the similarity between two objects. In its general definition, if the distance is small, two objects are very similar whereas if the distance is large we will observe a low degree of similarity. In real applications, whether high similarity is associated with small distance or with big ones, strictly depends on the adopted metric or algorithm.

3.2.4.1 Cross-Correlation Based Similarity Measurement

A widely used similarity function is the cross-correlation function (more detail are given in Section 2.1). In signal processing, the cross-correlation is a measure of similarity of two series as a function of their relative displacement. This is also known as a sliding dot product or sliding inner-product. It finds applications in pattern recognition, single particle analysis, case-based reasoning, audio signal processing, event recognition and more [41, 42, 43, 44, 45, 46].

The equation for cross-correlation can be derived from the basic correlation equation, by introducing a variable shift into one of the two functions (Equation 3.11). It does not matter which function is shifted with respect to the other, whether the signal x or y, the results would be the same. The correlation operation of Equation 3.11 is a series of correlations over different time shifts, k.

$$r^*_{xy}[k] = \begin{cases} \sum_{n=1}^{N} x[n] \cdot y[n+k] & k \geq 0 \\ r_{xy}[-k] & k < 0 \end{cases} \tag{3.11}$$

In order to constrain the cross-correlation in the range $[-1, 1]$, the normalized cross-correlation, $\hat{r}_{xy}$, is used (Equation 3.12)

$$\hat{r}_{xy}[k] = \frac{r_{xy}[k]}{\sqrt{r_{xx}[0] r_{yy}[0]}} \tag{3.12}$$

where $r_{xx}[0]$ and $r_{yy}[0]$ indicate the auto-correlations at zero lag of the signals x and y.

In order to extract a single score value, the maximum absolute value is taken from $\hat{r}_{xy}$. If value is small ($\rightarrow 0$) then the signals are uncorrelated (low similarity). If value is high ($\rightarrow 1$) then the signals are highly correlated (high similarity).

The cross-correlation operator requires signals sampled at the same frequency.

3.2.4.2 DTW Based Similarity Measurement

Dynamic time warping (DTW) is a well-known technique to find an optimal alignment between two given (time-dependent) sequences under certain restrictions (see Section 2.2 for more details). Intuitively, the sequences are warped in a non-linear way to match each other.

DTW has been applied to temporal sequences of video, audio, and graphics data [47, 48, 49]. In practice, any data that can be turned into a linear sequence can be analyzed with DTW. An advantage of the DTW algorithm relates to its ability to cope with time deformations and different speeds associated with time-dependent data.

In time series analysis, dynamic time warping (DTW) has also been used for measuring similarity between two temporal sequences, which may vary in speed, or sampled differently [50]. This enables the possibility to use signatures built on a dataset with different sampling frequencies than the one using in the test, or different than the sampling frequency of the fall detection device. This property is an advantage compared to the cross-correlation technique which requires signals equally sampled. For instance, similarities in walking could be detected using DTW, even if one person walks faster than another, or in case of accelerations and decelerations during an observation.

The temporal sequences are "warped" non-linearly in the time dimension to determine a measure of their similarity independent of certain non-linear variations in time. This sequence alignment method is at the base of time series classification techniques.

The use of a non-linear approach for the similarity measure involves a greater complexity compared to one involved in the cross-correlation.

The DTW algorithm intrinsically computes the "distance" between the two temporal sequences (whose metrics can be chosen) whose value is a measure of the similarity. If value is low ($\rightarrow 0$) then the signals are highly correlated (high similarity). If value is high ($\rightarrow \infty$) then the signals are highly uncorrelated (low similarity).

3.2.5 Classification

Classification is the final step in the entire falls and ADLs detection strategy. It must decide whether a given event belongs to a class or another. Historically, classification algorithm in the AAL context using low power wearable devices, have been primarily based on empirically found thresholds acting on some type of amplitude level (typically linear and angular acceleration amplitude) [51, 52, 53, 54, 55] or just on the analysis on the user position after fall. Although extensively used, thresholds acting just on amplitude levels, are strongly influenced by the characteristic of the user (if a user is particularly tall or obese, this many results in acceleration level beyond the thresholds even in the absence of a fall event), exogenous factor and poor selectivity. The ones based on static user's position suffer from false-negatives since they can be easily triggered by ADL having axes direction compatible with a fall type.

These disadvantages are sophistically removed thanks to the intrinsic nature of the score value: they are based on a measure of similarity rather than a simple amplitude. This allows the adoption of simple classification algorithms for the detection phase.

Two classifiers are now introduced. It must be underlined that major advantages of what is going to be described rely on their low computational demand and adaptability to several different application contexts. The classification strategies have been specifically thought for their implementation in a real power-limited embedded system where, more complicate classification approaches, such as the ones based on machine learning techniques, can be hardly implemented.

3.2.5.1 Threshold-Based

The threshold-based classification algorithm (abbreviated as TH) compares the extracted scores with threshold values, to define the potential class or classes to which the unknown event belongs. An event is classified as belonging to a specific class if the score value overpasses, or not, a predefined threshold. Whether we control the threshold's overpass or it's opposite, depends on the nature of the score value. If the score is computed using the cross-correlation (high similarity is associated with high score value) the threshold's overpass is considered. If the score is computed using the DTW (high similarity is associated with low score value) values that do not overpass thresholds are considered.

To define optimal threshold values for each class of the addressed events, the ROC theory has been used (see Section 2.3). The ROC curve theory provides theoretical support to the classification problem where a classifier is required to map each instance to one of two classes [56]. The general strategy adopted by the ROC theory allows us to identify thresholds maximizing a selected performance index (Sensitivity, Specificity, Accuracy and so on) assessing the classification methodology. In this application, the intersection between the specificity and sensitivity curves has been adopted as the selection criteria for threshold identification [35].

It must be observed that the result of the classification strategy above described can lead to multiple classifications (an unknown pattern could be recognized as belonging to different classes) and unclassified events (an unknown pattern could be classified as not belonging to any of the considered classes of events).

3.2.5.2 Absolute Minima Value

This classifier is the easiest classifier one can design and implement.

To understand this classifier, some considerations should be made. The TH classifier is totally able to work even in the presence of a single score value. Using Table 3.1 as an example, a TH classifier can say if Event 1 or Event N belongs to the class expressed by Signature 1 only by comparing the score value with the threshold. In the case of the Absolute Minima Value (AMV) classifier, the event having the highest similarity

Table 3.1: Example of a score vector built having N events and 1 signature.

	Signature 1
Event 1	Score_1
Event 2	Score_2
...	
Event N	Score_N

Table 3.2: Example of a score vector built having N events and M signatures.

	Signature 1	**Signature** 2	**...**	**Signature** M
Event 1	Score_{11}	Score_{12}		Score_{1M}
Event 2	Score_{21}	Score_{22}		Score_{2M}
...				
Event N	Score_{N1}	Score_{N2}		Score_{NM}

value, among the M signatures, is defined as belonging to that class. To clarify, let us use Table 3.2. Event 1 is said to belong to the class defined by Signature 2 if Score_{12} is:

- The highest value in the row in case of similarity based on cross-correlation
- The lowest value in the row in case of similarity based on DTW

It is now clear that, for this method to fully work, an unknown event must be compared to multiple signatures.

Chapter 4

Assessment of the Fall Detection Strategy

This chapter features results obtained by means of the classification methodology presented in Section 3. Results coming from this section will prove the goodness and reliability of the proposed methodology by also using dedicated metrics, such as Sensitivity, Specificity, Accuracy, and F1-Score.

4.1 Falls and ADLs Dataset

Many falls and ADLs datasets can be found in the literature. In order to select a proper one, some basic requirements have been imposed for the selection:

1. all activities must be well documented;
2. raw data must be freely available;
3. must contain both falls and ADLs;
4. reported in a peer-reviewed paper.

Following these requirements, four datasets have been identified:

1. MobiFall [57]: twenty-four volunteers having age between 22 and 42 years old performed nine types of ADLs and four types of falls

using a Samsung Galaxy smartphone. Only nine subjects performed falls and ADLs, while the remaining 15 performed only falls (three times each);

2. tFall [58]: only ten participants between 20 and 42 years old. It is made up of eight types of falls (503 total recordings with two smartphones), and one week of continuous ADL recordings with all participants carrying smartphones in the pockets or in an handbag;

3. DLR [59]: sixteen subjects between 23 and 50 years old. It is made of six types of ADLs, and the authors did not specify the conditions of the falls (they belong to a single group). Acquisitions are too short for a consistent analysis.

4. Project gravity [60]: three participants (ages 22, 26, and 32) performed 12 types of falls and seven types of ADLs with a smartphone in the pocket;

5. SisFall [40]: thirty-eight volunteers divided into elderly people and young adults. The elderly people group (age between 60 and 75 years old) was formed by 15 participants (8 male and 7 female), and the young adults group (age between 19 and 30 years old) was formed by 23 participants (11 male and 12 female). In total have been acquired 34 types of events, 15 falls and 19 ADLs, with several trials each, for a total of 2706 ADL and 1798 falls.

The SisFall dataset is the one containing more participants, types of activities and recordings than all the other publicly available datasets. More specifically, none of the other datasets includes elderly people, which is a big drawback, and the variety of activities and the number of subjects is limited compared to the SisFall. Additionally, all the other datasets have been acquired using smartphones in the pocket, which is a different approach compared to the methodology under assessment. The SisFall instead has been built using a belt buckle sensor node.

Those properties made this dataset suitable for our assessment.

4.1.1 SisFall Dataset

In this section, more details on the adopted dataset are provided.

All the acquisitions were recorded with an embedded device integrating an ADXL345 accelerometer (configured for ± 16 g, 13 bits analog to digital converter), a MMA8451Q accelerometer (± 8 g, 14 bits ADC) and an ITG3200 gyroscope ($\pm 2000^{\circ}/s$, 16 bits ADC). Nevertheless, only acceleration data acquired with the ADXL345 sensor (sampling frequency f_s of 200 Hz) was used in the assessment phase. The device was fixed to the waist of the participants whose orientation of the sensor (Figure 4.1) presents the positive z-axis in the forward direction, the positive y-axis in the gravity direction, and the positive x-axis pointing to the right side of the subject.

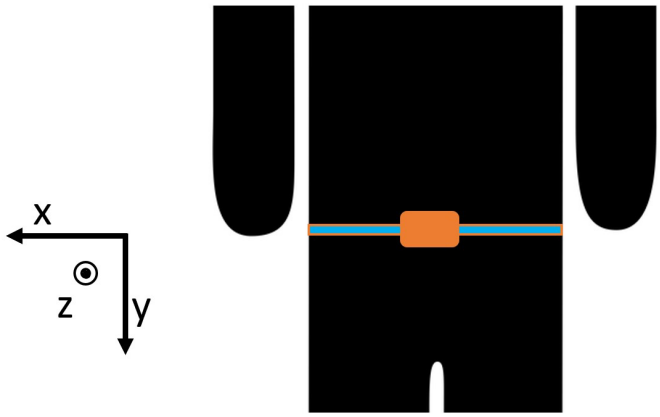

Figure 4.1: Position of the measurement system on the human body.

4.1.1.1 Types of Fall

As previously stated, 15 different types of fall have been acquired in the SisFall dataset. Falls are of major interest in this work since they represent the dangerous events that must be promptly detected. Working with a large set of falls for the system assessment, is a huge advantage since the reliability of the fall detector can be evaluated in a robust way. A detailed list of the falls included in the dataset is given in table 4.1.

Table 4.1: Types of falls included in the SisFall dataset. Data from [40].

Code	Activity	Duration	Trials
F01	Fall forward while walking caused by a slip	15 s	5
F02	Fall backward while walking caused by a slip	15 s	5
F03	Lateral fall while walking caused by a slip	15 s	5
F04	Fall forward while walking caused by a trip	15 s	5
F05	Fall forward while jogging caused by a trip	15 s	5
F06	Vertical fall while walking caused by fainting	15 s	5
F07	Fall while walking, with use of hands in a table to dampen fall, caused by fainting	15 s	5
F08	Fall forward when trying to get up	15 s	5
F09	Lateral fall when trying to get up	15 s	5
F10	Fall forward when trying to sit down	15 s	5
F11	Fall backward when trying to sit down	15 s	5
F12	Lateral fall when trying to sit down	15 s	5
F13	Fall forward while sitting, caused by fainting or falling asleep	15 s	5
F14	Fall backward while sitting, caused by fainting or falling asleep	15 s	5
F15	Lateral fall while sitting, caused by fainting or falling asleep	15 s	5

4.1.1.2 Types of ADLs

The 19 types of ADLs were selected based on activities that are similar (in acceleration waveform) to falls, and activities with high acceleration that can generate false positives. Also in this case, a detailed list of the acquired ADLs is given in Table 4.2. A large set of ADLs allows to verify the capability of the algorithm to reliably distinguish common daily activities from falls.

4.1.1.3 Participants

The database was generated with the collaboration of 38 volunteers: 15 elderly and 23 young adults. Table 4.3 shows age, weight, and height of each group. The elderly group was made up of healthy and independent

Table 4.2: Types of ADLs included in the SisFall dataset. Data from [40].

Code	Activity	Duration	Trials
D01	Walking slowly	100 s	1
D02	Walking quickly	100 s	1
D03	Jogging slowly	100 s	1
D04	Jogging quickly	100 s	1
D05	Walking upstairs and downstairs slowly	25 s	5
D06	Walking upstairs and downstairs quickly	25 s	5
D07	Slowly sit in a half height chair, wait a moment, and up slowly	12 s	5
D08	Quickly sit in a half height chair, wait a moment, and up quickly	12 s	5
D09	Slowly sit in a low height chair, wait a moment, and up slowly	12 s	5
D10	Quickly sit in a low height chair, wait a moment, and up quickly	12 s	5
D11	Sitting a moment, trying to get up, and collapse into a chair	12 s	5
D12	Sitting a moment, lying slowly, wait a moment, and sit again	12 s	5
D13	Sitting a moment, lying quickly, wait a moment, and sit again	12 s	5
D14	Being on one's back change to lateral position, wait a moment, and change to one's back	12 s	5
D15	Standing, slowly bending at knees, and getting up	12 s	5
D16	Standing, slowly bending without bending knees, and getting up	12 s	5
D17	Standing, get into a car, remain seated and get out of the car	25 s	5
D18	Stumble while walking	12 s	5
D19	Gently jump without falling (trying to reach a high object)	12 s	5

Table 4.3: Age, height and weight of the participants. Data from [40].

	Sex	**Age**	**Height (m)**	**Weight (kg)**
Adults	Male	60-71	1.63–1.71	56–102
	Female	62-75	1.50–1.69	50–72
Elderly	Male	19-30	1.65–1.83	58–81
	Female	19-30	1.49–1.69	42–63

subjects, and none of them presented gait problems.

Young adults performed ADLs and falls. Elderly people did not perform falls and activities D06, D13, D18, and D19 due to physician recommendations. Additionally, some elderly people did not perform some activities due to personal impairments. One single subject, 60 years old, simulated both falls and ADLs.

4.2 Assessment Strategy

The proposed assessment strategy is depicted in Figure 4.2. Some steps are already familiar since introduced and explained in Section 3. In addition to that, some new functions, specifically implemented for the assessment, have been included:

1. K-fold cross validation;

2. Definition and analysis of the method performances;

The implementation of the K-fold cross-validation has been done according to the *leave-one-out* strategy using $K = 10$.

To graphically validate each step of the methodology, up to the final classification, four events, two falls and two ADLs, are used as a reference. The selected falls are F01 and F02, respectively a type of forward and backward fall. The selected ADLs are D03 and D10, respectively a type of jogging and a type of sitting. It must be specified that those events will be the one graphically shown in the work, but all the events are used in the assessment.

Another points to be clarified regards the different acquisition length of some events. While each fall has an equal sample length, ADLs do

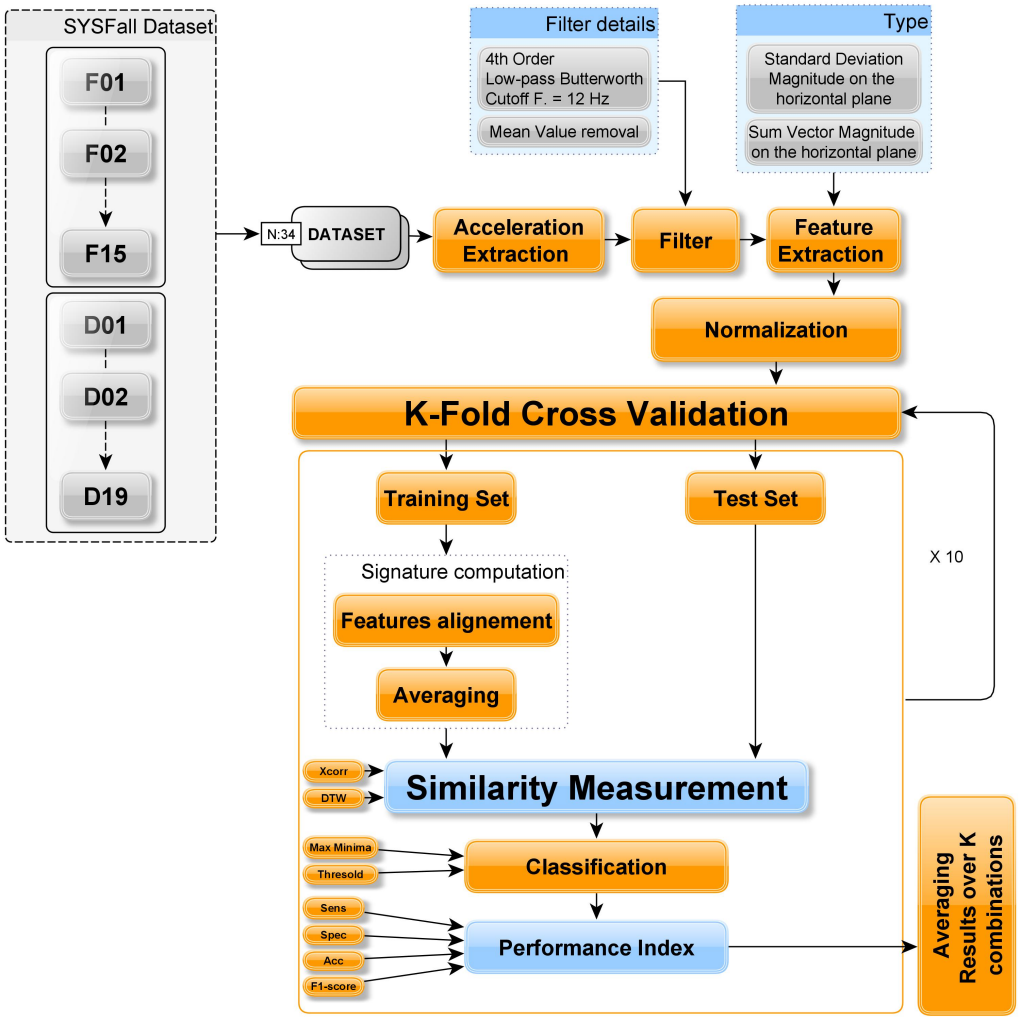

Figure 4.2: General structure of the adopted assessment strategy.

not. Events from D01 to D06 are periodic activities and hence, reducing their dimension, still preserve the nature of the event itself. To make compliant the ADLs dimension with the falls ones, every ADL has been reduced/extended to 15s. The signal extension has been done by appending zeros at the end of the vectors.

4.2.1 Pre-Processing Results

The pre-processing is made up of the filtering, features extraction and normalization stages.

Starting from the raw accelerations, the output of each step is shown from Figure 4.3 to Figure 4.6. The normalization is not shown since it just produces a scaling of the feature and its result has already been included in Section 3.2.2.3. Notes on the accelerations figures: the 3 axes, x, y and z are referred as data1, data2 and data3.

As anticipated, features built using SDM are less prone to over-fitting, which is a wanted result when one needs to adequately capture the underlying structure of the inertial data. This conclusion will be supported by numerical results later on in this chapter.

4.2.2 Cross Validation

Cross-validation is a statistical method generically used to estimate the skill of a model to generalize to an independent dataset. It is commonly used to compare and select a model for a given predictive modeling problem because it is easy to understand, easy to implement, and results in estimates that generally have a lower bias than other methods.

The goal of cross-validation is to test the model's ability to predict new data while avoiding problems like overfitting or selection bias.

Cross-validation involves partitioning a dataset into complementary subsets, performing the analysis on one subset, the training set, and validating the analysis on the other subset, the testing set. This procedure can be repeated K times, using different partitions. If cross-validation is repeated K times, then it takes the name K-fold cross-validation. Finally, the validation results are averaged to give an estimate of the model's predictive performance.

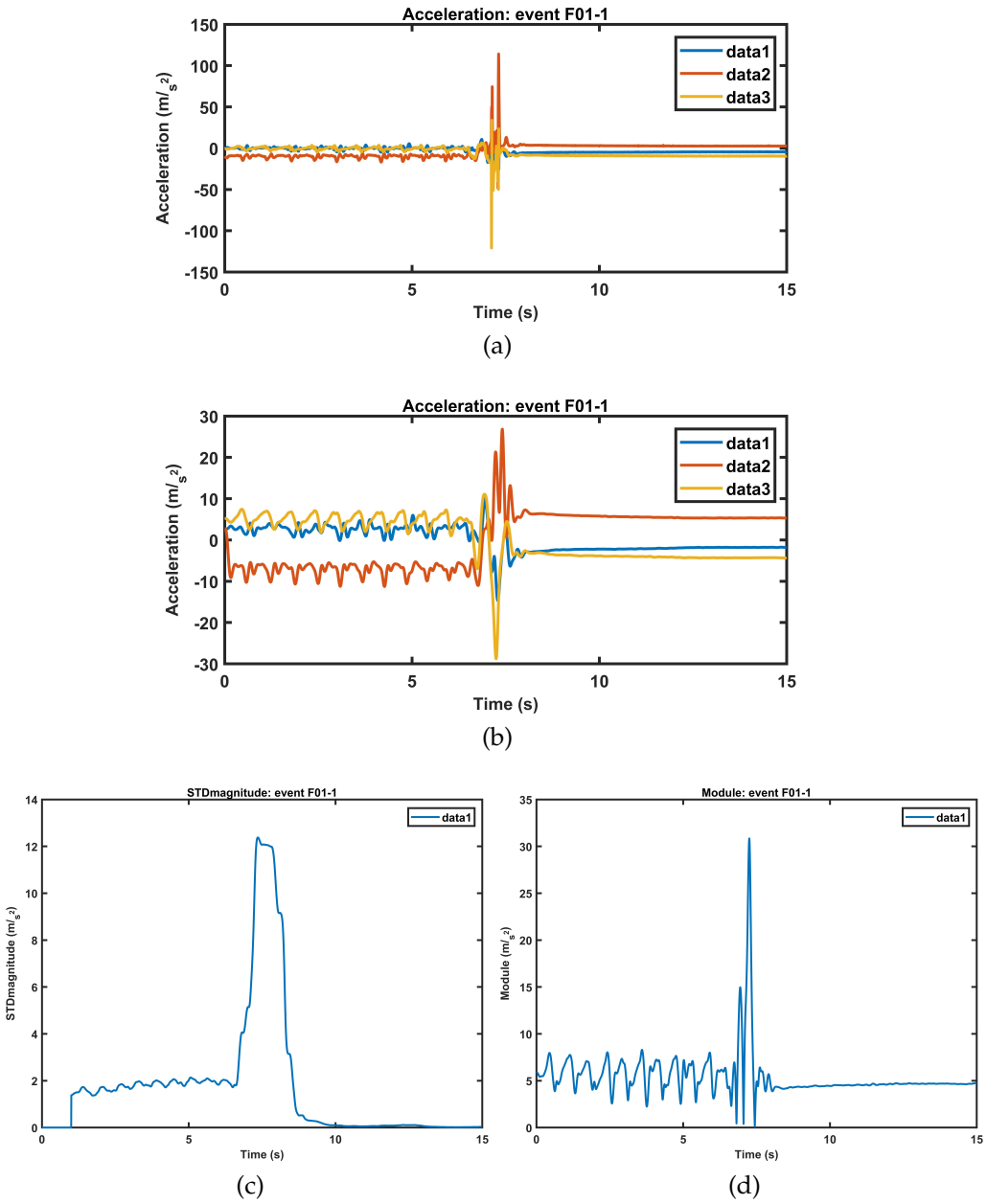

Figure 4.3: F01 event. (**a**) Raw acceleration; (**b**) filtered and zero centered; (**c**) SDM feature; (**d**) SVM feature.

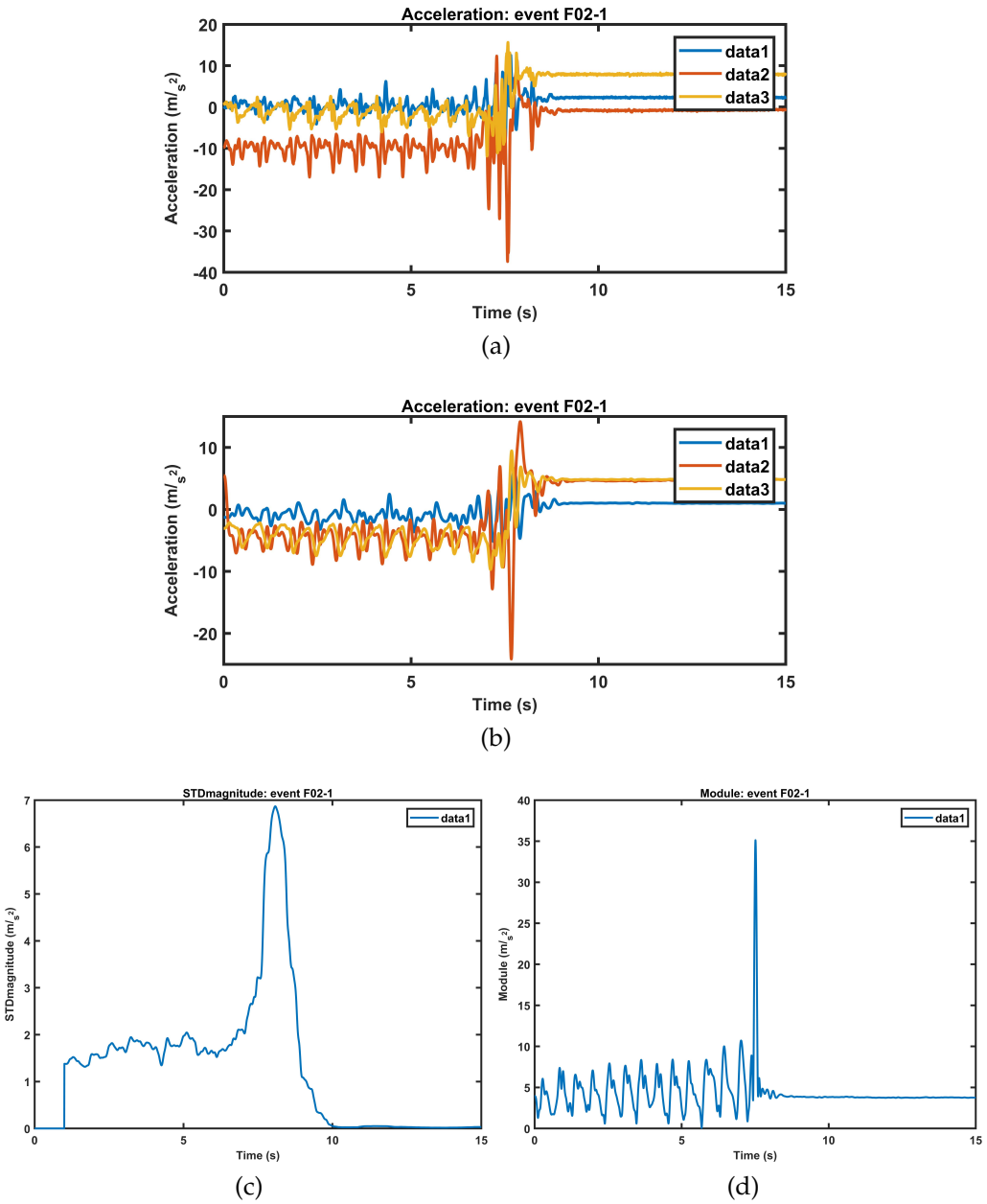

Figure 4.4: F02 event. (**a**) Raw acceleration; (**b**) filtered and zero centered; (**c**) SDM feature; (**d**) SVM feature.

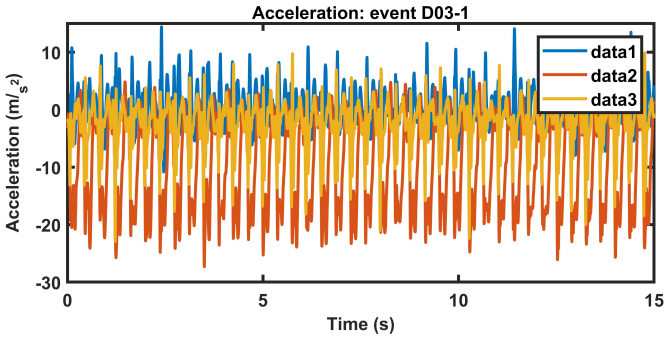

(a)

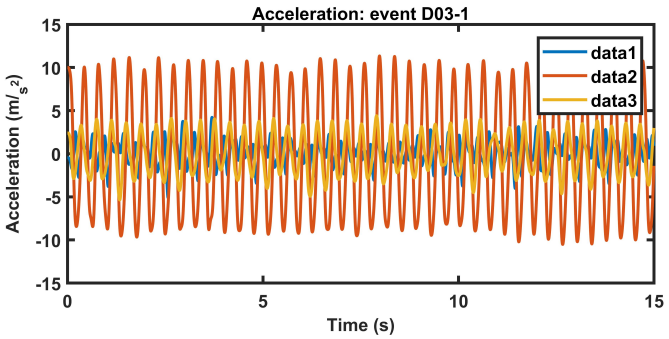

(b)

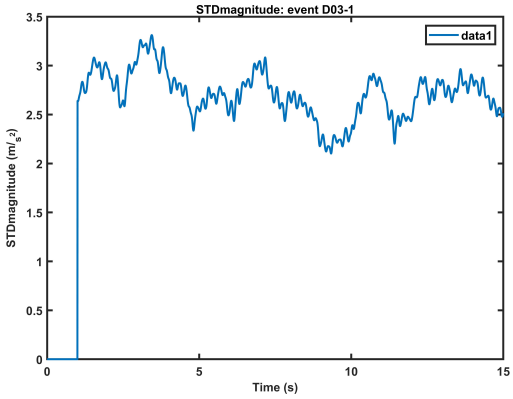

(c)

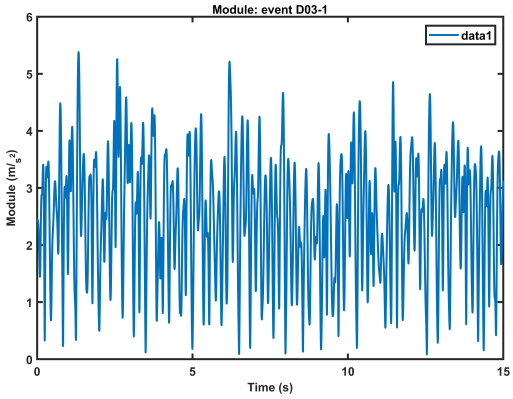

(d)

Figure 4.5: D03 event. (**a**) Raw acceleration; (**b**) filtered and zero centered; (**c**) SDM feature; (**d**) SVM feature.

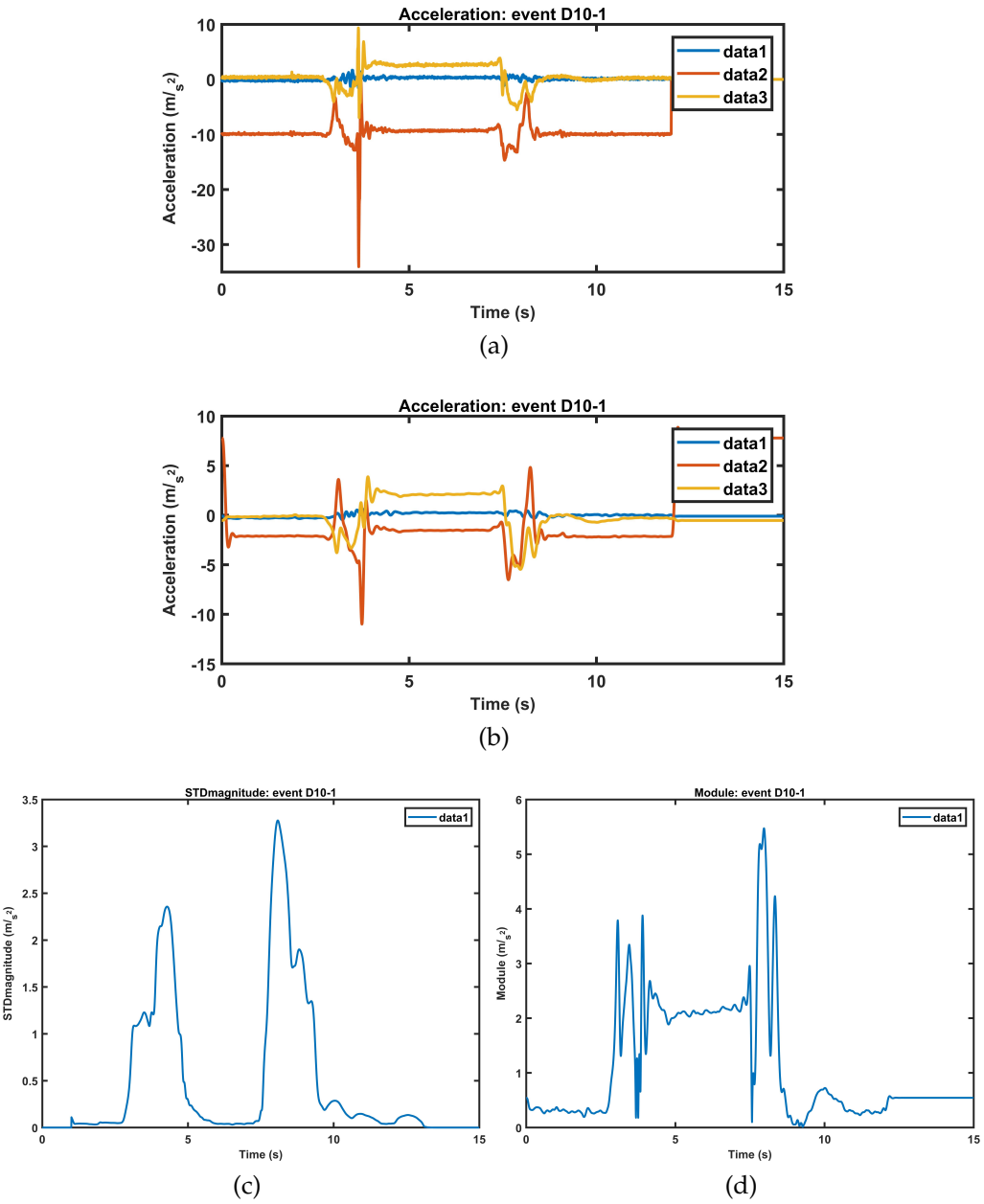

Figure 4.6: D10 event. (**a**) Raw acceleration; (**b**) filtered and zero centered; (**c**) SDM feature; (**d**) SVM feature.

In this work, K has been fixed to 10 and used the leave-one-out approach.

The K-fold cross-validation has been implemented in the following way (see Figure 4.2):

1. Each class of event (F01 – D19) has been divided into 10 Folds (subset);
2. Roughly every subset contain the same number of event (division doesn't always result in integer numbers);
3. K-1 folds are used as a training set and the signature/template is built on that;
4. A similarity measurement is performed;
5. Classification;
6. Performance indexes are calculated;
7. Steps from 3 to 6 are repeated 10 times (since $K = 10$) changing training and test subset;
8. Performance indexes are finally averaged.

4.2.3 Events' Signatures

Events' signatures for the 34 classes included in the dataset have been computed following the steps given in Section 3.2.3: 1) alignment and 2) averaging.

The alignment process for each of the four selected class of events, is given Figure 4.7 to Figure 4.10.

It must be specified that, for the sake of clarity, only 10 features have been shown in the figures.

Since the SDM is less prone to data overfitting, in the sense that it produces a waveform having smoother variations compared to the SVM, it facilitates the alignment process in all circumstances. The presence of feature oscillations in the SVM waveform, before the fall occurrence, contribute negatively to the alignment phase which, just to remind, is

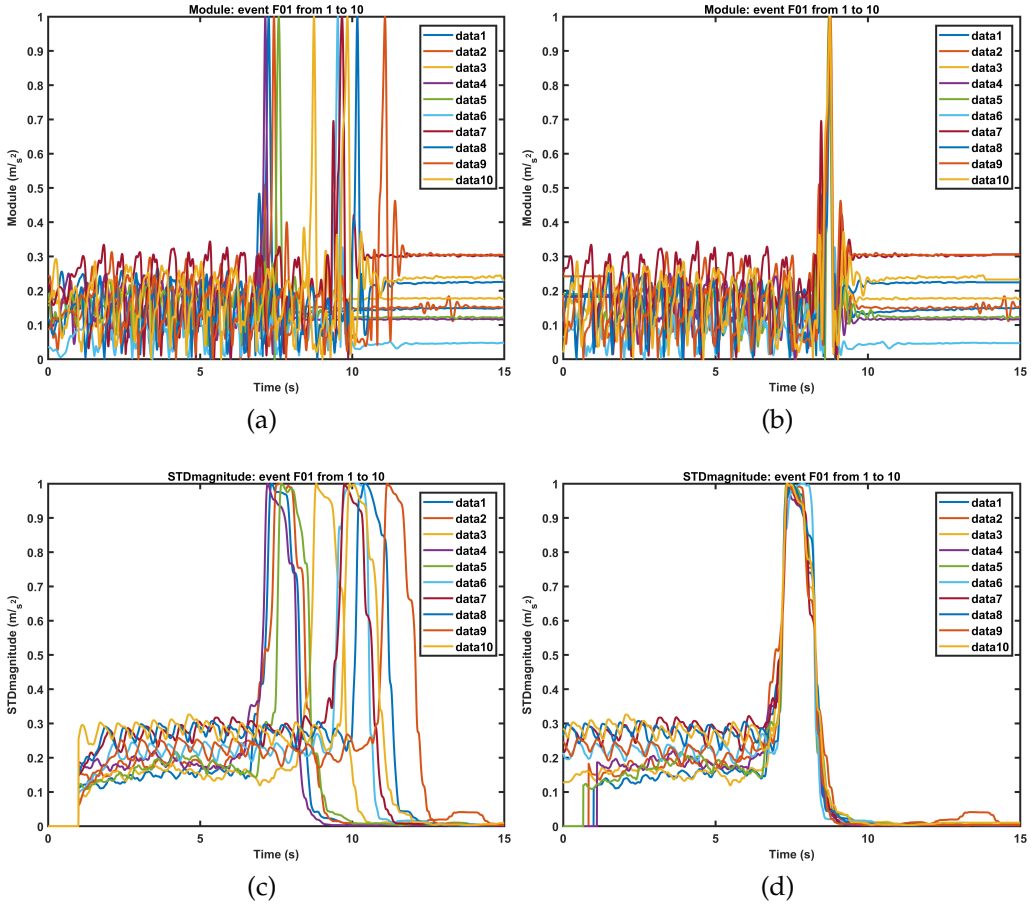

Figure 4.7: F01 signature generation process. (**a**) Misaligned SVM feature; (**b**) aligned SVM feature; (**c**) misaligned SDM feature; (**d**) aligned SDM feature.

based on the cross-correlation. The adoption of the SDM-based feature produces a signature that is less "representative" of a specific class of fall but well generalizes an entire set of possible falls. This property of "generalization" improves consistently the capability of the method to distinguish falls from ADLs.

The complete list of signatures, for a given K (K coming from the K-fold cross-validation), are shown from Figure 4.11 to Figure 4.14.

The property of "generalization" of the SDM features is now clearly

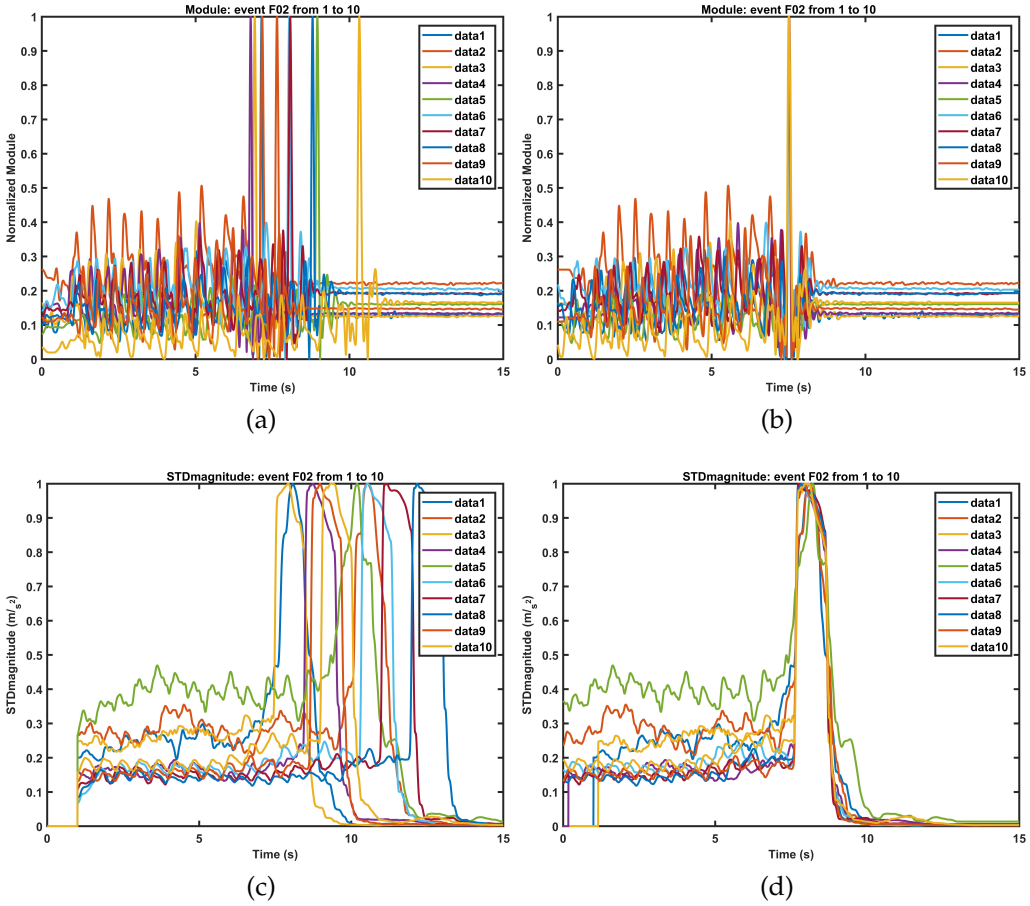

Figure 4.8: F02 signature generation process. (**a**) Misaligned SVM feature; (**b**) aligned SVM feature; (**c**) misaligned SDM feature; (**d**) aligned SDM feature.

evident. All the 15 classes of addressed falls (Figure 4.11) show similar shapes although representing different falls. Same conclusion can be drawn from the 19 classes of ADLs (Figure 4.13). Periodic events, such as jogging and walking, have basically the same signature, as well as sitting events. On the contrary, SVM features show more specific shapes (Figure 4.12 and Figure 4.14). Also, in some cases, ADLs SVM features show similar shapes to some type of falls contributing negatively during classification.

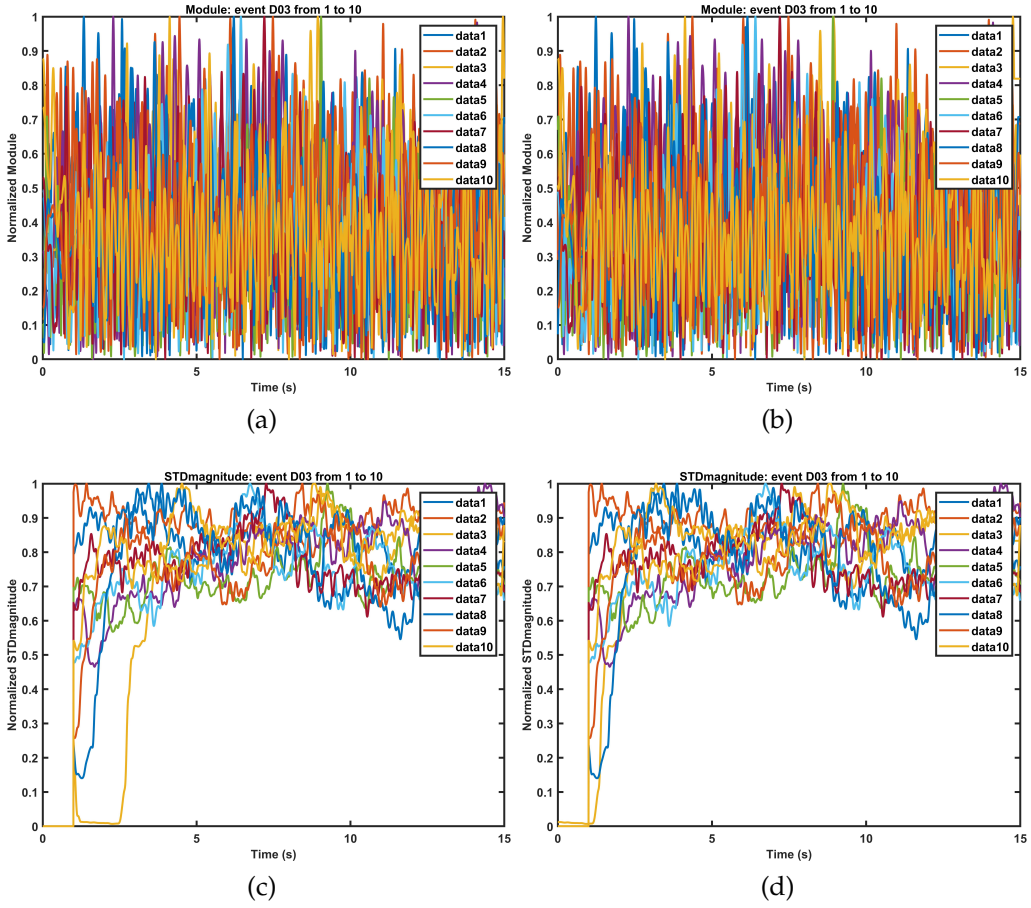

Figure 4.9: D03 signature generation process. (**a**) Misaligned SVM feature; (**b**) aligned SVM feature; (**c**) misaligned SDM feature; (**d**) aligned SDM feature.

4.2.4 Similarity Measurements and Classification

The similarity measurement is the procedure giving rise to the scores vector the classification algorithm will use. The implemented similarity measures are based on cross-correlation and DTW. In both cases, the measure outputs a single number measuring the degree of similarity between signatures and an unknown event (more specifically, the feature of the unknown event). Unlike cross-correlation, which is normalized, DTW-

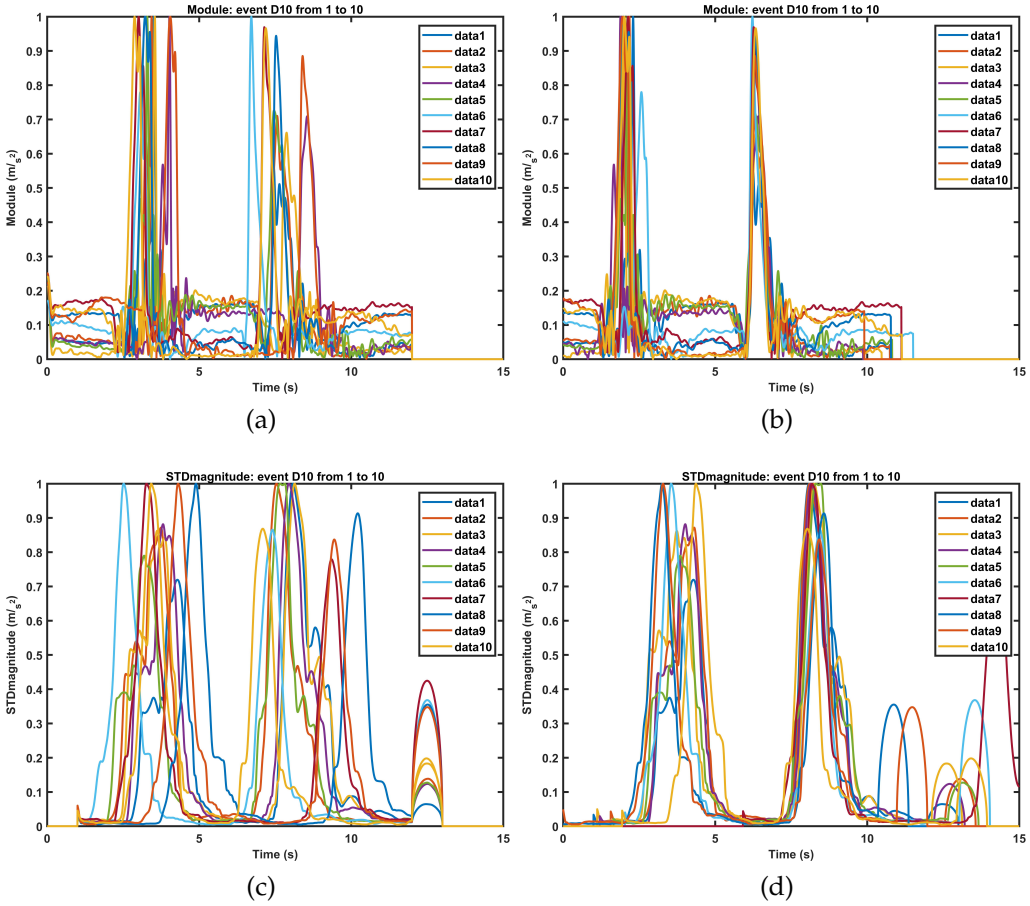

Figure 4.10: D10 signature generation process. (**a**) Misaligned SVM feature; (**b**) aligned SVM feature; (**c**) misaligned SDM feature; (**d**) aligned SDM feature.

based scores are not constrained between $[-1, 1]$ thus producing scores reaching high values. To clearly understand how both techniques work when applied to features, examples of score matrices computed either through cross-correlation (on both the SDM and SVM feature) or through DTW (on both the SDM and SVM feature) are shown from Table 4.4 to Table 4.7.

Let us focus on the SDM and SVM based scores. Under the same similarity measure, SDM-based scores produce a much clear separation

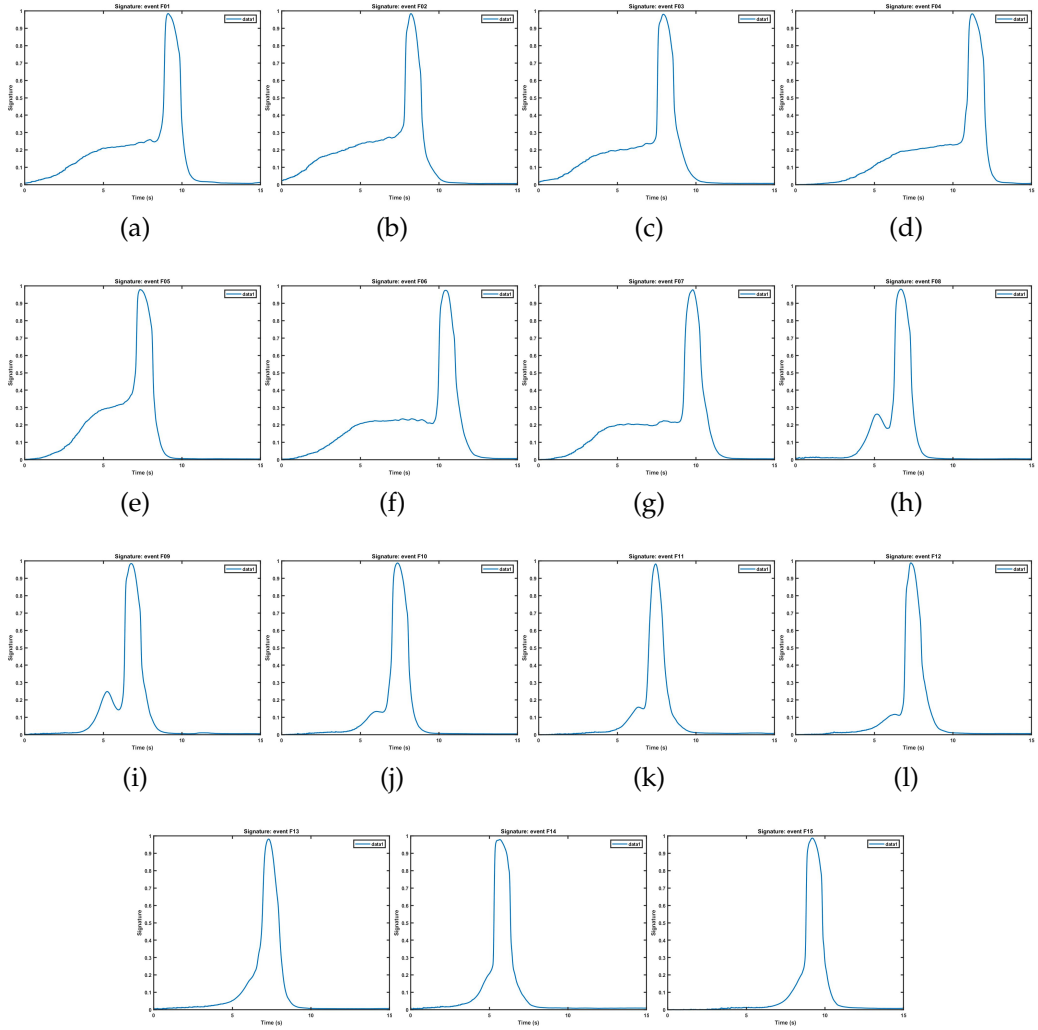

Figure 4.11: SDM-based signatures. From (**a**) to (**o**) are mapped events from F01 to F15.

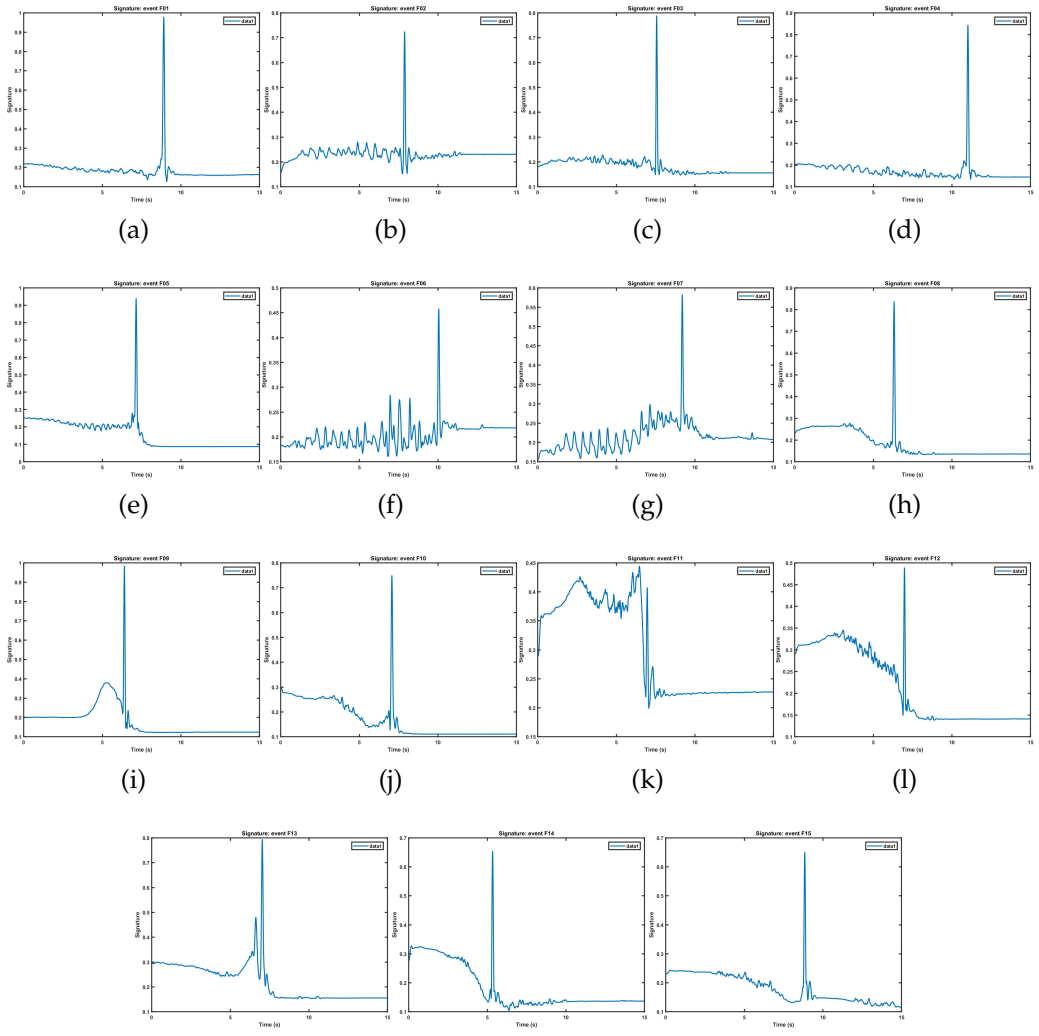

Figure 4.12: SVM-based signatures. From (**a**) to (**o**) are mapped events from F01 to F15.

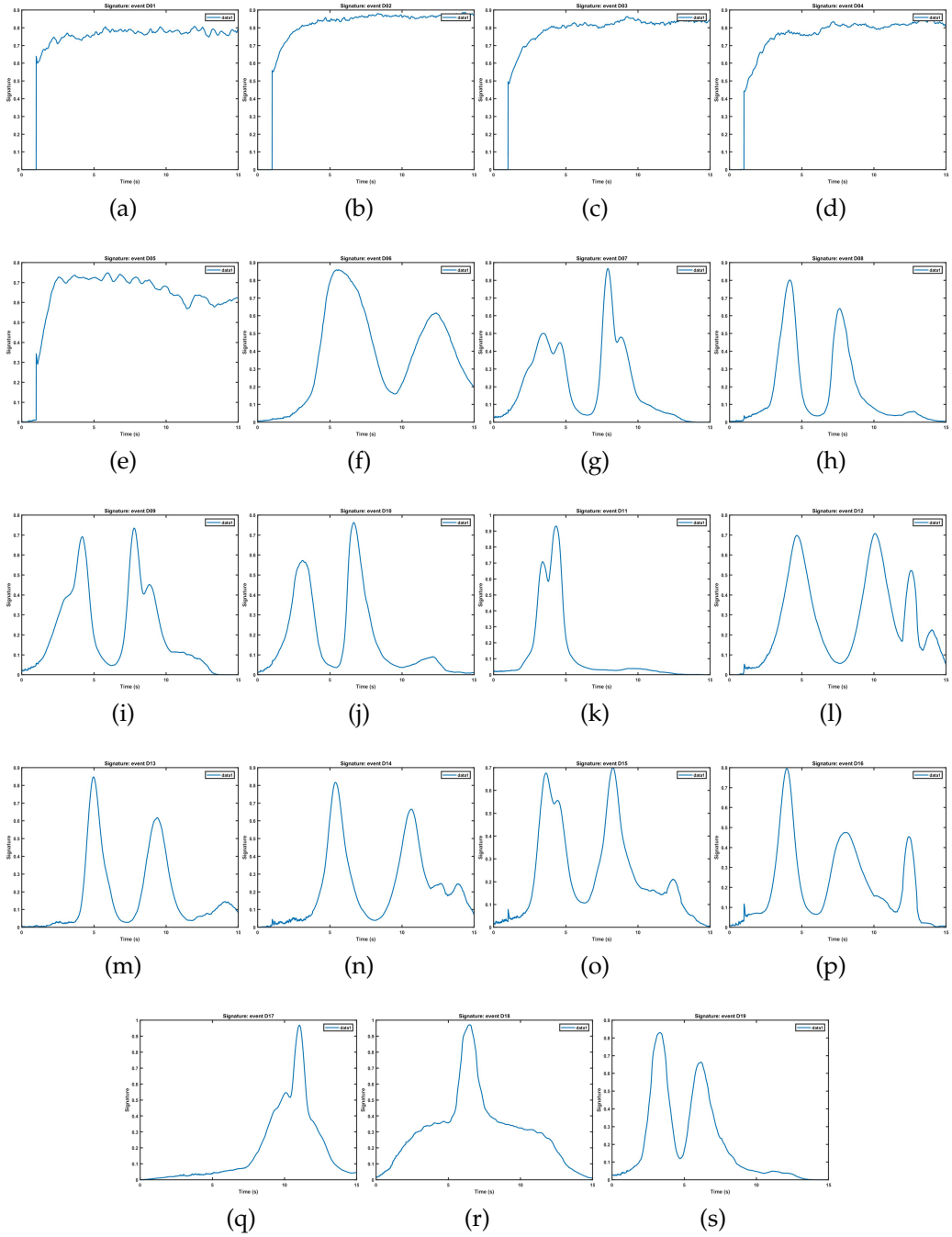

Figure 4.13: SDM-based signatures. From (**a**) to (**s**) are mapped events from D01 to D19.

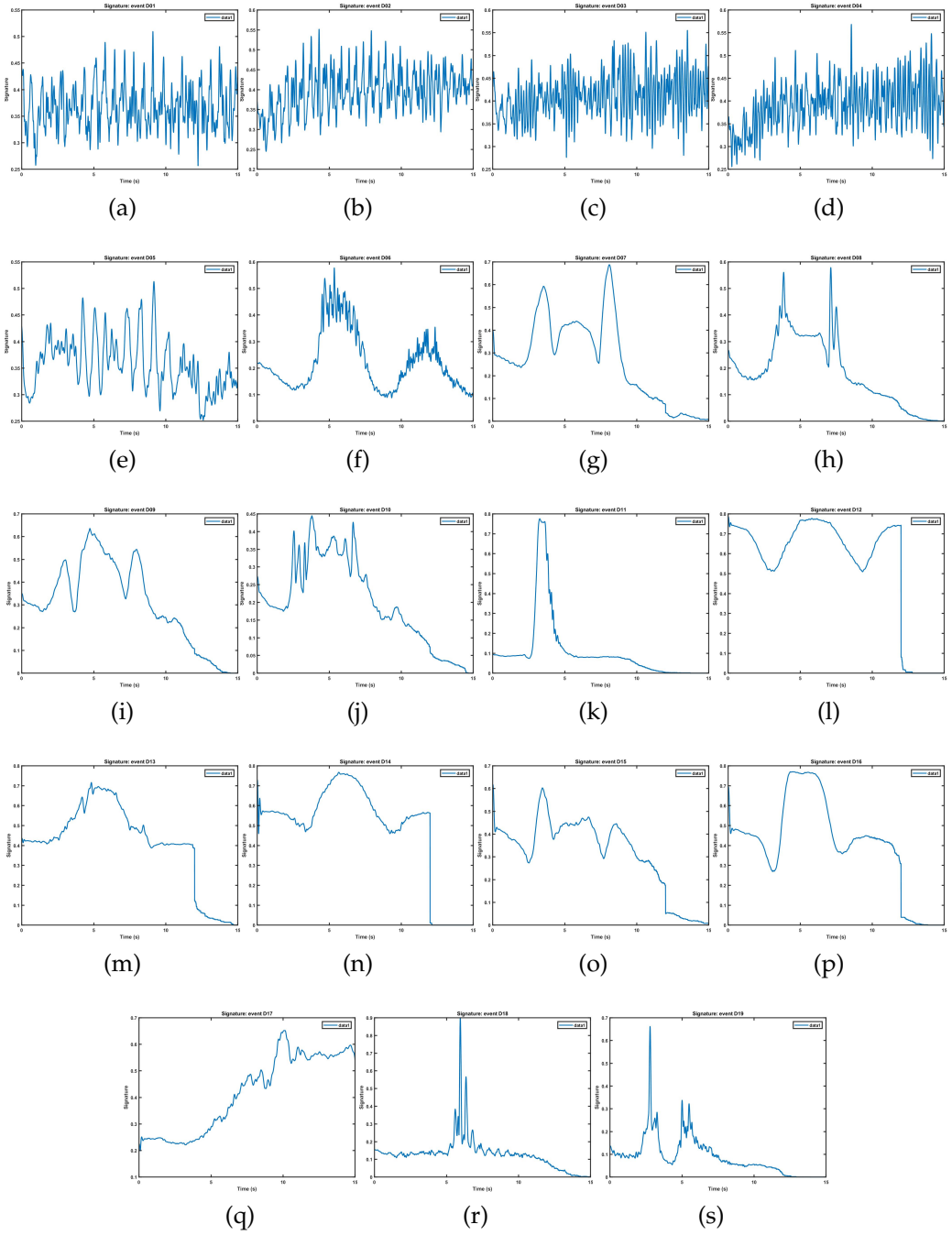

Figure 4.14: SVM-based signatures. From (**a**) to (**s**) are mapped events from D01 to D19.

between falls and ADLs. Common similarity values between falls and falls' signatures are greater than 0.9 (using cross-correlation) while between falls and ADLs' signatures are generically lower than 0.7. Similar considerations can be done in the case of DTW. This clear separation is blurred in the case of SVM-based scores.

These findings have a direct impact on the classification performances. Classification rules have been based on the type of separation the method wants to highlight:

- **Falls vs Non-Falls (C1):** we are only interested in detecting a fall, no matter the type, and be able to differentiate them from ADLs;
- **Inter-Class (C2):** we are interested in detecting a specific type of event, no its general class. If an F01 event occurs we want to be able to classify it as belonging to the F01 class. Since this represents a challenging task, classes addressed in this scenario are reduced only to falls and, specifically, to three classes of fall: FF (forward falls), BF (backward falls) and LF (lateral falls). Since most classes are representative of similar events, such as F01, F04 and F05, they have been grouped together.

Adopted classification techniques are:

- **Absolute Minima Value (AMV)**
  - DTW similarity: it assigns an unknown event to the class showing the lowest score value;
  - Cross-correlation similarity: it assigns an unknown event to the class showing the highest score value;
- **Threshold based (TA):** this introduces a level of complexity compared to the previous one. An optimal threshold is determined using the ROC curves theory.
  - DTW similarity: it assigns an unknown event to the class having a score value lower than the threshold;
  - Cross-correlation similarity: it assigns an unknown event to the class having a score value greater than the threshold;

While the AMV classifier does not require any further computation, the TH one requires the threshold definition. In case the C1 rule is used, only one threshold is required while, in case rule C2 is used, three different thresholds are needed. As depicted in Section 2.3, for the ROC curves to work, a positive and negative distribution must be defined. Both distributions have been defined taking the maximum score value row-wise using only the fall columns as shown in Table 4.8. Those are the distributions on which the thresholds have been identified for each run of the cross-validation.

Table 4.4: Example of a reduced scores matrix using the SDM feature and the cross-correlation as similarity measurement. The reported rows are just 1 single example among the n values corresponding to a given K.

	F01	F02	F03	F04	F05	F06	F07	F08	F09	F10	F11	F12	F13	F14	F15	D01	D02	...	D19
F01	0,99	0,98	0,98	0,99	0,97	0,98	0,98	0,96	0,95	0,96	0,95	0,95	0,97	0,95	0,95	0,55	0,56		0,76
F02	0,98	0,98	0,96	0,98	0,95	0,98	0,98	0,88	0,87	0,87	0,86	0,86	0,88	0,85	0,85	0,68	0,68		0,8
F03	0,98	0,98	0,97	0,98	0,94	0,99	0,98	0,9	0,89	0,89	0,88	0,88	0,89	0,88	0,88	0,64	0,64		0,77
F04	0,99	0,99	0,98	0,99	0,95	0,99	0,99	0,93	0,92	0,92	0,91	0,92	0,92	0,92	0,92	0,62	0,62		0,76
F05	0,97	0,97	0,96	0,96	0,97	0,95	0,96	0,88	0,87	0,86	0,85	0,85	0,87	0,85	0,84	0,63	0,64		0,83
F06	0,98	0,98	0,96	0,98	0,93	0,99	0,98	0,88	0,88	0,87	0,86	0,87	0,87	0,86	0,86	0,67	0,68		0,79
F07	0,97	0,97	0,96	0,97	0,93	0,98	0,98	0,91	0,9	0,9	0,89	0,9	0,9	0,89	0,89	0,63	0,63		0,74
F08	0,92	0,91	0,93	0,92	0,92	0,89	0,91	0,99	0,99	0,98	0,98	0,97	0,98	0,98	0,98	0,4	0,41		0,72
F09	0,91	0,9	0,94	0,92	0,91	0,9	0,92	0,99	0,99	0,99	0,99	0,99	0,98	0,98	0,99	0,4	0,41		0,72
F10	0,91	0,9	0,94	0,92	0,92	0,89	0,91	0,98	0,99	0,99	0,99	0,99	0,99	0,99	0,99	0,42	0,42		0,74
F11	0,94	0,94	0,96	0,95	0,94	0,94	0,95	0,98	0,98	0,98	0,99	0,98	0,98	0,97	0,97	0,5	0,5		0,75
F12	0,9	0,89	0,93	0,91	0,89	0,89	0,91	0,97	0,98	0,99	0,99	1	0,98	0,99	0,99	0,39	0,39		0,74
F13	0,92	0,91	0,93	0,93	0,93	0,89	0,91	0,98	0,97	0,99	0,98	0,97	0,99	0,98	0,98	0,42	0,42		0,75
F14	0,92	0,9	0,94	0,92	0,92	0,9	0,92	0,98	0,98	1	0,99	0,99	0,99	1	1	0,4	0,41		0,74
F15	0,91	0,91	0,93	0,92	0,93	0,88	0,91	0,97	0,96	0,97	0,96	0,95	0,98	0,97	0,97	0,44	0,44		0,74
D01	0,61	0,62	0,58	0,59	0,56	0,64	0,6	0,43	0,43	0,41	0,42	0,42	0,43	0,43	0,42	0,99	0,99		0,67
D02	0,63	0,64	0,6	0,62	0,57	0,67	0,63	0,45	0,45	0,42	0,42	0,42	0,44	0,42	0,41	1	1		0,66
...																			
D19	0,87	0,87	0,88	0,87	0,9	0,86	0,86	0,81	0,81	0,79	0,78	0,79	0,8	0,78	0,77	0,6	0,61		0,96

Table 4.5: Example of a reduced scores matrix using the SVM feature and the cross-correlation as similarity measurement. The reported rows are just 1 single example among the n values corresponding to a given K.

	F01	F02	F03	F04	F05	F06	F07	F08	F09	F10	F11	F12	F13	F14	F15	D01	D02	...	D19
F01	0,87	0,91	0,94	0,87	0,94	0,89	0,89	0,9	0,89	0,92	0,89	0,88	0,93	0,84	0,88	0,9	0,89		0,75
F02	0,91	0,96	0,94	0,91	0,87	0,95	0,96	0,89	0,88	0,88	0,92	0,89	0,92	0,86	0,91	0,96	0,96		0,77
F03	0,87	0,9	0,93	0,85	0,93	0,87	0,87	0,9	0,89	0,92	0,88	0,88	0,92	0,83	0,87	0,88	0,88		0,74
F04	0,9	0,93	0,95	0,86	0,91	0,9	0,9	0,89	0,88	0,9	0,87	0,86	0,91	0,83	0,86	0,9	0,9		0,77
F05	0,81	0,84	0,85	0,83	0,87	0,82	0,8	0,92	0,91	0,85	0,9	0,9	0,88	0,88	0,88	0,84	0,82		0,8
F06	0,9	0,97	0,96	0,91	0,89	0,95	0,94	0,89	0,88	0,89	0,91	0,88	0,92	0,86	0,9	0,95	0,95		0,73
F07	0,88	0,96	0,94	0,89	0,86	0,94	0,94	0,85	0,88	0,85	0,88	0,85	0,9	0,82	0,87	0,94	0,94		0,78
F08	0,8	0,8	0,84	0,75	0,89	0,74	0,77	0,9	0,94	0,84	0,85	0,84	0,87	0,83	0,81	0,76	0,75		0,77
F09	0,9	0,93	0,94	0,91	0,89	0,92	0,91	0,96	0,98	0,9	0,97	0,95	0,94	0,91	0,94	0,94	0,93		0,81
F10	0,84	0,86	0,88	0,86	0,87	0,84	0,81	0,92	0,9	0,92	0,92	0,95	0,89	0,93	0,91	0,86	0,85		0,8
F11	0,92	0,97	0,95	0,92	0,85	0,97	0,96	0,9	0,91	0,87	0,94	0,9	0,93	0,86	0,92	0,97	0,97		0,78
F12	0,91	0,94	0,94	0,93	0,91	0,93	0,91	0,95	0,93	0,94	0,98	0,98	0,94	0,96	0,96	0,94	0,93		0,79
F13	0,84	0,85	0,87	0,86	0,88	0,84	0,81	0,92	0,89	0,92	0,93	0,95	0,9	0,98	0,92	0,85	0,83		0,81
F14	0,87	0,9	0,93	0,87	0,94	0,89	0,88	0,93	0,88	0,95	0,9	0,92	0,93	0,88	0,89	0,89	0,88		0,75
F15	0,91	0,94	0,94	0,92	0,91	0,94	0,92	0,93	0,87	0,95	0,95	0,96	0,94	0,95	0,95	0,95	0,94		0,75
D01	0,87	0,9	0,89	0,87	0,81	0,91	0,89	0,86	0,83	0,84	0,88	0,86	0,87	0,85	0,88	0,9	0,9		0,68
D02	0,89	0,93	0,9	0,9	0,82	0,92	0,91	0,87	0,85	0,85	0,9	0,87	0,87	0,86	0,9	0,93	0,93		0,69
...																			
D19	0,68	0,65	0,69	0,62	0,73	0,6	0,65	0,74	0,72	0,69	0,71	0,73	0,72	0,74	0,68	0,61	0,62		0,83

Table 4.6: Example of a reduced scores matrix using the SDM feature and the DTW as similarity measurement. The reported rows are just 1 single example among the n values corresponding to a given K.

	F01	F02	F03	F04	F05	F06	F07	F08	F09	F10	F11	F12	F13	F14	F15	D01	D02	...	D19
F01	30,23	24	28,15	29,99	23,52	31,04	25,9	29,86	28,72	26,12	26,17	29,33	33,13	30,85	28,64	1219	1342		142,09
F02	55,62	50,75	56,82	59,71	43,23	55,34	49,35	36	40,77	52,96	48,87	57,88	51,4	47,68	45,79	1279	1388		152,3
F03	68,04	66,01	73,4	75,72	53,95	65,64	67,37	36,73	40,93	61,89	56,12	64,95	58,95	52,24	51,26	1330	1458		164,78
F04	41,08	35,85	39	42,43	38,19	38,25	34,63	28,39	23,3	40,13	37,2	43,99	45,47	39,45	38,88	1224	1335		158,56
F05	154,13	141,85	153,95	165,76	71,45	169,7	167,87	66,54	72,71	65,95	64,23	64,07	65,86	61,46	57,35	1453	1555		163,69
F06	66,27	66	69,55	73,98	67,92	71,77	66,15	44,09	44,75	72,13	63,05	74,67	70,79	60,85	61,04	1255	1365		178,41
F07	81,07	73,84	78,55	83,05	68,87	75,57	71,15	43,22	39,48	76,48	70,08	79,99	75,02	68,85	68,01	1200	1309		180,74
F08	23,88	34,29	28,92	21,23	20,06	21,43	22,18	14,67	13,66	18,83	21,33	20,85	20,61	22,75	20,94	1277	1425		151,33
F09	25,26	35,39	29,1	20,97	19,8	19,29	18,84	12,3	10,51	17,37	21,89	19,89	19,3	23,09	21,18	1231	1378		146,98
F10	11,2	17,93	13,31	8,88	9,41	8,83	9,05	6,85	10,21	7,31	9,49	8,39	8,56	10,59	8,88	1449	1629		133,74
F11	19,18	22,37	21,79	21,62	21,24	23,4	22,25	32,24	32,89	24,79	23,02	23,37	24,04	23,06	25,9	1066	1192		130,21
F12	10,97	18,15	11,67	8,76	9,91	11,02	8,63	12,63	15,13	6,58	8,19	6,61	7,53	8,39	7,57	1270	1428		131,33
F13	13,81	15,81	14,12	10,57	9,91	14,08	11,19	15,44	18,32	8,76	11,97	10,62	10,15	13,19	11,23	1362	1521		131,54
F14	10,01	20	12,79	7,48	6,68	11,08	8,19	12,48	16,04	5,81	8,58	7,37	6,98	8,21	6,8	1121	1246		137,42
F15	11,88	21,93	15,4	9,14	8,07	12,68	10,51	14,46	17,57	7,74	9,72	9,4	8,55	10,73	9,14	1136	1260		139,74
D01	1014	1151	1107	738,75	1195	880,62	926,58	1170	1135	1048	1036	1025	1067	1242	798,27	134,1	203,44		1259
D02	1163	1339	1299	820,83	1418	991,9	1062	1409	1371	1263	1259	1242	1293	1512	944,76	338,11	172,42		1691
...																			
D19	149,95	151,34	150,89	149,61	149,3	150,94	149,04	161,09	158,3	151,35	150,77	150,5	151,84	151,34	152,35	1409	1574		73,69

Table 4.7: Example of a reduced scores matrix using the SVM feature and the DTW as similarity measurement. The reported rows are just 1 single example among the n values corresponding to a given K.

	F01	F02	F03	F04	F05	F06	F07	F08	F09	F10	F11	F12	F13	F14	F15	D01	D02	...	D19
F01	68,75	178,99	60,51	56,07	132,79	149,22	145,95	74,14	88,54	109,59	297,62	140,22	133,9	109,44	71,02	428,97	476,32		249,79
F02	442,94	371,95	484,12	387,78	580,89	353,55	374,49	516,83	527,77	560,14	379,64	512,05	466,37	523,53	483,73	133,89	127,37		724,74
F03	117,37	223,95	117,27	90,92	127,81	199,08	202,48	94,56	99,56	91,55	374,97	146,86	177,12	112,03	80,14	507,21	548,19		209,17
F04	76,86	174,62	72,8	54,71	156,08	155,97	147,05	84,96	115,22	129,08	333,45	136,39	161,39	116,29	80,77	462,02	500,5		227,4
F05	156,16	248,33	155,76	143,1	103,22	254,54	250,51	120,77	102,26	78,86	298,68	137,84	155,66	119,79	92,73	458,56	537,53		203,04
F06	106,03	85,8	114,28	109,8	213,33	63,76	60,39	160,04	176,86	199,2	218,86	191	169,34	179,34	141,04	346,63	388,65		304,35
F07	141,04	75,22	160,04	128,63	251,39	69,72	67,34	189,97	210,01	225,68	163,09	211,47	206,51	200,54	176,39	291,7	337,37		346,44
F08	229,34	316,55	236,62	198,92	162,05	339,32	328,49	246,2	209,61	201,52	497,48	346,23	339,57	272,94	219,39	649,91	700,47		71,13
F09	212,22	103,26	214,61	252,38	265,84	186,71	139,1	173,34	217,51	228,48	63,29	151,15	111,57	176,88	217,3	237,41	307,4		389,37
F10	238,18	292,05	229,01	249,21	281,44	328,55	345,95	170,64	202,3	207,6	171,86	101,41	97,83	131,2	217,76	359,44	441,28		331,25
F11	601,59	530,03	666,79	560,58	725,68	628,07	554,54	638,29	685,83	715,49	584,02	725,31	594,3	679,45	642,59	282,96	244,42		867,3
F12	222,01	78,16	209,63	277,37	274,16	149,29	121,54	203,41	232,56	258,84	28,06	196,15	138,01	225,33	213,3	207	284,02		413,31
F13	180,34	273,55	193,3	181,79	151,46	307	319,02	110,14	85,88	75,57	224,32	66,22	99,03	57,75	112,53	405,49	493,62		256,29
F14	89,13	203,98	87,85	67,59	116,17	185,23	183,31	117,38	69,69	97,62	360,42	211,63	206,56	139,79	78,33	494,61	545,98		189,18
F15	423,69	334	474,31	413,29	536,69	385,91	381,42	449,11	516,72	444,89	189,24	373,44	399,07	380,51	427,87	155,69	227,55		613,97
D01	451,47	462,85	455,55	456,31	457,13	476,13	475	449,13	457,46	454,35	444,81	457,8	440,58	453,19	456,66	356,88	324		489,84
D02	540,5	548,84	549,34	553,46	598,07	621,47	561,65	573,43	590,73	606,51	594,31	597,57	525,73	583,37	580,92	525,35	463,81		676,14
...																			
D19	302,04	420,54	312,96	287,33	201,11	412,95	426,23	286,87	266,68	228,12	501,65	302,39	344,41	272,81	243,77	667,54	739,29		85,7

Table 4.8: Table showing how the positive and negative distribution have been defined. For each row, but only including scores produced by fall signatures (red values), the maximum value has been found. Maximum coming from falls rows are defined as positive distribution while maximum coming from ADLs rows as negative. The included values refers to the cross correlation similarity measurement using the SDM feature.

	F01	F02	F03	F04	F05	F06	F07	F08	F09	F10	D01	...	D09
F01	0,99	0,98	0,99	0,97	0,98	0,98	0,96	0,95	0,96	0,95	0,55		0,60
F02	0,98	0,98	0,96	0,98	0,95	0,98	0,88	0,87	0,87	0,87	0,68		0,62
D01	0,61	0,62	0,58	0,59	0,64	0,60	0,43	0,43	0,41	0,42	0,99		0,98
D09	0,62	0,61	0,61	0,57	0,59	0,60	0,63	0,60	0,58	0,58	0,98		0,99

4.3 Discussion

Before presenting the obtained results, let us provide some definitions. In case of a generic event class E, the following quantities can be defined:

- TP (true positive): events of type E correctly recognized as belonging to class E;
- FN (false negative): events of type E recognized as belonging to a class different than E;
- TN (true negative): events different from type E correctly recognized as belonging to a class different than E;
- FP (false positive): events different from type E recognized as belonging to class E.

In case the C1 rule (falls vs non-falls) is adopted for the classifier, only two classes are considered: 1) Falls and 2) ADLs. If any fall event is classified as belonging to any of the addressed fall classes, then this is a positive event classified as positive: TP. If any ADL event is classified as belonging to any of the addressed ADLs classes, then this is a negative event classified as negative: TN. If any fall event is classified as belonging to any of the addressed ADLs classes, then this is a positive event classified as negative: FN. If any ADL event is classified as belonging to any of the

addressed falls classes, then this is a negative event classified as positive: FP.

In case the C2 rules (inter-class) is adopted for the classifier, three classes are used. If an event of type x is classified as belonging to the x class, then this is a positive event classified as positive: TP. If an event different that type x is classified as belonging to any other classes than the x class, then this is a negative event classified as negative: TN. If an event of type x is classified as belonging to any other classes than the x class, then this is a positive event classified as negative: FN. If an event different that type x is classified as belonging to the x class, then this is a negative event classified as positive: FP.

Using the so calculated quantities, the following performance indexes will be used:

- Sensitivity (S_e): defined as the capability of the classifier to properly classify the events belonging to the positive distribution;

$$S_e = \frac{TP}{TP + FN} \tag{4.1}$$

- Specificity (S_p): defined as the capability of the classifier to properly classify the events belonging to the negative distribution;

$$S_p = \frac{TN}{TN + FP} \tag{4.2}$$

- Accuracy (A_c): defined as the number of correct decisions among the total number of test examples;

$$A_c = \frac{TP + TN}{TP + TN + FP + FN} \tag{4.3}$$

- F1-Score (F_1): defined as the weighted average of "precision" (the ratio of correctly predicted positive observations to the total predicted positive observations) and S_e;

$$F_1 = \frac{TP}{TP + \frac{1}{2}(FP + FN)} \tag{4.4}$$

Table 4.9: Performances of both classifiers using the cross-correlation as similarity measure (C1 rule).

Classifier ->	AMV		TH	
Feature ->	SVM	SDM	SVM	SDM
S_e	0,82	0,99	0,79	0,97
S_p	0,96	0,97	0,80	0,98
Acc	0,90	0,98	0,79	0,97
F_1	0,87	0,97	0,76	0,97

Table 4.10: Performances of both classifiers using DTW as similarity measure (C1 rule).

Classifier ->	AMV		TH	
Feature ->	SVM	SDM	SVM	SDM
S_e	0,68	0,98	0,98	0,99
S_p	0,97	0,89	0,91	0,87
Acc	0,85	0,92	0,50	0,92
F_1	0,79	0,91	0,61	0,91

It is worth recalling that, the aim of the assessment approach is to estimate the method performances in terms of reliability in fall classification.

To provide a fast and synthetic way to present the performances of the fall detector, taking into account all the discussed methods, comparative tables have been built. Starting with results coming from the C1 classification rule, Table 4.9 and Table 4.10 are provided.

Considering the C1 classification rule, independently of the adopted similarity measure, and classification type, the SDM feature always performs better than the SVM one. Moreover, the AMV classifier is generically slightly better than the TH ones, both with the cross-correlation and DTW similarity measures. However, it must be pointed out that the TH classifier can be even used with a single class of events to work (this advantage has been already explained in Section 3.2.5.2) while the AMV requires a representative list of both falls and ADLs classes. In case the method must be embedded into a physical device, this property can be

very helpful since the memory requirements can be optimized. Last, focusing on the SDM feature with the AMV classifier, the cross-correlation similarity is the one showing the highest performances.

The same analysis has been conducted for the C2 classification rule and obtained results are shown from Table 4.11 to Table 4.14.

Table 4.11: Performances of both classifiers using the SVM feature and the cross-correlation similarity measure (C2 rule)

	Classifier AMV			Classifier TH		
	FF	BF	LF	FF	BF	LF
Se	0,64	0,36	0,35	0,68	0,80	0,73
Sp	0,64	0,47	0,44	0,83	0,67	0,53
Acc	0,64	0,44	0,41	0,76	0,70	0,59
F1	0,62	0,23	0,26	0,72	0,55	0,52

Table 4.12: Performances of both classifiers using the SDM feature and the cross-correlation similarity measure (C2 rule).

	Classifier AMV			Classifier TH		
	FF	BF	LF	FF	BF	LF
Se	0,74	0,26	0,22	0,72	0,75	0,73
Sp	0,75	0,46	0,41	0,86	0,66	0,54
Acc	0,75	0,41	0,35	0,81	0,67	0,57
F1	0,72	0,17	0,17	0,79	0,51	0,51

Similarly to what previously done with the C1 rule, also in this case it is possible to highlight a proper selection of feature, similarity and classifier leading to the best possible results. In particular, once again the SDM-based feature proves to be the optimal choice along with the use of cross-correlation as similarity measure but, conversely to what obtained before, optimal results are obtained using the TH classifier. Even if performances are not as good as the one obtained using the C1 rule, although acceptable, it must pointed out that this second analysis is always

Table 4.13: Performances of both classifiers using the SVM feature and the DTW similarity measure (C2 rule).

	Classifier AMV			Classifier TH		
	FF	BF	LF	FF	BF	LF
Se	0,85	0,15	0,13	0,70	0,63	0,49
Sp	0,85	0,43	0,37	0,61	0,54	0,40
Acc	0,85	0,37	0,30	0,66	0,58	0,44
F1	0,84	0,10	0,10	0,67	0,60	0,47

Table 4.14: Performances of both classifiers using the SDM feature and the DTW similarity measure (C2 rule).

	Classifier AMV			Classifier TH		
	FF	BF	LF	FF	BF	LF
Se	0,69	0,25	0,29	0,75	0,72	0,55
Sp	0,72	0,46	0,45	0,54	0,51	0,35
Acc	0,70	0,41	0,40	0,69	0,62	0,45
F1	0,68	0,17	0,23	0,67	0,65	0,50

preceded by the first; to be more clear, once the general classification is done (fall vs non-fall) this second classification provides an additional information on the specific type of fall.

Finally, it can be affirmed that the proposed method guarantees incredible reliability and robustness in the fall detection task also when tested with common activity of daily life. Specifically, the optimal settings, which are the one made up of the SDM feature with the cross-correlation similarity measure and with both AMV and TH classifiers, are completely compliant with their integration in a low power embedded device.

Even if not discussed in this thesis, a first attempt of integration of the methodology in a low power embedded architecture, has been carried out in collaboration with the company STMicroelectronics, and published in [61]. In particular, the implemented functionalities are: SVM feature

along with a cross-correlation based similarity measurement and an AMV classifier. However, it must be specified that during that attempt, a custom made dataset has been used for testing purposes making impossible a one-to-one comparison with results obtained in this thesis. Since the aim was just to verify the feasibility of the embedded implementation, any optimization on the basis of real users' requirements has been done.

Chapter 5

Assistive Solutions for Postural Instabilities Analysis

In the introduction of this thesis, some hints on possible outcomes associate with an aging population have been given. Among them, we have seen falls, and a solution for their detection has been already proposed, and postural instabilities. Both events contribute substantially to the limitation of mobility and premature hospitalization and hence needs to be properly addressed.

Given the possible outcomes associated with postural instabilities, which are most of the time falls' precursors, solutions for their analysis and *classification* are then necessary.

Typical approaches are based on the analysis of variation of the body's Center Of Pressure (COP) in time while more advanced and specific techniques are based on the use of optical systems.

Using the COP variation in time, different features have been adopted by the scientific community to extrapolate useful information on the user postural status. Those features are totally independent from the hardware adopted for the construction of the COP.

Basically then, it must be made a distinction between the methodology for the postural analysis and the hardware (measurement system) adopted for data acquisitions.

For the sake of comprehension, an overview of the main adopted hardware and methods are proposed in the following section.

5.1 Approaches for Postural Sway Analysis - An Overview

The state of the art regarding solutions for postural analysis can be divided as a function of the hardware and signal processing solutions. Since a huge amount of methodologies are completely independent from the hardware, they are discussed separately.

5.1.1 Adopted Hardware

Hardware architectures for postural sway analysis may be divided as a function of the physical principle they use to reconstruct the COP or, more in general, the dynamics of the users while standing.

5.1.1.1 Force Platform

A first and more common solution is based on **Force Platform**.

Force platforms (Figure 5.1) measure the forces exerted by a subject during the execution of motor tasks (static and/or perturbed posture) in a fixed reference system in order to quantify balance, gait, and other biomechanical parameters. They may use different types of transducer, such as load cells, piezoelectric sensors, or capacitance gauge, to measure forces. Beyond vertical force, some force plates can measure shear forces (i.e. lateral and horizontal forces) [62].

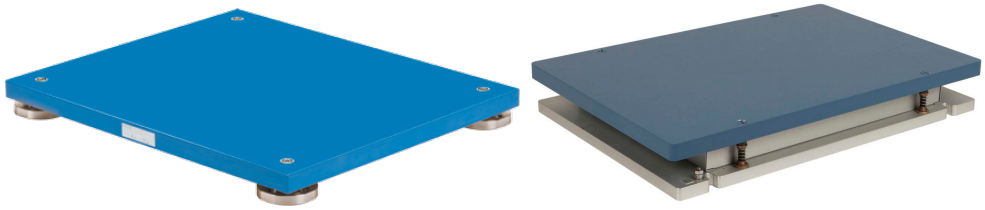

(a) (b)

Figure 5.1: Examples of two commercial force plates. (**a**) Kistler 9260AA; (**b**) A-Tech OPT400600.

Some examples of applications of force platform for postural analysis are the ones presented in [63, 64, 65, 66, 67, 68].

Although largely adopted for their capability to provide clinically precise and accurate measurements, these systems are very expensive (the actual price may depend on the number of measured components) and hence not affordable for end-users which require constant postural evaluation.

5.1.1.2 Sensorized Insoles

Measurement systems based on sensorized insoles may be differentiated according to the number and sensor's distribution inside them. The number of sensors has a direct influence on the type of analysis they can perform. As an example, we may find insoles providing a granular evaluation of the user's pressure distribution, by means of a large number of sensors (matrix), or just an evaluation of the vertical reaction forces (low number of sensors).

Advantages coming from the adoption of a large number of sensors rely on the possibility to properly analyze the plantar pressure distribution, to easily reconstruct the COP by a weighted average of the single pressure points, and to also measures the ground reaction forces.

Sensorized insoles have been widely used/developed in postural related researches [69, 70, 71, 72, 73] as much as produced by companies [74, 75, 76, 77]. Two examples of commercially available devices are shown in 5.2

5.1.1.3 Vision Systems

Visual systems are nowadays considered a Gold Standard in the area of motion analysis, with specific regards to gait analysis. This technology has been widely used in sports [78], neuroscience [79, 80], validation and control of computer vision [81] and robotics [82]. In the area of postural analysis, vision systems are always used in conjunction with other devices (force platforms, inertial systems, or similar) to have a complete motion analysis ranging from dynamical to static properties [83, 84, 85, 86].

Their working principle is based on the use of reflective markers (in

(a) (b)

Figure 5.2: Examples of two commercial senzorized insoles by (**a**) Moticon and (**b**) Retisense .

the infrared frequencies) to reconstruct users' movements, in the 3-D space, with an incredible resolution and accuracy. These systems are capable of measuring movements of the whole body; they can measure both gait and postural control, are highly accurate and precise, and hence widely used to compare new tools as well as to evaluate the benefit of therapeutic interventions (e.g., surgical procedures, pharmacological therapies, assistive devices, and exercise training programs). However, the high cost, long preparation time, and need for specialist staff to operate these systems are barriers to their wholesale adoption within routine clinical care [87]. Furthermore, even when clinically implemented, the choices regarding protocols such as different marker sets and biomechanical models, which are needed to quantify kinetics and kinematics, combined with the complexity of the outputs, can greatly influence the outcome and decisions based on the data collected [88]. That is why, very often, these systems are largely limited to research settings.

An example of commercial system produced by BTS (BTS Bioengineering) is shown in Figure 5.5 in Section 5.2.1.2

5.1.1.4 Inertial Systems

The use of wearable inertial sensors to monitor postural instability has been long recognized as a valuable and advantageous alternative to traditional solutions [89]. Examples are given in [90, 91, 92, 93, 94, 95, 96].

Since they are not yet recognized as robust clinical tools, compared with solutions based on vision or force plates, inertial solutions are often prone to validation [95, 97, 98, 99, 100].

As an example, in [95], the authors use an inertial sensor positioned on a belt and secured on the posterior trunk at the level of L5 lumbar vertebrae and the validation of the inertial solution has been performed using both a force plate and a motion capture system. Bivariate correlation analysis between data from the above systems and a study of the inertial sensor's sensitivity in case of different balance tasks have been presented.

Another is the one described in [97]. This study investigated the concurrent validity of one inertial motion sensor system (ViMove) for its ability to measure lumbar inclination motion, compared with the Vicon motion capture system. The authors found a clinically acceptable level of agreement between these two methods for measuring standing lumbar inclination motion in these two cardinal movement planes.

5.1.2 Methods

As previously stated, a primary way to clinically assess the postural status of a subject is to look at the variation of the COP in time. Classical clinical systems, such as the force platforms, or the instrumented insoles, are able to reconstruct the COP by only looking at the ground reaction forces. Systems based on vision must reconstruct the movements of the body's center of mass by kinematic models, similar to what happens in the case of inertial systems. Independently of the adopted technology a COP variation in time (an example is shown in Figure 5.3) is obtained. The COP variation in time is called **Stabilogram**. To be specific, the COP is built considering the relative variation of the Medio-Lateral (ML) and Antero-Posterior (AP) movements.

Main addressed features in the literature are the one from Equation 5.1 to Equation 5.10 [101, 102].

- Mean Velocity, defined as:

$$MV = \frac{1}{N-1} \sum_{i=1}^{N} v(i) \tag{5.1}$$

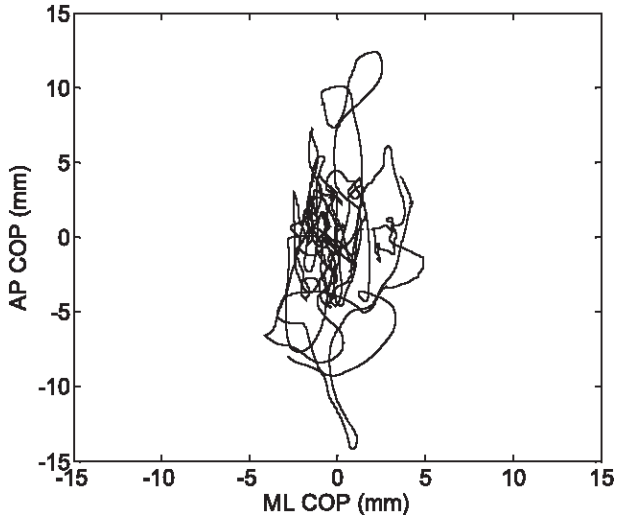

Figure 5.3: An example of a stabilogram. The x axis contains the ML displacement while the y axes the AP displacement.

which represents the average velocity of the body's center of mass. The term $v(i)$ is the instantaneous velocity defined as:

$$v(i) = \frac{|d_p(i+1) - d_p(i)|}{T} \tag{5.2}$$

where T represents the sampling period of the adopted measurement system. It basically provides information about the rate of change of the displacement, with respect to the time, without any reference to the direction of the movement;

- Rectangular area:

$$A_r = (D_{AP}^{max} - D_{AP}^{min})(D_{ML}^{max} - D_{ML}^{min}) \tag{5.3}$$

where DAP and DML are the AP displacement and ML displacement.

- Root Mean Square (RMS) displacement:

$$D_{RMS} = \sqrt{\frac{\sum_{i=1}^{N} d_p(i)^2}{N}} \tag{5.4}$$

where $d_p(i)$ represents the distance between two adjacent points on the stabilogram;

- Displacement Range of the projection of the center of mass:

$$DR = max(d_p) - min(d_p) \tag{5.5}$$

- Total Displacement:

$$TD = \sum_{i=1}^{N} |d_p(i+1) - d_p(i)| \tag{5.6}$$

- Elliptical area which includes 95% of the stabilogram plot:

$$CEA_{95\%} = \pi ab \tag{5.7}$$

where the terms a and b represent the two semi-axes of the ellipse and can be evaluated as it follows:

$$a = CSF\sigma_{AP} \tag{5.8}$$
$$b = CSF\sigma_{ML} \tag{5.9}$$

where CSF is a Confidence Scaling Factor whose value, in the case of the 95% ellipse, is 2.4477 while σ_{AP} and σ_{ML} are the standard deviations of DAP and DML, respectively, estimated by considering the dispersion of the two signals on the time windows of 10s shifted by 200ms.

- Total Power (T_P) [103]:

$$T_P = \sum_{i=1}^{N} S_x(i) \tag{5.10}$$

where S_x is the power spectral density of the COP signal.

Another interesting theory which has been applied to postural analysis is based on the Wavelet transform [104, 105, 106, 107, 108, 109] (a complete theoretical background can be found in [110, 111, 112]). This theory

has been extensively used in many scientific areas, ranging from physics studies to audio signal processing, denoising, compression/decompression, or for their ability to be localized in both time and frequency. The latter property, in particular, enable the possibility to discover non-periodic variations (i.e. abrupt changes) inside a signal, which make this theory interesting for signal processing algorithms.

As an example, in [104], the Wavelet theory is used to quantitatively analyze the postural status of a subject, comparing obtained results with control ones (obtained from healthy users), while no classification is given on the basis of that results. In [105] the wavelet theory has been exploited for the detection of the "critical point interval (CPI)" indicating a variation of the user's postural control strategy.

Wavelet theory in the context of postural analysis is hence primarily used only to quantify the subject's motor properties while final conclusions and remarks are demanded to physicians.

5.1.3 Discussion

Although brief, this review of the state of the art allows making some conclusions.

One of the first things to focus on, is the utility, or final target, of an assistive solution addressing postural instabilities. Clearly, for a solution to be really assistive, it must have a direct effect on the subjects, by increasing their safety during everyday life. For this reason, wearable solutions are the most appropriate. Although from a clinical standpoint, vision systems or force platforms are the preferred architectures, these cannot provide a direct effect on the user but can only help neurologists in assessing the user pathology in structured environments. Conversely, wearable systems, i.e inertial solutions, may provide continuous monitoring of the user's postural sway during everyday life. This is a big advantage compared to other solutions since it allows to monitor improvements/aggravations of the user status, in real-time, thus enabling the possibility to also validate pharmacological therapy and/or medical directives.

From a methodology point of view, most of the reported features have proved to have a good capability in providing an estimation of the user's

postural status. Nevertheless, since wearable solutions are the most convenient, attention must be given to power requirements. Also, the use of the Wavelet theory for the classification task, for classes such as stable and unstable, is worth to be investigated since there is a lack of researches addressing this problem.

Moreover, discussed approaches, with particular regard to the validation (assessment) of inertial solutions, mainly focus on the comparison between the proposed solution and reference systems (e.g. based on vision motion tracking solutions or on force plates) or against a clinical score [113], while any or poor attention is given to the comparison of possible classification results. The validity of the proposed approaches is, in general, assessed by using different bivariate correlation-based methodologies adopting different indexes like the Pearson and the Intraclass Correlation Coefficient (ICC).

For this reason, part of the doctoral activity has been devoted to the problem of postural analysis. In particular, two main activities will be presented: a system for postural instability analysis, with relative validation through a Gold Standard, and a Wavelet-based approach for postural classification. In the former case, features computed on top of the COP graph are used, with a consequent classification based on thresholds while, in the latter, features are built on top of the transformed signals and classified by mean of a K-Nearest Neighbour classifier.

5.2 A System for Postural Analysis

The advantages coming from the possibility to monitor the user's postural instabilities (especially in case of patients affected by neurological disorders) have been already introduced many times. This could be of extreme importance for the neurologists, to promptly intervene by refining the administered therapies, and for every elderly to evaluate the risk of falls, especially for hospitalized subjects. A continuous monitoring of the postural sway of hospitalized patients provides the experts a way to gain a lot of information on the user's pathology progression and appropriately calibrate the therapies.

Typically, clinical maneuvers for the evaluation of the motor aspects

and postural instabilities involve test such as the Timed Up and Go (TUG) [114], the Pull Test (PT) [115], and the Tandem Walk (TW) [116].

However, the assessment of the postural status via the TUG, PT and TW tests require the interaction between the user and the neurologist, and hence it may be performed at discrete times, few times per year. Moreover, some tests require dedicated laboratory space and instrumentation to be used by specialized operators. Conversely, the continuous monitoring of the patient's postural behavior while performing the daily activities would be of strategic interest for the neurologist to achieve real-time information allowing the assessment of the user status evolution.

For this reason the use of a wearable inertial sensors to monitor postural instabilities has been proposed along with main adopted features and relative assessment.

The system would act like a "Holter" for the monitoring of the user postural sway while performing the daily activities at home. In particular, the system uses a sensing device that has to be worn by the user at the chest through a belt. The device adopts an inertial sensor to monitor the postural sway along the two main directions, AP and ML. A dedicated algorithm has been developed to extract a class of features from the stabilogram plot, obtained by combining the measured AP and ML displacements, useful for the assessment of postural behavior through a dedicated signal processing.

Two main advantages of the proposed methodology can be highlighted:

1. The possibility for neurologists to continuously monitor the patient's postural behavior while performing the daily activities;

2. No need for neither structured environments, such as dedicated laboratories and set up, nor specialized operators.

5.2.1 The Inertial Systems

As introduced, this activity aims to realize a reliable solution for the continuous monitoring of the user postural sway. In this scenario, both the measurement system and methodology need to be accurately tested.

Dealing with a wearable device, measurements and methods are strictly dependent and hence need to be assessed together.

The assessment phase is based on the results' comparison between the wearable inertial system, which will run the signal processing algorithm, and a reference system (or Gold Standard). The same methodology is applied to data acquired with both systems and results are compared.

Both system are now introduced.

5.2.1.1 Wearable Inertial Measurement System

The realized prototype is shown in Figure 5.4a. It is equipped with a low-power 3-axis digital accelerometer (Analog Devices ADXL345) set at ± 2 g with a full resolution of 10 bit and a sensitivity of 256 LSB/g. A microcontroller (Arduino Pro Mini exploiting an Atmel ATMega328P microcontroller at 8 MHz) has been adopted to acquire data from the accelerometer by the Inter-Integrated Circuit, I2C, protocol through the native Two Wire Interface (TWI).

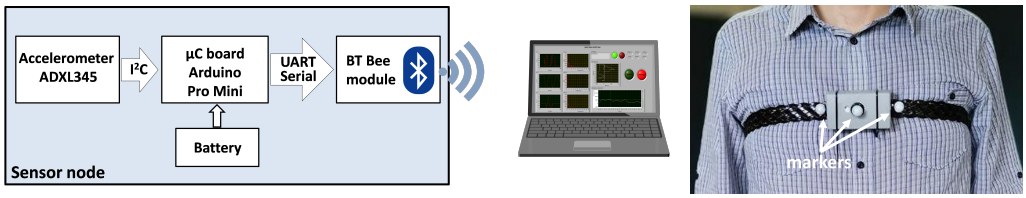

(a) (b)

Figure 5.4: (**a**) Schematization of the user node (IEEE, 2019). (**b**) The lab-scale prototype of the sensor node worn by the user with the reflecting markers used for the trajectories reconstruction by the reference motion capture system.

To speed up the development and debug of both the system and methodology, data is acquired and transmitted to a PC running a dedicated NI LabVIEW Virtual Instrument (VI) implementing the methodology.

The communication between the node and the PC takes place by a Bluetooth (BT) connection. Data from the accelerometer is acquired with a sampling frequency of 40 Hz and transmitted via BT. The device is powered by a rechargeable 3.7 V Lithium Polymer (LiPo) battery with a

capacity of 1400 mAh. The sensor node embeds also the battery charging unit. As shown in Figure 5.4b, the node must be worn tightly on the chest through a belt.

It should be pointed out that, to evaluate the inertial system reliability in quantifying postural instability in both clinical settings and home environments, the validation of the inertial sensor node by using a reference standard is mandatory.

5.2.1.2 Reference System: the Gold Standard

Experiments aimed at the assessment of the inertial system have been performed in the Gait Analysis facilities of the University Hospital Policlinico of Catania, Italy, through the system for motion analysis BTS GAIT-LAB (BTS Bioengineering) representing the gold standard in this domain. The reference system, shown in Figure 5.5, integrates a high precision SMART-DX 6000 Optoelectronic System and a sensorized floor.

For the validation, only the optoelectronic system has been used. The system adopts 6 infrared digital cameras with a maximum resolution of 2.2 Mpixel, an acquisition frequency at the maximum resolution of 340 fps and an accuracy lower than 0.1 mm in the monitoring volume of 4x3x3 m^3. During tests, images have been acquired with a frequency of 100 Hz. The volume monitored by the reference system has been defined, during the calibration phase, following the procedure indicated by the manufacturer. In particular, a volume of 4x1.5x3 m^3 has been considered which refers to the central part of the carpet, as shown in Figure 5.5. The system accuracy, estimated by accomplishing the calibration procedure, is better than 0.1 mm. This result is compliant with the information reported by the manufacturer.

The system reconstructs the 3D trajectories of passive markers reflecting the infrared light radiated by the illuminators placed on the cameras. During experiments, three markers have been placed on the sensor node (shown in Figure 5.4b). Data from the optoelectronic system have been acquired and pre-processed by using the BTS Smart Capture, BTS Smart-Tracker and BTS Smart-Analyzer tools which allows the management of the process of system calibration, data acquisition and motion analysis. The reconstructed displacements of the sensor node have been then ex-

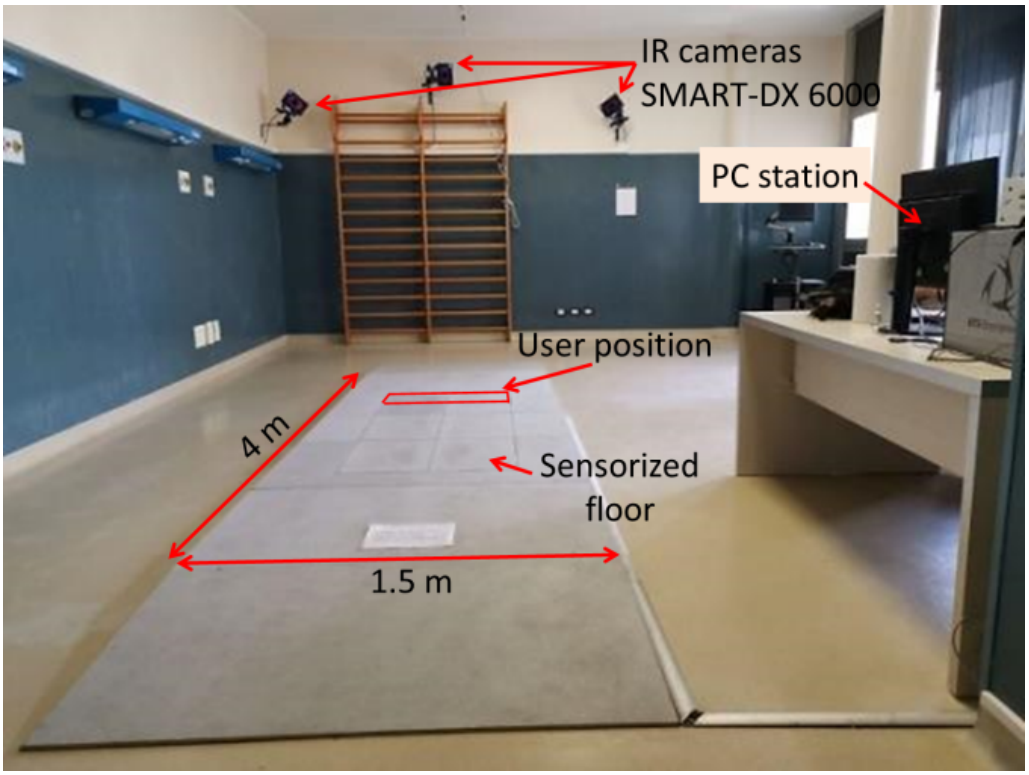

Figure 5.5: The reference system Smart-DX (BTS Bioengineering) installed in the Gait Analysis Lab of the University Hospital Policlinico of Catania, Italy, used for the sensor node assessment.

ported in text files for post-processing.

5.2.1.3 Synchronization Between Systems

To synchronize both systems, during the assessment phase, a trigger event has been expressly generated at the beginning of each trial asking the user to move the trunk up and down. The evaluation of the features from data acquired by the worn device starts at the end of such an event. In particular, the end of the variation of the position of the marker along the vertical direction has been then used as a starting point to process, offline, the data acquired from the reference system.

Nevertheless, it should be considered that the comparison between the

two systems has been performed by comparing features extracted from the two related stabilograms which make this approach quite insensitive to slight time mis-synchronization between the two systems.

5.2.2 Features for Postural Analysis

The adopted methodology for the continuous postural behavior monitoring uses inertial data from the sensor node to reconstruct the movements of the user's trunk in the two main directions: AP and ML. The displacements, DAP and DML, are then combined to reconstruct the trajectories (stabilogram) of the sensor node's center of mass. An example of obtained displacements, in both AP and ML directions, are shown in Figure 5.7.

The methodology is based on a clinically validated theory, typically applied to COP reconstructed by means of force platforms, where users' COP variation has been evaluated projecting the body's center of mass under the feet while the user maintains an upright posture [117].

It must be highlighted that postural sway should be assessed during the static posture of the user and hence the effects of dynamics introduced by the daily activities performed by the user, such as walking, must be properly considered and removed.

With the aim to perform continuous monitoring with fast detection of the instability dynamics, a continuous data processing has been developed in order to compute a suitable set of features on time windows of 10s shifted by 200ms one to each other. The selected time window is in line with the state of the art [101, 102, 118], while the window overlap has been defined empirically by observing the system behavior for time shifts belonging to [25, 500] ms. The adopted value does not introduce a significant delay: a 200ms shift has been observed to represent a good compromise between the computational demanding and the need for a continuous postural sway monitoring, without affecting a reliable detection of potentially unstable dynamics.

To assess the user postural behavior a set of features has been extracted from the stabilogram plots. To such aim, the filtered accelerations measured by the sensor node are used to estimate the user's chest angular

displacements, θ_{pitch} and θ_{roll}:

$$\theta_{pitch} = arctg\left(\frac{a_z}{\sqrt{a_y^2 + a_z^2}}\right) \tag{5.11}$$

$$\theta_{roll} = arctg\left(\frac{a_y}{\sqrt{a_x^2 + a_z^2}}\right) \tag{5.12}$$

and then AP and ML displacements, DAP and DML, respectively, as follows:

$$D_{AP} = H_1 tan\left(\theta_{pitch}\right) \tag{5.13}$$

$$D_{ML} = H_2 tan\left(\theta_{roll}\right) \tag{5.14}$$

where: a_x, a_y and a_z are the accelerations along the x, y and z axes of the reference system, in line with the ones of the inertial system (as shown in Figure 5.6), H_1 and H_2 are the height of the sensor node with respect to the user's ankles and waist, respectively.

Stabilograms, related to the reference system, are reconstructed from the measured displacements of the reflective marker. In addition to DAP and DML, main features considered in the present work, which have been extracted from the stabilogram plots, are the one introduced in Equation 5.1 to Equation 5.9.

The above features have been selected among others available because of their simplicity which make them suitable to be easily implemented on a microcontroller platform.

5.2.3 Experimental Assessment

The experimental assessment is extremely important to quantify the quality of the adopted solution and for identifying features that maximize its performance. Each of the features previously introduced has been used and compared along with the others. In the following, some details regarding users and obtained features' values are given.

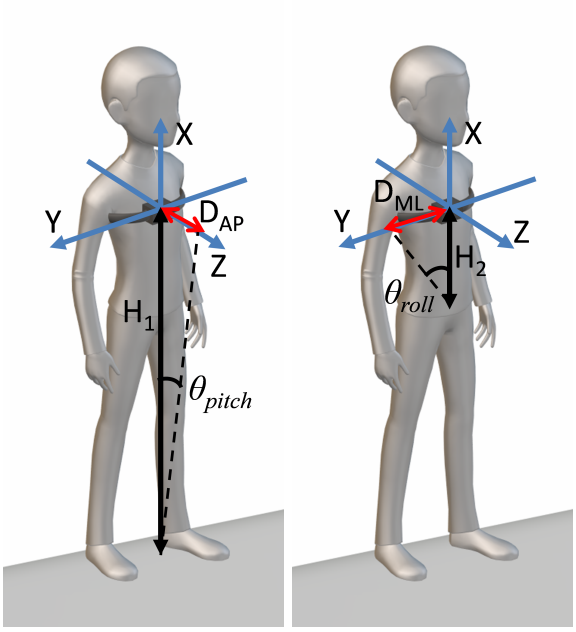

(a) (b)

Figure 5.6: The reference system adopted for the evaluation of the user's chest AP (**a**) and ML (**b**) displacements.

5.2.3.1 Users Involved

The assessment has been conducted with subjects having age in the range of [23, 60] years with an average age of 34 years. The height of participants ranged between 1.62 and 1.89 m, with a mean value of 1.73 m. In this first phase of the system assessment, users in good health conditions have been involved. It is worth noting that, although results reported in this work are related to a set of "healthy" users miming instability dynamics under the supervision of the neurologists, the main targets of this activity deal with fundamental and mandatory steps aimed at investigating both the wearable unit and the classification methodology, as well as the definition of a performance index rating the reliability of the classification outcome. All the above investigations are mandatory before conducting experiments with real users. Moreover, the involvement of real patients in the assessment of the continuous postural sway monitoring

strategy with instability dynamics requires a long procedure of approval by the hospital's ethics committee and the recruitment of patients with their manifestation of consent.

5.2.3.2 Experimental Rules

The users have been requested to worn the sensor node with the reflective markers attached and perform different trials, standing still and simulating typical postural instabilities in the AP or/and ML directions, observed in real unstable patients. To this aim, non-physician participants were instructed by neurologists which have supervised all trials.

Features have been evaluated on data with a time length of 60 s. To this aim, a first calibration phase of the inertial system is performed to evaluate the offset on the output voltage of each axis by asking the user to stand still upright maintaining the balance for 10 s. The raw acceleration data were then filtered with a band-pass filter in the range [0.01, 0.60] Hz to remove the higher frequency dynamics not attributable to the chest sway due to the postural instability. The filter has been empirically defined by observing the acceleration signals, in the frequency domain, and selecting the range of frequencies which allows reconstructing a stabilogram showing similar trajectories to the one obtained by the reference system with compatible displacement ranges (in both AP and ML directions). In particular, data from the accelerometer have been filtered through a zero-phase digital filtering process aimed to preserve the signal characteristics using a 2^{nd} order band-pass Butterworth Infinite Impulse Response (IIR) digital filter. In order to properly design the filter, the spectral contents of acquired signals has been analysed, leading to a frequency band of [0.01, 0.6] Hz. The obtained results are shown in Figure 5.7.

A total of 48 trials have been considered valid for the sake of system performance assessment.

5.2.3.3 Discussion

For each trial, features have been computed by the stabilograms reconstructed from data provided by both the inertial and the reference system.

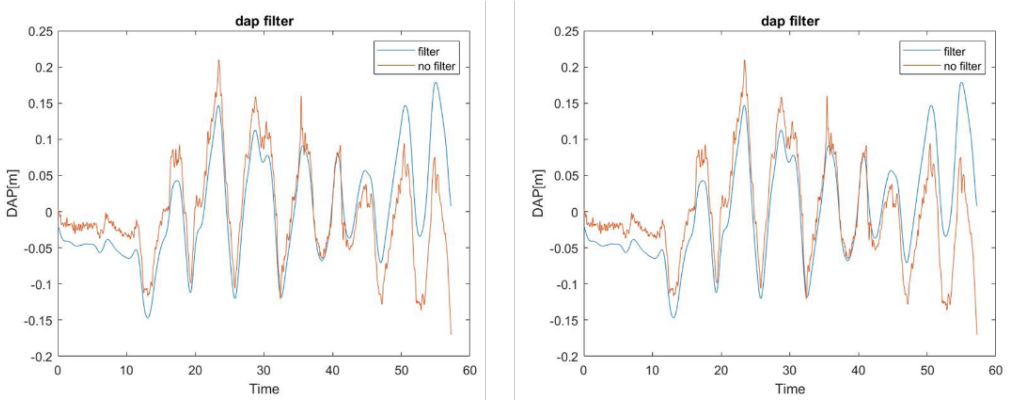

Figure 5.7: DAP and DML distances before and after the filtering process. Both distances are obtained using an unstable case.

Figure 5.8 shows the values of features evaluated for each trial for both the inertial (left column) and the reference system (right column). For clarity, trials have been organized in classes of simulated dynamics (stable behavior, AP or ML instabilities, as well as a combination of AP-ML dynamics) as indicated in Figure 5.8a. The cases of stable postural behaviors and unstable postural behaviors have been represented by different markers, in order to highlight the possibility to adopt a threshold-based methodology for the classification between stable and unstable.

It should be observed that differences in the absolute value of the features, estimated by the two systems, are due to the different methodologies (one from optical signals and one from accelerations) adopted to reconstruct the user dynamics. As can be observed by the results presented in Figure 5.8, trends estimated by the wearable and the reference systems, in terms of clustering stable and unstable behaviors, agree.

The features values, or scores, can now be given as input to the classifier.

5.2.4 The Postural Classification

As introduced for the fall detection methodology, one of the easiest classification techniques one can realize in the case of a low-power embedded device is based on thresholds.

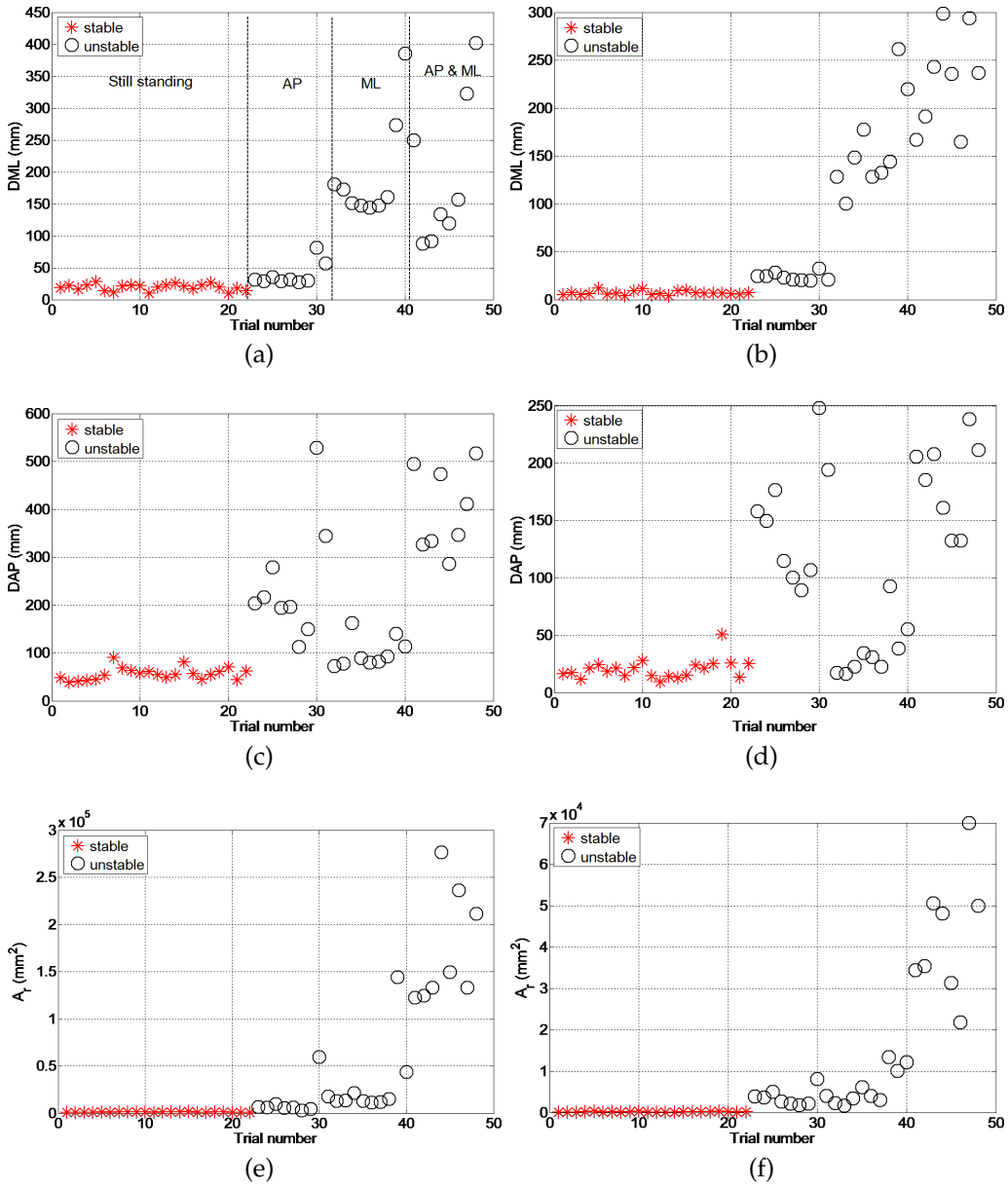
stable
unstable
Still standing
AP
ML
AP & ML
DML (mm)
DAP (mm)
Trial number
(a)
(b)
(c)
(d)
(e)
(f)

Figure 5.8

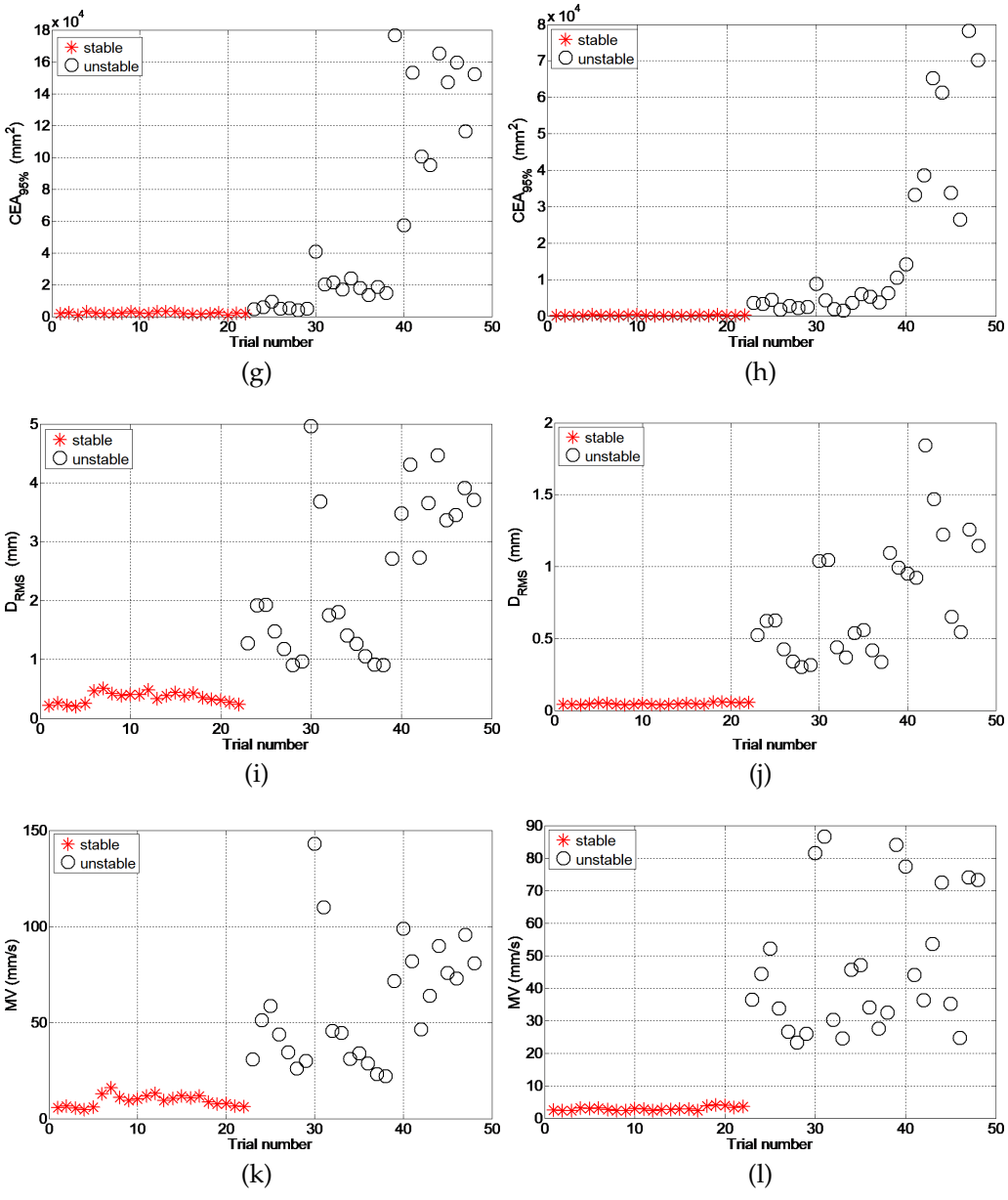
x 10^4
stable
unstable
CEA95% (mm2)
Trial number
(g)
x 10^4
stable
unstable
CEA95% (mm2)
Trial number
(h)
stable
unstable
DRMS (mm)
Trial number
(i)
stable
unstable
DRMS (mm)
Trial number
(j)
stable
unstable
MV (mm/s)
Trial number
(k)
stable
unstable
MV (mm/s)
Trial number
(l)

Figure 5.8

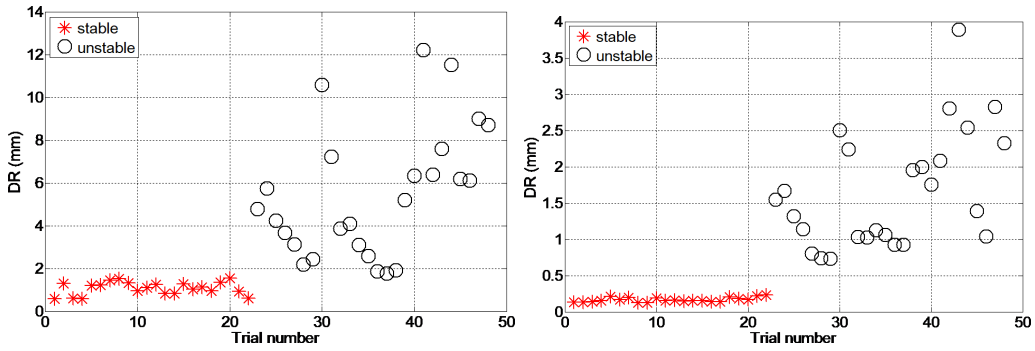

(m) (n)

Figure 5.8: The values of the features evaluated for each trial for both the inertial (left column) and the reference system (right column).

To implement a threshold-based classification strategy, optimal threshold values, for each of the considered features, have been defined by the Receiver Operating Characteristic (ROC) theory (see Section 2.3 for more details) where TP, TN, FP and FN, have been defined using the following rule: a TP if a stable case is classified as stable, a TN if an unstable case is classified as unstable, a FP if a stable case is classified as unstable and a FN if an unstable case is classified as stable.

The optimal threshold value has been estimated adopting an analytical approach searching for the minimum distance, d, between the upper left corner, having coordinates $(0, 1)$ and the points on the ROC curve [113]:

$$\min_{d} d = \sqrt{(1 - TPR)^2 + FPR^2} \tag{5.15}$$

where TPR and FPR represent the True Positive Rate (Sensitivity) and the False Positive Rate (1-Specificity), respectively. The so computed thresholds, J_{th}, for each of the considered features are given in Table 5.1.

Features have been compared with thresholds thus obtaining a set of binary features, $J_{f,bin}$, where the symbols 0 and 1 have been used to indicate that the value of the considered feature, for the specific trial, is lower or higher than the threshold, respectively. Just as a reference, two examples of obtained binary features for the DAP and DML features are shown in Figure 5.9.

Table 5.1: Optimal estimated thresholds for the considered features for both the inertial and the reference systems.

Index	Optimal Threshold	
	Inertial Device	BTS SMART DX
DAP	70.96 mm	29.66 mm
DML	28.33 mm	14.27 mm
Ar	2397.20 mm^2	513.11 mm^2
CEA	3586.70 mm^2	894.32 mm^2
RMS	0.75 m	0.06 m
MV	19.02 mm/s	4.68 mm/s
DR	1.67 mm	0.25 mm

Subsequently, to have a synthetic index for the postural behavior classification (where classes are stable and unstable) the average value of the binary features, $\overline{J_{f,bin}}$, for each trial, has been computed. The adopted rule for the sake of classification considers as belonging to the class of unstable behaviors the trials showing at least 50% of features with values higher than the respective thresholds.

It should be observed that DAP and DML features are very specific for instabilities along the AP and ML directions, respectively. Specifically, the DAP binary feature is 0 in the case of instabilities only in the ML direction

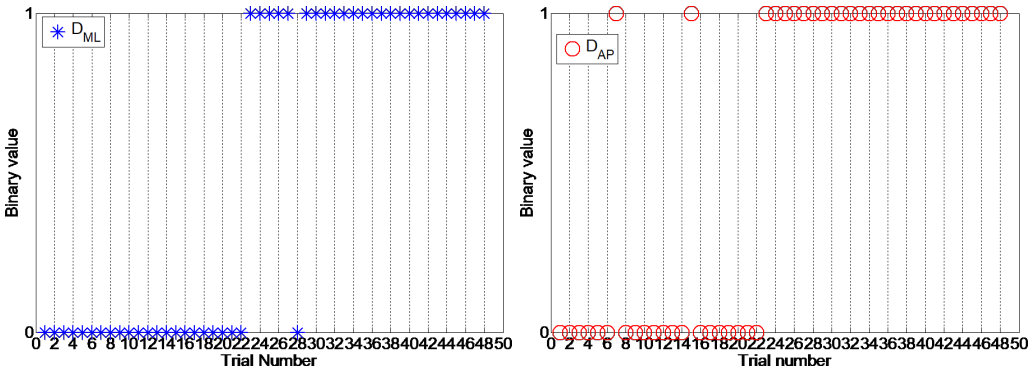

(a) (b)

Figure 5.9: Two examples of binary features. **(a)** DML and **(b)** DAP.

and vice-versa, which could lead to misclassification. Consequently, these two indexes have been combined by a logic OR operator before evaluating the average binary index.

By comparing the average binary index with the 0.5 threshold, the following stability index, J_s, has been defined:

$$J_s = \begin{cases} 0 & \overline{J_{f,bin}} < 0.5 \\ 1 & \overline{J_{f,bin}} > 0.5 \end{cases} \tag{5.16}$$

The behavior of J_s, estimated for the inertial device, is shown in Figure 5.10, where the predicted postural behavior is compared with the a priori knowledge of users dynamics recorded during the trials. As it clearly emerges the classification task performs very well. In order to assess the

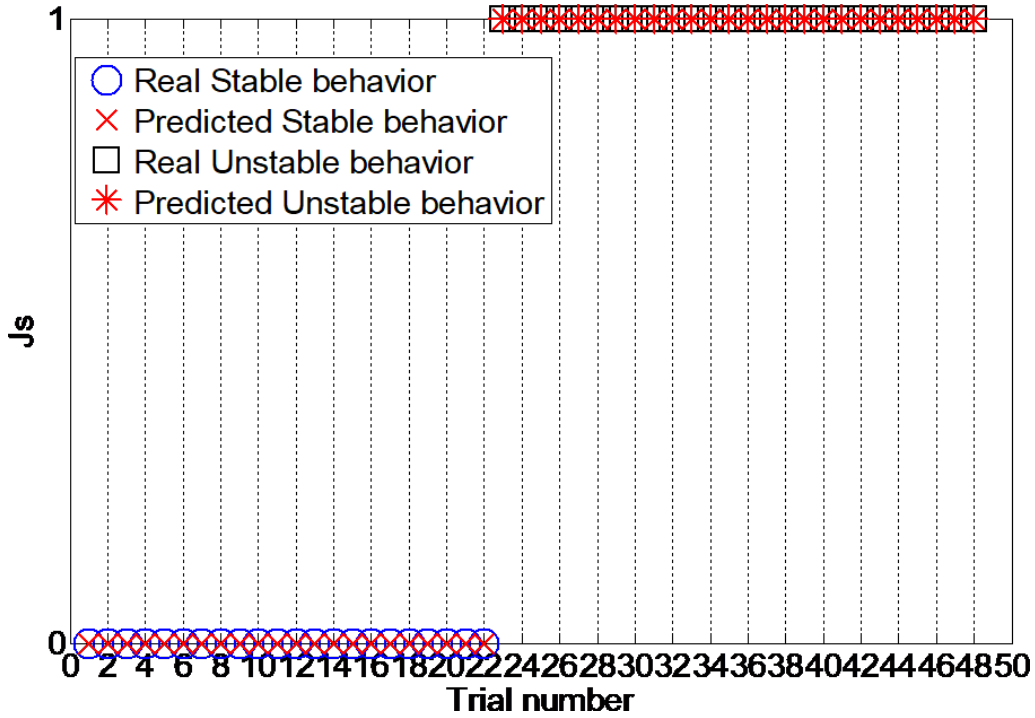

Figure 5.10: The index J_s, estimated for the inertial device. The predicted postural behavior is compared with the a priori knowledge of users dynamics recorded during the trials.

classification performance the following index can be adopted:

$$J_c\% = 100\left(1 - \frac{1}{N}\sum_{i=1}^{N}(J_{s,i} - J_k)\right) \tag{5.17}$$

where N is the number of trials and J_k is the binary array of the a priori knowledge of user dynamics recorded during the trials. The above index evaluates the percentage normalized error of the proposed strategy in performing the classification task. In particular, the higher is the value of the above index, the higher is the performance of the classification methodology with $Jc\% = 100$ in case all the trials have been correctly classified.

As can be observed, full classification success has been obtained. Once again, although results are related to a set of "healthy" users, it should be considered that the main target of this activity is the development of a methodology for the assessment of the continuous postural sway monitoring strategy, concerning both the wearable unit and the classification methodology, as well as the definition of a performance index rating the reliability of the classification outcome.

5.2.4.1 Reliability of the Classification Outcome

To rate the quality of the classification outcome, a reliability index, RI, has been defined as schematized in Figure 5.11. It is important to underline that, being RI aimed to rate the reliability of the classification outcome, in this case, the a priori knowledge about the user dynamic cannot be exploited.

The procedure starts by evaluating, for each trial, the normalized distance, J_F, between features J_f, and the related optimal thresholds J_{th}. J_F is an array where each element (one per each considered feature) provides an estimation of the feature robustness in performing the classification task.

Consequently, the vector J_p is built as the product by the J_F and $J_{f,bin}$ for each of the addressed features. In case of n number of features, the J_p vector is of size $1 \times n$. It must be recalled that, since DAP and DML features are very specific, an OR operation could be necessary: if both

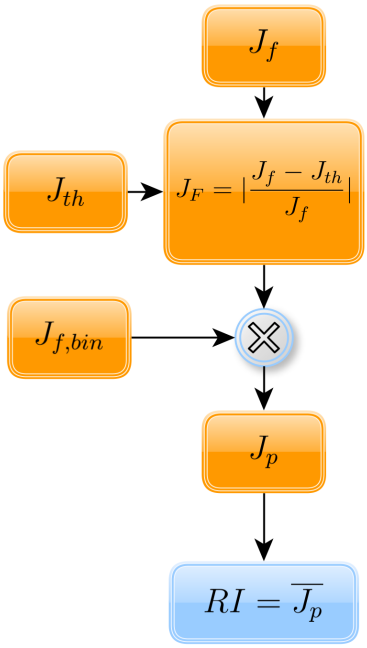

Figure 5.11: The processing algorithm aimed at the evaluation of the reliability index, RI.

binary features are equal then their average is computed otherwise the OR operation is done.

An index of reliability, RI, for each trial, can be obtained by averaging values in J_p:

$$RI\% = 100\overline{J_p} \tag{5.18}$$

This index aims to define a "quality index", associated with the classification results, in order to evaluate the reliability of the information provided by each specific test. This performance index is useful to declare the "rate of truth" of each pattern classified as stable or unstable. This could be an interesting information for a neurologist in order to assess the reliability of the specific test (not of the methodology).

Figure 5.12a shows the RI index obtained for the wearable device while, the RI index evaluated for the reference system, is shown in Figure 5.12b. It is easy to see that results obtained from the investigated system are consistent with information provided by the reference system thus

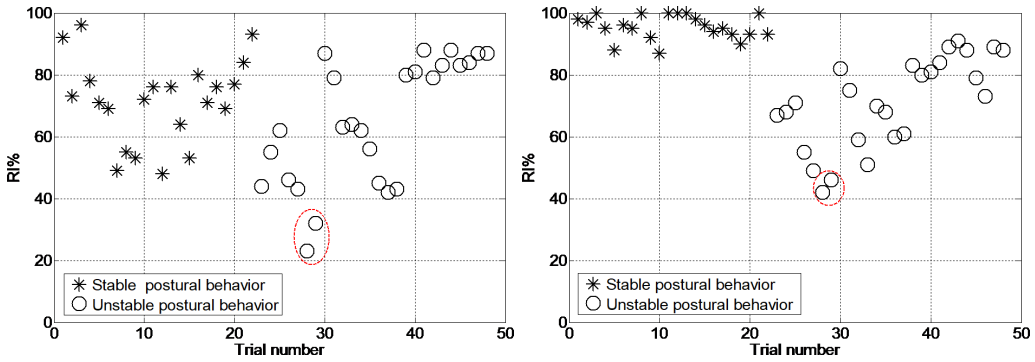

Figure 5.12: The reliability index, RI, obtained for **(a)** the wearable device, **(b)** the reference system.

confirm the viability of the proposed approach.

As can be observed by results shown in Figure 5.12, the RI index assumes high values for many of the test patterns, while for some cases, values in the range $[40, 60]\%$ have been achieved. Overall estimation of the reliability of the proposed approach can be evaluated by averaging the RI for the set of trials considered through this work obtaining average reliability of about 70% for the classification outcomes. The latter result states that some of the performed postural sway observations (showing a low value of the reliability index) merit to be repeated or extended.

As it emerges, two trials (specifically two cases of instabilities along the AP direction), highlighted in Figure 5.12a, show a lower value of the RI index: 0.23 and 0.32, respectively. The same two trials show lower values of RI also for the reference system as indicated in Figure 5.12b. Using a graphical representation of the considered trials in a DAP vs DML plot, as shown in Figure 5.13a, it easily emerges that the two trials with lower RI reside at the very close border of the stability region. The stability region has been represented as a circle including all the trials with stable dynamics and radius equal to the maximum estimated value of the displacement along the AP and ML directions. For the sake of comparison, the same plot for the reference system is shown in Figure 5.13b. It is possible to observe that results obtained from both the two

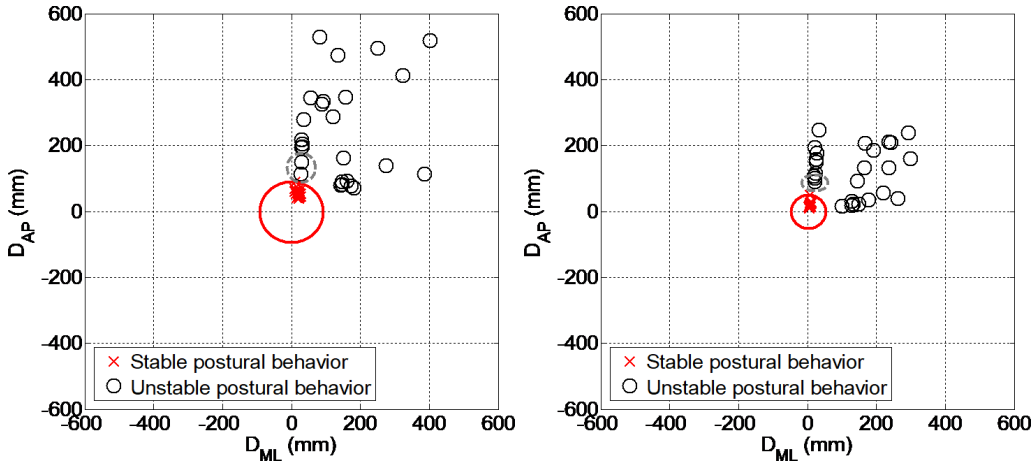

Figure 5.13: Scatter plot of the DAP vs DML for **(a)** the wearable device and **(b)** the reference system.

systems are clustered in a similar way and that the two considered trials are at the border area between the stability and instability zones.

It is worth to underline that, considering the reliability of the classification outcome, a comparison with the state of the art is not easy to be performed. In fact, from what emerges from a literature search, available papers addressing the problem of postural instability monitoring through the use of inertial devices mainly focus on the comparison between the proposed solution and reference systems (e.g. based on vision motion tracking solutions or on force-plates) or against a clinical score [113]. The validity of the proposed approach is, in general, assessed by using different bivariate correlation-based methodologies adopting different indexes like the Pearson and the Intraclass Correlation Coefficient (ICC).

Assessment approaches reported in the literature mainly aim to compare the trajectories of the user body reconstructed with the proposed solution with that measured by the reference system. The reliability index (Equation 5.18) proposed through this work is intended to define a "quality index" associated with the classification output and aimed to evaluate its reliability.

Finally, it should be considered that the solution presented in this

work does not claim to replace traditional high-cost solutions aimed at the clinic postural instability assessment but to support the neurologist with information about postural dynamics of the monitored patient while performing the normal activities of the daily living. Such information is now not available to the neurologist. In this perspective, although the proposed solution needs further investigations, the obtained results are very encouraging.

5.2.5 Conclusions

The main target of the solution proposed was to realize an automatic real-time wearable device aimed at the continuous monitoring of the user's postural behavior while performing daily activities. The device could be of strategic interest for the physicians to gain continuous information on the user pathology or its progression/ regression as a consequence of the pharmacological therapy or the rehabilitation tasks.

The sensing node could also be considered a node of a network of assistive devices installed at home or in care facilities, aimed at the monitoring and assistance of the user to improve his quality of life. In particular, the work primarily focused at the experimental assessment of the device by using a gold standard addressing the following novel aspects, which represent also a valuable advancement concerning solutions proposed in the State of the Art:

- The methodology developed for the classification of stable and unstable postural behaviors;
- The experimental assessment of the device;
- The assessment of the postural sway monitoring strategy;
- The definition of a performance index rating the reliability of the classification outcome.

Results shows the possibility to use the inertial device for the monitoring of postural sway and the developed classification algorithm, based on the evaluation of a set of features obtained from the stabilogram plots, with good performances. In particular, in the case addressed through this

work a full classification success has been obtained with overall reliability of about 70%.

Future efforts would be dedicated to the assessment of the device performance with a larger number of tests involving also real patients affected by postural instabilities. Moreover, while in this phase data processing and classification are in charge of a tool developed in LabVIEW, efforts to implement the processing algorithm on board of the wearable node are in progress.

5.3 A Wavelet-Based Approach to Postural Classification

In the brief review of the state of the art has been shown that there is a growing interest in the use of metrics based on frequency analysis and non-linear tools [119, 120]. This growing interest is mainly due to research suggesting that increased CoP movements do not necessarily indicate an impending postural destabilization [121, 122, 123]. Therefore, alternative measures may be useful to reliably characterize postural sway. To address the limitations coming from the linear measures of sway (that only examine the magnitude of postural movements), studies have started to use time-dependent non-linear measures to analyze CoP data with interesting results [124, 125, 126, 127]. Although non-linear time-dependent measures have proven to be a valuable tool in assessing the health of the postural system they do not provide information regarding specific body reactions involved in the postural control [108].

Wavelet decomposition, since can examine many different timescales at different time instants, may provide useful results to identify changes in posture control, due to aging or disease, leading to metrics enabling a more robust way to classify postural status. Since pieces of information on the posture control are hidden in different timescales, the DWT is adopted for the proposed methodology.

In this Section, the DWT is exploited on the COP signals to evaluate postural instability during quiet standing.

5.3.1 Proposed Methodology

A general overview of the proposed method is given in Figure 5.14.

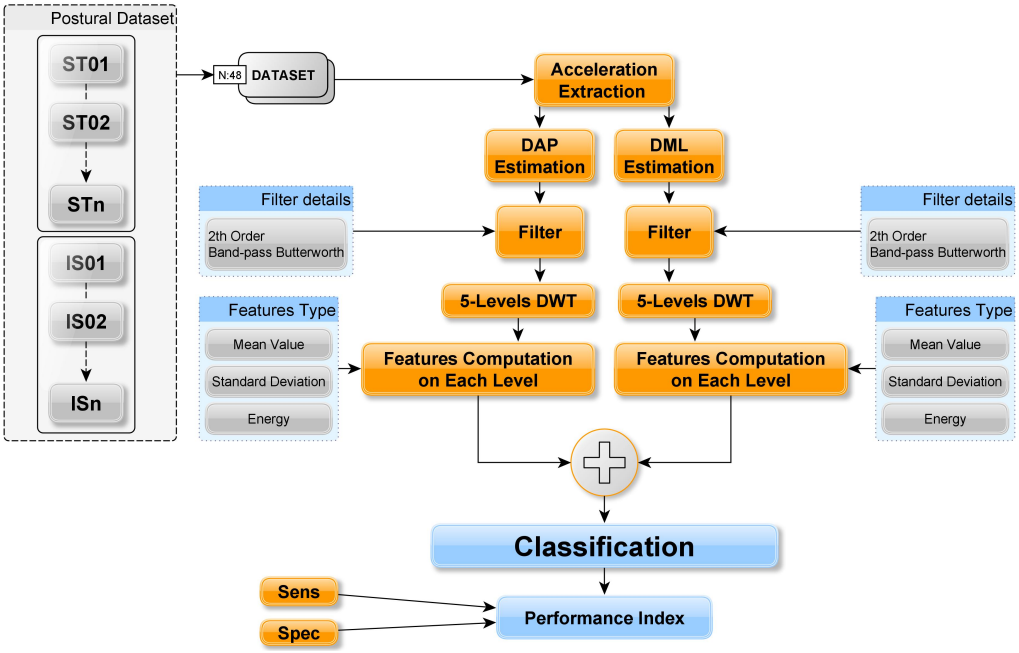

Figure 5.14: General structure of the wavelet-based methodology.

Since public dataset for postural instabilities researches are not yet available, the dataset acquired in Section 5.2.3 has been also used for the validation of this methodology. To be specific, during the experimental assessment presented in Section 5.2.3 only a subset of the entire acquisitions has been used; some of the acquisitions were discarded due to a synchronization issue between the reference system and the inertial one. Since no validation with a reference system is addressed in this section, the entire dataset can be used. It is made of 72 acquisitions divided into 28 stable cases (ST) and 44 unstable cases (IS) acquired by subjects having age in the range of [23, 60] years with an average age of 34 years. The height of participants ranged between 1.62 and 1.89 m, with a mean value of 1.73 m.

After the extraction of the acceleration components and relative filtering, the DAP and DML distances are computed as shown in Section

5.2.2.

Now, the DWT is applied to the just calculated DAP and DML distances; the DWT can be only computed on time-dependent function and hence can be only used on the single directions (AP or ML) rather than the entire stabilogram. In particular, a 5-level DWT is used.

Using each level of the transformation, 3 different features, namely Mean Value (MV), Standard Deviation (STD), and Energy (E) content have been used; these features are computed in both the transformed DML and DAP distances. Giving the wavelet transform $T(a,b) = \int_{-\infty}^{+\infty} x(t)\psi_{a,b}(t)dt$, where $x(t)$ represents the time series data and $\psi_{a,b}(t)$ represents a wavelet at timescale t_a and time instant b, features are defined as follow:

$$MV(a) = \frac{1}{K(a)} \sum_{k=0}^{K(a)} T(a,k) \tag{5.19}$$

$$STD(a) = \sqrt{\frac{1}{K(a)-1} \sum_{k=0}^{K(a)} (T(a,k) - MV(a))^2} \tag{5.20}$$

$$E(a) = \sum_{k=0}^{K(a)} T(a,k)^2 \tag{5.21}$$

at timescale a and K number of samples in the transformed signal.

Since we are interested in a complete evaluation of the user's postural status, i.e. in both in the AP and ML directions, the obtained features are added one by one; as an example, the STD of the transformed DML is added along with the STD of the transformed DAP. The final result of this procedure is the creation of a score matrix that will later be passed to the classifier (see Section 5.3.3 for more details).

Finally, some indexes are computed to evaluate the classification performances of the classifier.

5.3.2 Obtained Results

An example of a result coming from the DAP and DML computation of an unstable case, with relative filtering, has been already presented in Figure 5.7.

Starting from the filtered DAP and DML distances, the 5-level DWT is computed for both stable and unstable cases. Two examples of relative output, for a stable and an unstable case, are presented in Figure 5.15 and Figure 5.16 respectively.

It can be noticed how the Wavelet Coefficients (WCs) have greater amplitude for lower frequencies (detail WCs d5, d4, and d3) than for higher (detail WCs d2 and d1); this result is directly reflected on the computed features that consequently will show bigger value for those WCs having a higher amplitude and lower for the WCs having smaller amplitude.

Since obtained features cannot be all graphically represented, just two examples will be provided, representing respectively, features' value for a specific user in case of stable and unstable postural sway simulations (Figure 5.17). Once again, although users are simulating postural instabilities, these have been validated by neurologists which constantly overviewed the entire acquisitions.

As previously introduced, all the features show higher value in the case of d_3, d_4, and d_5. It must be specified that, at this point of the analysis, features computed on the transformed DAP and DML distances have been already summed together. That is why, since detail WCs d_1 and d_2 do not contribute substantially compared with the others, these levels are then neglected in the remaining consideration.

An aspect that deserves to be pointed out, relies on the nomenclature reported in Figure 5.17. In case of instabilities, the figure uses the name IS, AP and ML; although we are always addressing postural instabilities, different names have been given to differentiate instabilities which have been simulated in a preferential direction (AP or ML) or not (both AP and ML). A consequence of a preferential direction in the simulation of the instability has to do with the amplitude of the values of the features which are lower than what it could be obtainable in case of instabilities simulated in all directions. Nevertheless, all the addressed instabilities are considered as belonging to a single class throughout the analysis.

Finally, all computed features for each of the 72 simulations, are compared together in Figure 5.18.

Figure 5.18 allows to make the following conclusion: any clear separation can be highlighted just looking at one single feature, no matter

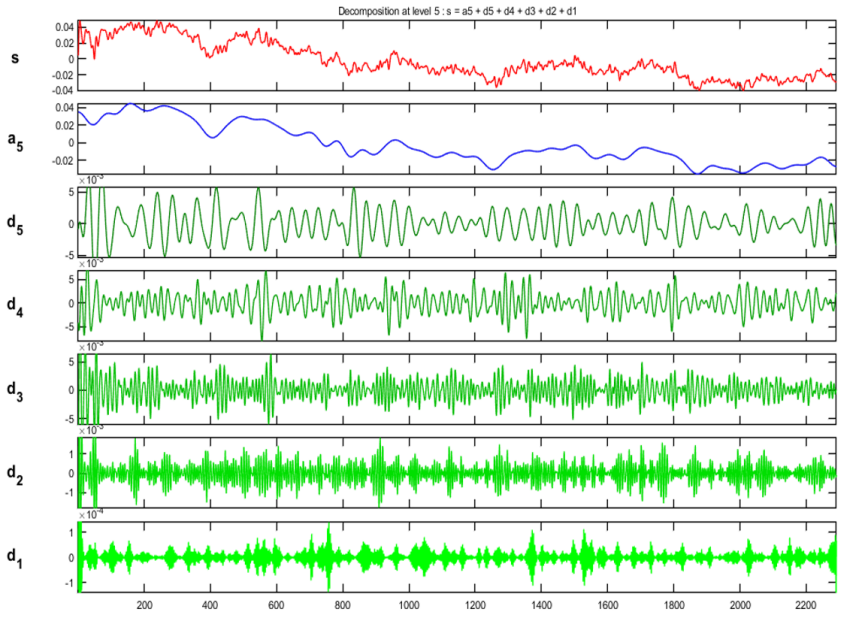

(a)

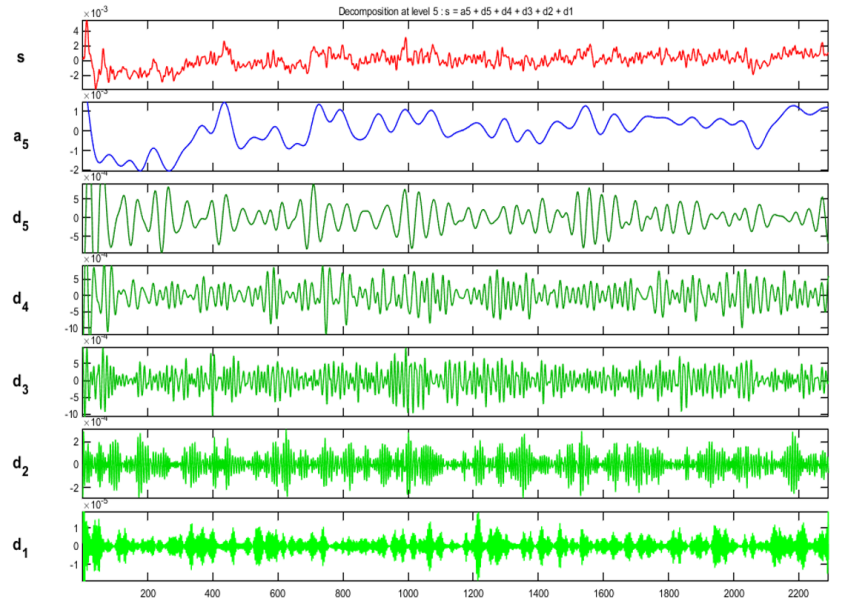

(b)

Figure 5.15: 5-level DWT for both DAP **(a)** and DML **(b)** distances in case of a stable case.

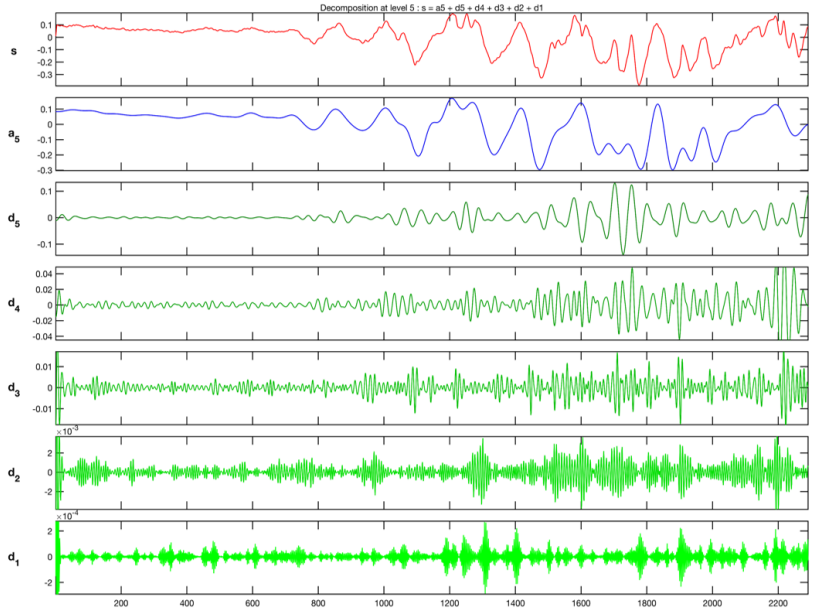

(a)

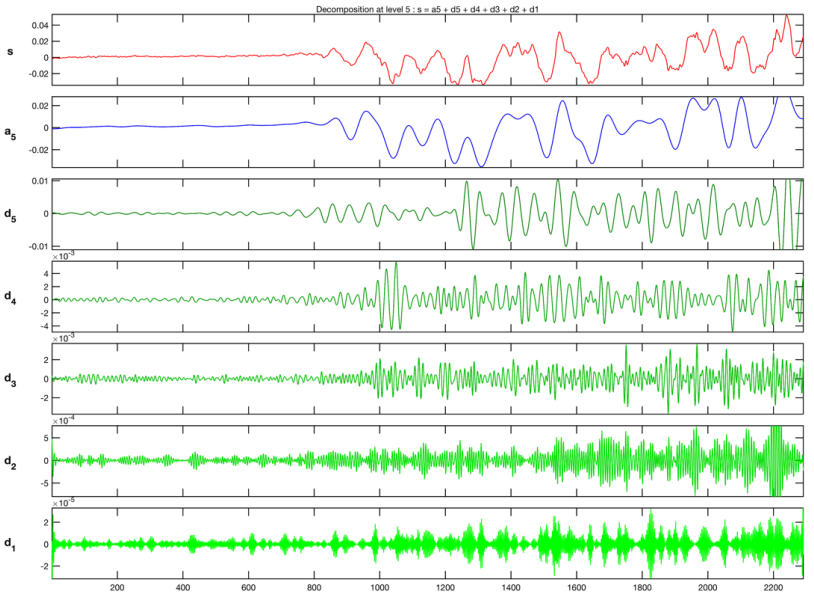

(b)

Figure 5.16: 5-level DWT for both DAP **(a)** and DML **(b)** distances in case of an unstable case.

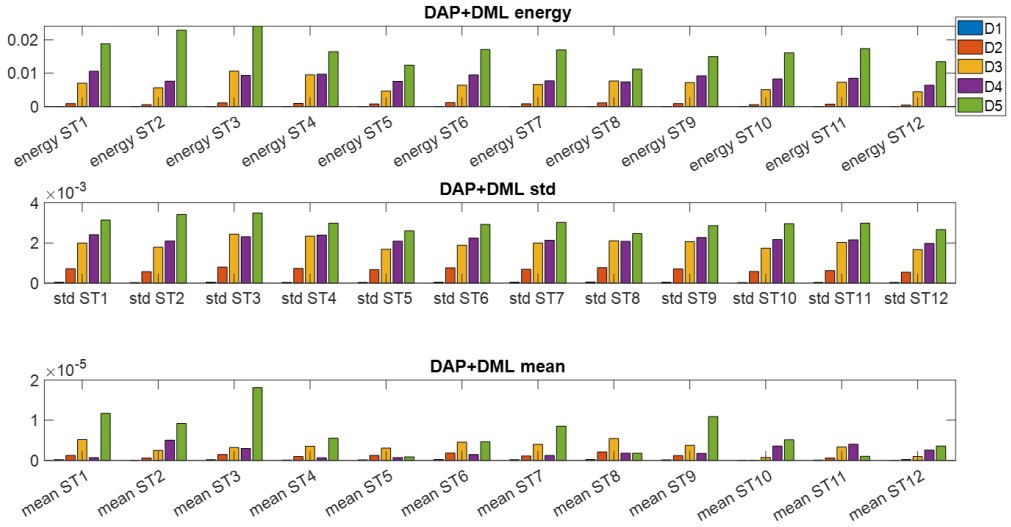

(a)

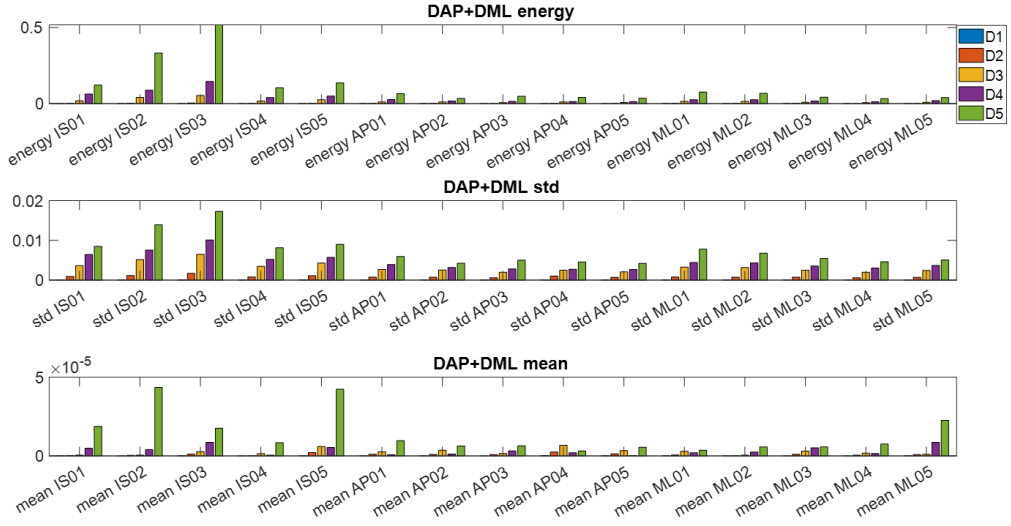

(b)

Figure 5.17: Bar plot of the DAP + DML features for **(a)** stable simulations and **(b)** unstable simulations.

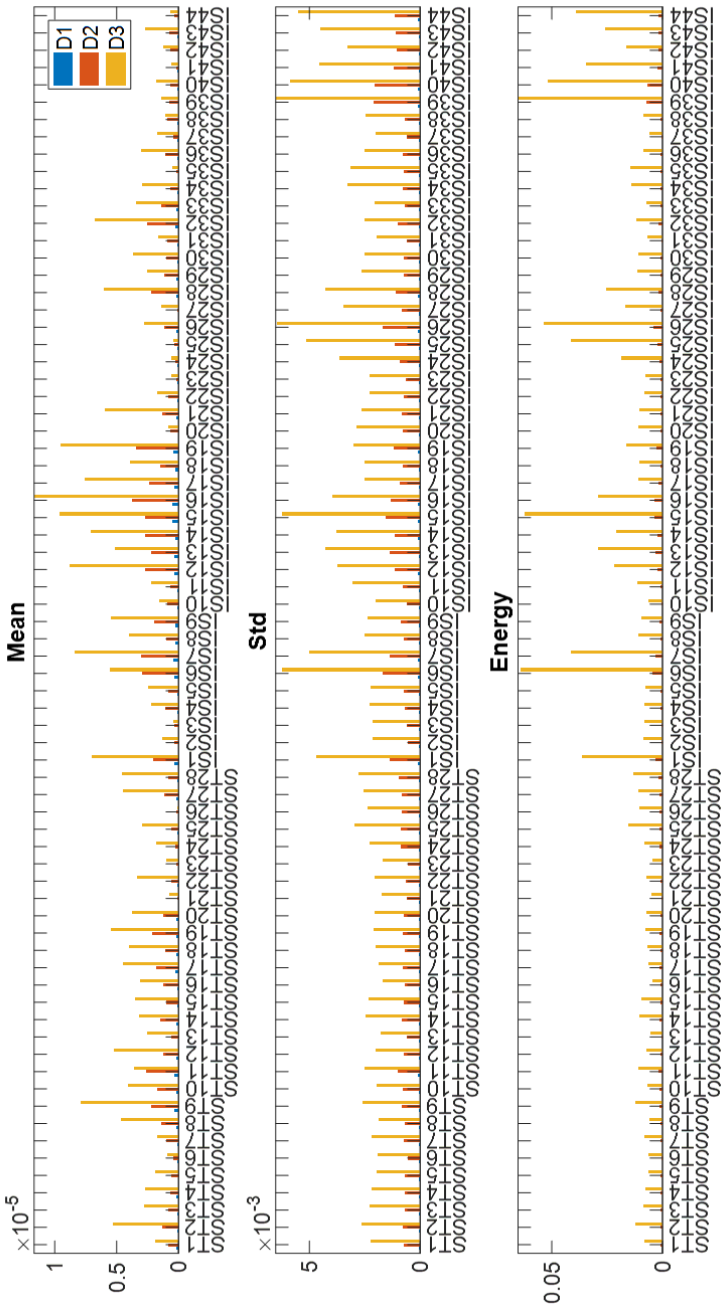

Figure 5.18: Computed features for each of the 72 simulations where detail d1 and d2 have been neglected

the WC level; although the *E* feature is the one resulting in a slightly more clear distinction between stable and unstable cases (in accordance to [104]), this is not sufficient for a reliable classification. Moreover, a direct consequence of the absence of a separation between the classes just based on the amplitude of the features, involves the impossibility to use a simple classifier, such as the ones based on thresholds. A more complex classifiers needs then to be used.

Even though the use of the DWT may appear too complex to be performed on a low-power microcontroller, different works have proved the opposite [128, 129, 130].

5.3.3 Classification and Performance Indexes

The possibility to use a simple threshold-based classifier for the classification task has been denied due to the behavior of the adopted metrics. The choice of alternative solutions must be done taking into account properties such as computational power and memory requirements.

A good trade-off between the above-mentioned properties can be obtained by a K-Nearest Neighbors (KNN) algorithm.

K-Nearest Neighbors essentially relies only on the most basic assumption underlying all prediction: that observations with similar characteristics will tend to have similar outcomes. Nearest Neighbor methods assign a predicted value to a new observation based on the plurality of its K "Nearest Neighbors" in the training set. KNN classification is one of the most fundamental and simple classification methods where the output depends on whether KNN is used for classification or regression: in classification, the output is a class membership. An object is classified by a plurality vote of its neighbors, with the object being assigned to the class most common among its K nearest neighbors. In regression, the output is the property value for the object. This value is the average of the values of K nearest neighbors.

The neighbors are taken from a set of objects for which the class (for classification) or the object property value (for regression) is known. This can be thought of as the training set for the algorithm, though no explicit training step is required. For more details refer to [131].

A reason why this specific classifier has been chosen for this appli-

cation relies on the possibility to generalize the distance measure from the K nearest neighbour to a distance measure from a specific cluster or region (built collecting altogether the instances of a specific class); since these regions may be defined off-line through a training set, the classification can be only performed by computing simple distance measurements between the unknown set and the class regions. This advantage is particularly convenient in case of its implementation in a low power embedded device.

The KNN classifiers offer a certain amount of flexibility in terms of adopted metrics, for the distance computation, and the number of neighbours; these are called hyperparameters. MATLAB provides an efficient tool for the optimization of this hyperparameters through a function called "fitcknn". This function analyzes the effect of different metrics and different values of K on an objective function to minimize.

Another parameter to be defined has to do with the number of score values. In total, the score matrix is made up of 72 rows (72 events) and 9 columns (where each column is a specific feature computed on a specific detail coefficient - 3 features by 3 selected detail coeff.). One may right away declare that the more features are included the more robust the classification will be. This is not always right since some type of features may contribute negatively in the capability of the classifier to discriminate the addressed classes. Moreover, many of the features could be redundant.

To methodically verify the above-introduced problem, we optimally train (using the fitcknn function) a KNN classifier, using all the possible combination of the score matrix, employing two objective functions to maximize; these combinations starts from the use of a single column ending with the use of the entire matrix. The used objective functions are based on typical metrics adopted in the case of binary classifier: Sensitivity S_e and Specificity S_p. For the sake of the S_e and S_p computation, TP, TN, FP and FN, have been defined using the following rule: a TP if a stable case is classified as stable, a TN if an unstable case is classified as unstable, a FP if a stable case is classified as unstable and a FN if an unstable case is classified as stable.

The optimization procedure is listed below:

- having the score matrix of size 72x9 a list of all the possible combi-

nations of $1, 2, ..., 9$ columns is built. This procedure results in 511 combinations;

- for each combination, the optimal hyperparameters are computed, producing an optimal KNN model (metric + K value);
- the optimal model is used to classify each event in the combination;
- compute S_e and S_p;

The output of this procedure gives the value of the S_e and S_p for each possible combination. As previously stated, the described optimization procedure allows to conclude that some features produce a deterioration of the classifier' performances and some of them are even redundant.

Many combinations results to behave optimally leading to $S_e = 1$ and $S_p = 1$. Among the combinations behaving optimally, the one obtained with the lowest number of combinations is used; specifically, detail d_3 of the STD and d_5 of the E are selected. Optimal hyperparameters are: euclidean distance with K=1.

Using the so defined score matrix, the following steps are used to assess the performance of the classifier:

- the score matrix is divided into a training set and a test set;
- the optimal KNN model is trained on the training set;
- obtained model is used to classify the test set;
- compute S_e and S_p;

Results obtained show a $S_e = 0.9$ and $S_p = 1$ which makes this classifier suitable for the postural classification task.

5.3.4 Conclusion

The Wavelet transformation has been addressed for the sake of postural sway classification since can highlight important postural control mechanisms in the human body. From an engineering point of view, this interesting property makes the wavelet transformation suitable for the identification of postural instabilities.

In particular, a 5-level DWT is used to decompose the computed distances and 3 main metrics have been defined on that.

This adopted metrics, computed for each timescale, are used to build the score matrix to be given to the classifier. Since no distinction between stable and unstable cases could be done just looking at features' amplitudes, a slightly more complex classifier needs to be used rather than a simple threshold-based one. In particular, a KNN classifier has been used since it allows the possibility to define regions (where each region represents a specific class) and to perform a distance measurement based on that. Moreover, to further reduce the computational burden of the entire classification procedure, the size of the score matrix has been optimized and the optimal classifier's hyperparameters have been found.

Results show the suitability of the developed methodology for the classification between stable and unstable dynamics, also from a computational point of view.

Further efforts need to be done in the full integration of the methodology in an embedded device and to provide a reliability index quantifying the reliability of the single classification.

Chapter 6

An Assistive Solution for the User's Habits Monitoring

6.1 Introduction

Dietary habits and a wrong lifestyle have been widely associated with age-related functional decline [132, 133, 134, 135, 136].

A direct consequence of a wrong lifestyle in terms of intake of nutrients, water and physical activity, leads to an increase of the probability to incur in mobility and physical decline with a consequent augmented fatigue and dependency in daily activities [137].

Constant monitoring of these subjects, through relatives or caregivers, is not always possible nor economically sustainable in the long run. For this reason, different technological solutions have been proposed by the scientific community aiming at monitoring users in terms of activity rate, nutrition, and hydration quality [138]. Those aspects are particularly important since a proper activity (in terms of an active lifestyle) and a correct nutrition/hydration can reduce the incidence of age-related trauma such as fall and postural instability.

Regarding falls, both exercise and an active lifestyle have a relevant effect on improving older people's balance with a consequent reduction in the risk of falling [139]. Nevertheless, very often, the elderly tend to forget, or neglect, the physical activity they have been asked to perform.

Usually, the responsibility to monitor the elderly has always been associated with caregivers, both professionals and family members, while, nowadays, automatic solutions for the daily activities monitoring, based on low-cost wearable devices, have been proposed. The primary aim of these solutions is to control fundamental parameters (especially geriatric parameters) such as the patient's mobility, the activity rates, user's habits, and ADL (Activity of Daily Living) [140].

Another area in which technology has an important role deals with solutions aiming at increasing awareness or providing reminders to eat and drink regularly. Both app or wearable systems have been proposed for the sake of monitoring wrong hydration or nutrition. These solutions provide a mechanism to monitor abnormal user's behavior, which might indicate nutrition or dehydration scarcity and, according to that, provide reminders to users and caregivers. Obli is one example. It is a balance meant to measure the fluid intake by weighing a bottle placed on top of it [141]. It uses visual and auditory signals in order to provide feedback when the fluid intake is not adequate. The authors have proved that the use of Obli increase the average fluid intake both 6 weeks and 6 months after the interventions began. Major drawbacks of this kind of solution consist of the inability to monitor more users sharing the same environments but using different or private bottles, and it is just meant to monitor hydration.

In the field of Active Assisted Living radio-frequency identification (RFID) technology has found increasing applicability. Examples of its use are the one discussed in [142, 143, 144, 145, 146].

Focusing on applications involving the user's habits monitoring, devices presented in [141], [145] and [147] are very interesting. The solution in [141] can provide an acoustic and visual alert, in case the fluid intake is inadequate, but it requires a static and fixed balance. Moreover, it does not provide the possibility to monitor more users sharing the same environments but using different or private bottles. The solution in [145] uses RFID for monitoring the arm activity in daily life. The system can read tags manipulated with one specific arm while does not consider handled object with the other hand. This strongly reduces the usability of this system for real applications. The architecture proposed can be used in the case of single users in a home environment while does not provide a way

to monitor simultaneously more users. Moreover, there is not any association between the handled object and user. The solution in [147] allows to monitor deviations from normal patterns of behavior which might indicate nutrition or dehydration scarcity but it does not allow to monitor the intake of nutrients, handled objects, or explored areas.

Concerning the aforementioned issues, an RFID based system, designed to monitor user's habits, such as the use of food/beverage/drugs is presented and assessed in this chapter. Also, the same solution can be effectively applied to monitor home appliances, exploitation of the indoor environment, and the activity rate.

To properly contextualize this activity, it must be considered that the presented device is a key component of the NATIFLife project [7]. The project aims at developing an innovative framework of assistive devices which could improve elderly autonomy. The development of an integrated platform of assistive technology, which is open to the integration of traditional and innovative solutions, can produce an improvement of the life quality of elderly and people with mobility impairments. In detail, the project aims at the assessment of the user habits, activity rate, nutrition and hydration, as well as the use of home appliances.

The RFID system aims at integrating, in the NATIFLife platform, functionalities such as food/beverage monitoring as well as a unique identification of the user living the environment. The main idea is to monitor the interaction between the user and generic targets (food, beverage, etc.) positioned in front of the user. To such aim, the user has to wear the RFID reader, while each target of interest is labeled by a passive tag.

Advantages of the adopted technology as respect to other solutions, such as vision systems, switches, or other sensors, are related to its low invasiveness, good flexibility in terms of tags distribution, re-allocation and quantity, ease of use and installation. All the above-mentioned features are mandatory while addressing effective assistive devices. It must be underlined that similar applications in literature make us of static devices, to be placed in the environment, or uses device-dependent measurement systems(in case of water intake, some propose the use of sensorized bottle or the use of inertial sensors in the bottle itself). As previously stated, those solutions do not provide a flexible way to monitor user's behavior nor they provide a way to understand which user is doing what.

In order to properly design this AT device, and successively assess the solution in a real scenario, specific attention has been given to the optimization of the system characteristics, in terms of physical dimensions, power consumption, and reading range. Moreover, since the monitoring of the user should not be subjected to high false-positive behavior, resulting in a miss-confidence of the solution from the user, a measurement campaign has been specifically performed to define objects' position constraints removing the multiple objects identification when the device is used in a real context. Finally, an assessment procedure is presented aiming at testing the system reliability when it is used in a scenario simulating a common domestic area.

6.2 The RFID System

The system is made up of an embedded architecture including an RFID reader (M6E-MICRO by Thing Magic), a power management system, a 1400 mAh rechargeable battery (3,7 V), and a Serial to Bluetooth converter (RN42XVP-I/RM 2.1) for device-smartphone communication. A schematization of the system is given in Figure 6.1.

Each item/furniture to be monitored is provided with flexible passive tags that represent an easy and economical way to provide objects with a basic level of identification.

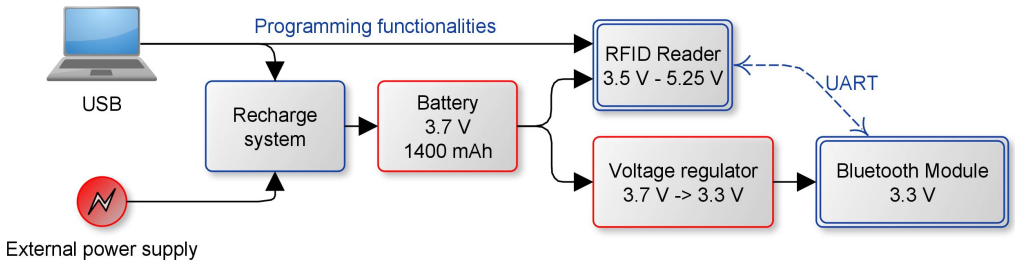

Figure 6.1: Block diagram of the hardware architecture

In the case considered of an assistive device supporting frail people in homelike environments, the device architecture is somehow constrained by the application. In particular, dimensions should be compatible with

a comfortable and wearable device, tags must be non-invasive and cheap and the power budget should allow a reasonable device's operation time. Based on the above consideration, the following choices have been done:

- Antenna maximum dimension has been fixed to 3 cm by 3 cm;
- Selected tags are: AD-227m5 (Avery Dennison).

To properly operate the system, an Android App has been developed. It handles different routines specifically developed to guarantee continuous communication with the RFID reader and a Graphical User Interface that allows users to manage/associate unknown tags, check device temperature, and errors. Being more specific, it allows associating with each detected tag a unique nickname (generally the nickname identify the detected objects) and the possibility to share tag EPC (Electronic Product Code), associate nickname, and detection time with an HTTP server.

The device, specifically prototyped for this application, is shown in Figure 6.2 while the final appearance of the system and its use by a real user are shown in Figure 6.3.

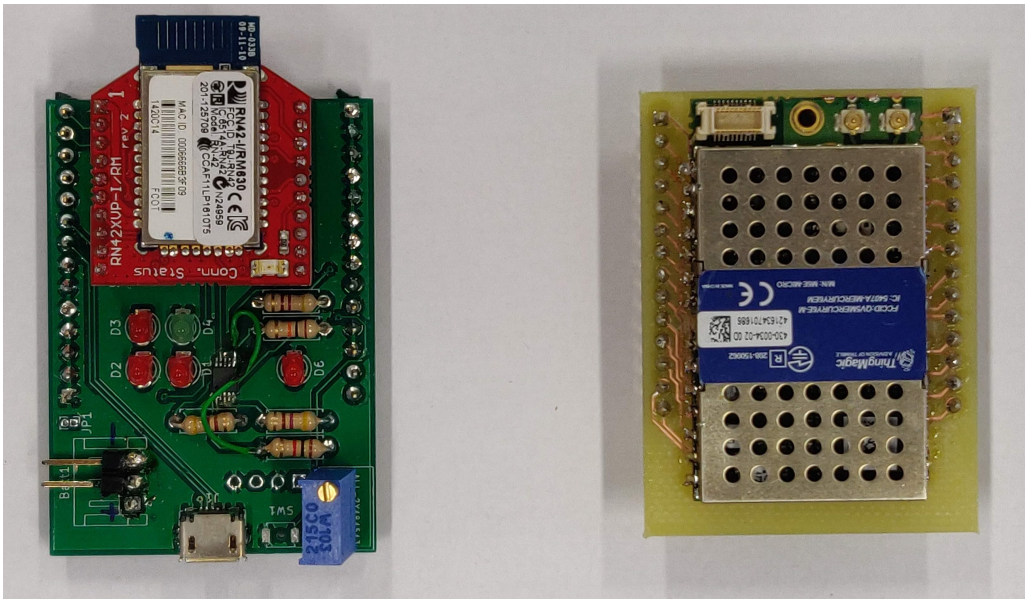

Figure 6.2: A real view of the device components.

(a) (b)

Figure 6.3: This figure shows (**a**) the final appearance of the device and (**b**) the system worn by a real user.

6.2.1 Integration in the NATIFLife Project

As previously stated, the device is a key component of the NATIFLife project and it specifically aims at the assessment of user habits and activity rate, by monitoring user's exploitation and navigation of indoor environments, as well as the use of equipment such as furniture and food/beverage related tools. Without an identification system, the NATIFLife platform cannot either associate the use of specific equipment to a specif user nor it can monitor the exploitation of the environment of a user. Moreover, beverages and food monitoring will allow us to estimate the user's habits in terms of nutrition intake and hydration. These requirements highlight the great importance of this assistive solution in the context of the project.

6.3 System Characterization

As previously introduced, the main goal of the RFID system is to detect the end-user proximity to furniture and/or food and drink in a homelike environment. This is fundamental to assess the user's activity rate, habits, hydration and nutrition.

In order to correctly detect the target - furniture, a tool, food or drink, or a location - the user is interacting with, two main aspects need to be addressed: the maximum operating range of the system in terms of the

maximum allowable distance between the antenna, worn by the user, and the tag applied to the target; the minimum distance between two tags (identifying two different targets) thus avoiding any cross detection of multiple tags in a specific reading range. The idea behind this system is to assess the user's habits and to monitor its actions; basically, if the user is using a cooking tool or handing a bottle of water. Each object is labeled by a dedicated TAG with a unique code in such a way the user interaction with that object can be identified. The problem arises when more objects are in the same area and the RFID system detects them (multi-object detection) simultaneously; the system will not be able to understand which is the object the user is interacting with and that is the reason behind the need of avoiding cross detection.

It must be underlined that objects are not supposed to be positioned in specific locations. The only constraint to be fulfilled is the minimum distance between two tags, allowing for reliable tags discrimination.

The above features are usually constrained by needs coming from the practical use of the device. In particular, for the addressed application, the target operating range of the device (antenna-tag distance) has been fixed to 30 cm, which is the typical range where an object is easily used by hands, while the minimum inter-tag distance will be fixed based on the characterization results (see Section 6.3.2).

The solution developed offers different degrees of freedom to fulfill the above specifications, such as the antenna dimensions, the tag type, and the reader output power. In the following section, measurement strategies adopted to fix the optimal reader's output power, fulfilling the antenna-tag distance specification, are presented.

6.3.1 Reading Range vs Reader's Output Power

This analysis aims to assure the target reading range while assuring the lowest device's power consumption. The RSSI (Received Signal Strength Indication) is used for the sake of identifying the areas in which the irradiated power is sufficiently high to power up the passive tag. Specifically, 4 different values of the reader's output power have been investigated, namely: 25 dBm, 20 dBm, 15 dBm, and 10 dBm.

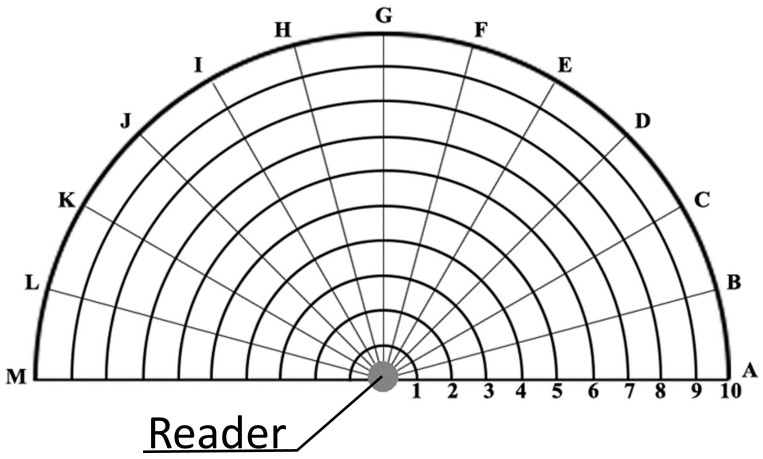

Figure 6.4: Selected measurements points for the system's reading range evaluation.

6.3.1.1 Experimental Setup

Measurements have been taken along the grid shown in Figure 6.4. In detail, each point in the chart, for a given angle, is spaced from the previous of 5 cm. Addressed distances range from 5 cm to 50 cm. The addressed angles are in the range of $[0, 180]^\circ$ with a step of 15°. In total, 130 measurement points (intersections) have been investigated. The reasons why the measurements have been taken just along a semi-circumference rather than the total circumference reside in two main reasons: 1) the back radiation gain of the adopted antenna is negligible as respect to the front radiation gain and 2) the final application does not expect readings for objects placed at the back of the user wearing the device.

The measurement protocol consists of the following steps:

1. Fixing the reader's output power, starting with the maximum value (25 dBm);

2. Placing the tag at a fixed distance from the antenna (e.g. 5 cm, combination 1-C);

3. Moving the tag on each of the 13 angular positions while keeping the distance from the reader antenna (e.g. 1-A, 1-B, . . . , 1-M);

4. Measuring the tag emitted power for each measurement point;
5. Increasing the distance from the emitter by 5 cm and repeat points 3 and 4;
6. Repeating every step with a different reader's output power, decreasing by 5 dBm until the requirements are not met.

This procedure allows for building an irradiation diagram representing the output power as a function of the angle/distance parameters, guaranteeing the detection of the tag placed in every of the measurement points. This strategy has led to the identification of the minimum power guaranteeing the desired reading range of $\sim$ 30 cm with a detection angular range of $\pm 45^{\circ}$. Such an operating domain has been defined by the specific application, considering a typical user-target interaction area in case of handled objects (food, beverage, drugs).

This preliminary phase, which was conducted in a laboratory set-up, has been carried out taking into account all the necessary steps to avoid interfering material to be placed between reader and tag or strong electromagnetic interference in the surrounding area.

6.3.1.2 Experimental Results and Device's Operation Time

Obtained results have been arranged in such a way to show the tag irradiated power when it is placed in the measurement points shown in Figure 6.4, thus facilitating the comprehension of the combination of angle/distance allowing a reliable tag detection.

Results obtained for each of the considered power are shown in Figure 6.5. This figure is built as an interpolation of the RSSI measures as a function of the reader power, reader-tag distance, and angle.

An analysis of the plots reported in Figure 6.5 allows us to draw the following conclusions:

- **25 dBm** (Figure 6.5a): this power value produces a reading range up to 50 cm in the whole cone of acceptance ($\pm 45^{\circ}$), as indicated by the bold line highlighted in the plot;
- **20 dBm** (Figure 6.5b): this power setting shows similar behavior compared to the previous one;

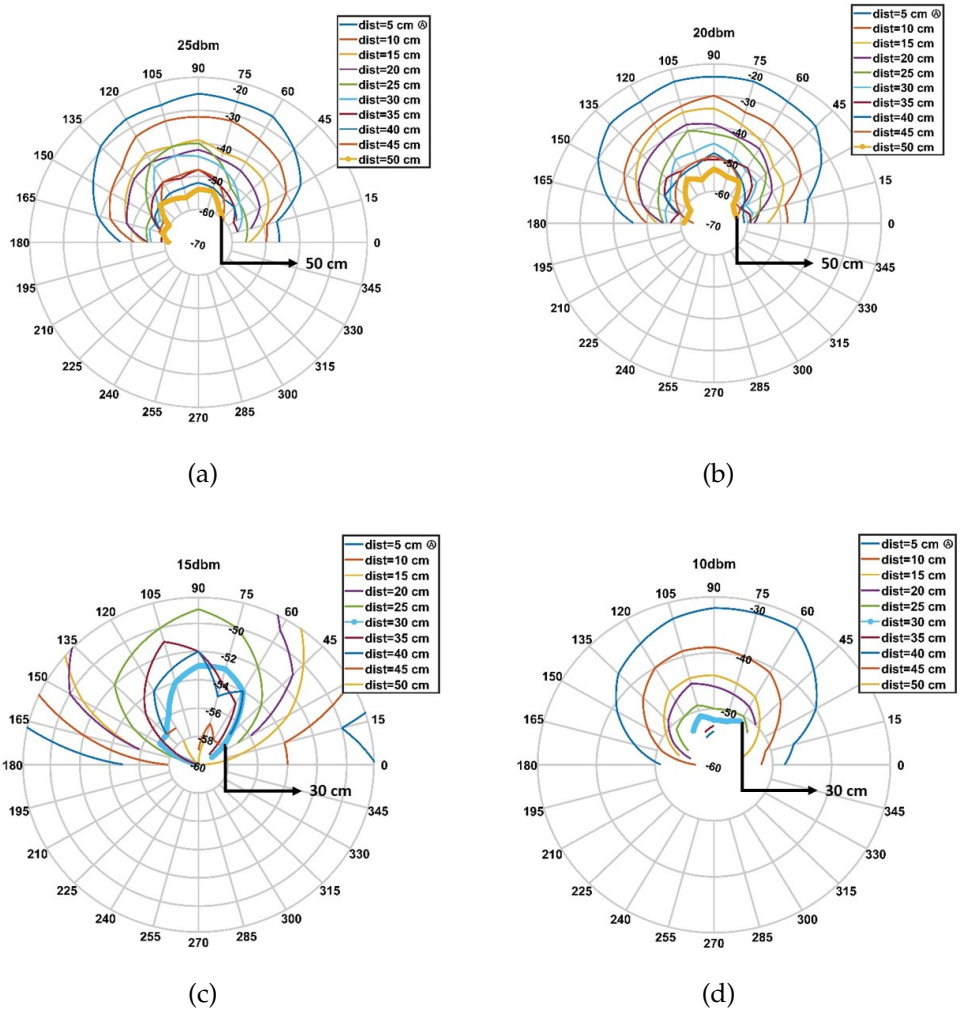

Figure 6.5: Characterization results. (**a**) shows the tag irradiated power when the output power is fixed to 25 dBm, (**b**) when fixed to 20 dBm, (**c**) when fixed to 15 dBm and (**d**) when fixed to 10 dBm.

- **15 dBm** (Figure 6.5c): analyzing the target range, which is the one highlighted by the bold line (30 cm), full coverage is guaranteed in the entire angular range of operation ($\pm 45°$). Nevertheless, greater distances, namely 40 cm, 45cm e 50 cm can still be achieved; however, it must be clarified that those values are not guaranteed in the

desired angular range but are spotted measures within the measurements' points. These results make the following power the optimal choice for the application's requirements. For the sake of clarity, the plot reports only results related to a distance range of 25 cm to 50 cm.

- **10 dBm** (Figure 6.5d): this last power has been investigated trying to understand if a further power reduction could have been possible or not. As clearly visible by the bold line, the target reading range is not guaranteed within the angular range of operation.

In conclusion, it can be affirmed that the optimal reader's output power, covering the desired interaction area, is equal to 15 dBm, which allows a suitable user-target interaction in the whole operation area (defined by a distance of 30 cm, in the range $[-45°, 45°]$). Moreover, both from a theoretical analysis and test, with the selected power of 15 dBm, the battery life has been estimated to be around 5 hours. The power required by the RFID module, in reading mode, is around 1 Wh. Using a battery of 1400 mAh with 3.7 V the total available power is 5 Wh. Nevertheless, it must be pointed out, that any smart control has been integrated into the device taking into account prolonged inactivity (resting or sleeping) which could drastically improve battery life.

The first conclusion can hence be summarized as follows: in case the end-user handles objects in the above-defined working range, the system assures the identification of user-targets interaction. Of course, the above working range has been defined conservatively, assuring a full range of tag identification. As can be observed by results obtained, in the central area of the working range the system can detect tags positioned up to 50 cm. This consideration allows affirming that in a real scenario, where the interaction between end-users and items (beverage, food, etc. positioned on a working table) have to be monitored, it would be suggested to put targets at a minimum distance of 50 cm from the line of action of a potential end-user.

6.3.2 Multiple-Objects-Identification (MOI)

As already described, an aspect worthy of consideration during assistive devices development is the maximization of the user confidence and trust. Consequently, the reliability of the system is a mandatory characteristic to avoid users' miss-confidence. One of the peculiar characteristics which should be fulfilled by the system under investigation is high robustness against MOI. Basically, in order to guarantee the expected reliability in following user activities inside the living environment, the system should identify just one tag at a time and MOI must be avoided.

In particular, the above investigation is mandatory in case the RFID system would be used to identify objects positioned next to the end-user, e.g. just to notify the user of the proximity of the target or to monitor the closeness to specific targets (user traceability). In this case, the user is not required to necessarily handle the target.

It is hence necessary to analyze the system behavior in the presence of more than one tag in the working range of the system, to determine the minimum distance between tags assuring high selectivity of the identification procedure. This is mandatory to properly set the position of tags associated with different services or tools in a real scenario.

6.3.2.1 Experimental Setup

The measurement survey has been performed by a dedicated set-up represented by the working area shown in Figure 6.6.

The experiment consists in observing the system behavior in case two tags are positioned within the rectangular area. The main task to be achieved is the estimation of the minimum inter-tag distance avoiding MOI.

Circles represent the measurement points, shifted one from another by 10 cm. The black triangle at the bottom defines the reader's position. For each measurement, one tag (labeled as "#1") is fixed in the position defined by (Row (i), Column(j)), chosen as the reference position, and a second tag (labeled as "#2") is moved along all the other points belonging to the same Row. For the sake of completeness, it must be underlined that only combinations of tags belonging to the same row (lines of operation

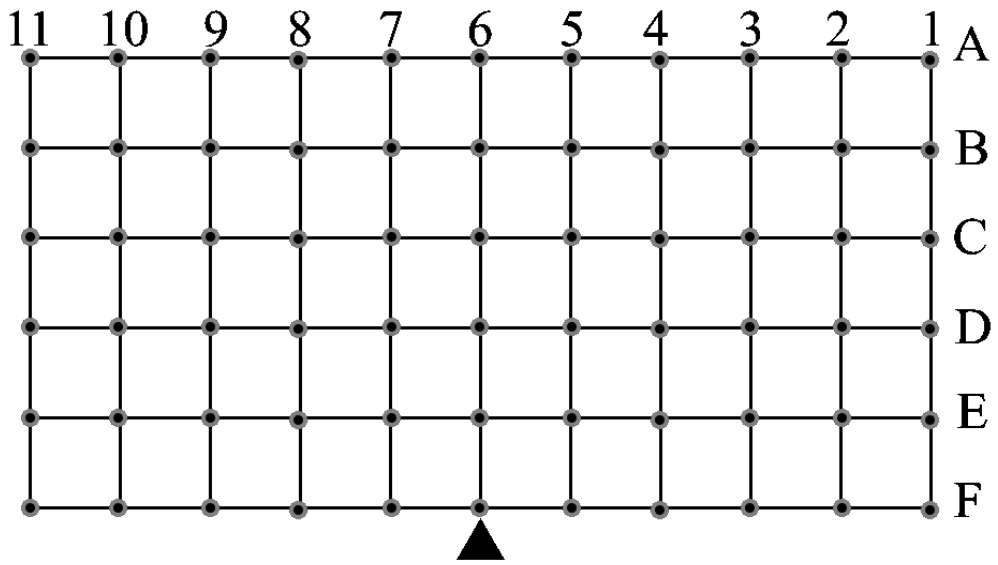

Figure 6.6: Working area adopted to assess the system behaviour in terms of MOI. Dimensions are 100 cm by 50 cm with each step measuring 10 cm.

in front to the user) have been investigated, which represents the worst case in terms of MOI.

6.3.2.2 Experimental Results

Obtained results, in terms of detected or missed readings, are given in Figure 6.7.

As an example, Figure 6.7a shows results related to the case in which measurement surveys have been accomplished by positioning successively the fixed tag #1 in the first column of each row meanwhile the tag #2 is moved on the corresponding row from column 2 to column 11. For each of the combination produced employing this strategy the plot reports a "0" in case the system does not detect the presence of tags, a "1" or a "2" in case the system detects one of the two tags, and a "1/2" in case both tags are detected (MOI). The dark vertical cells show the position of

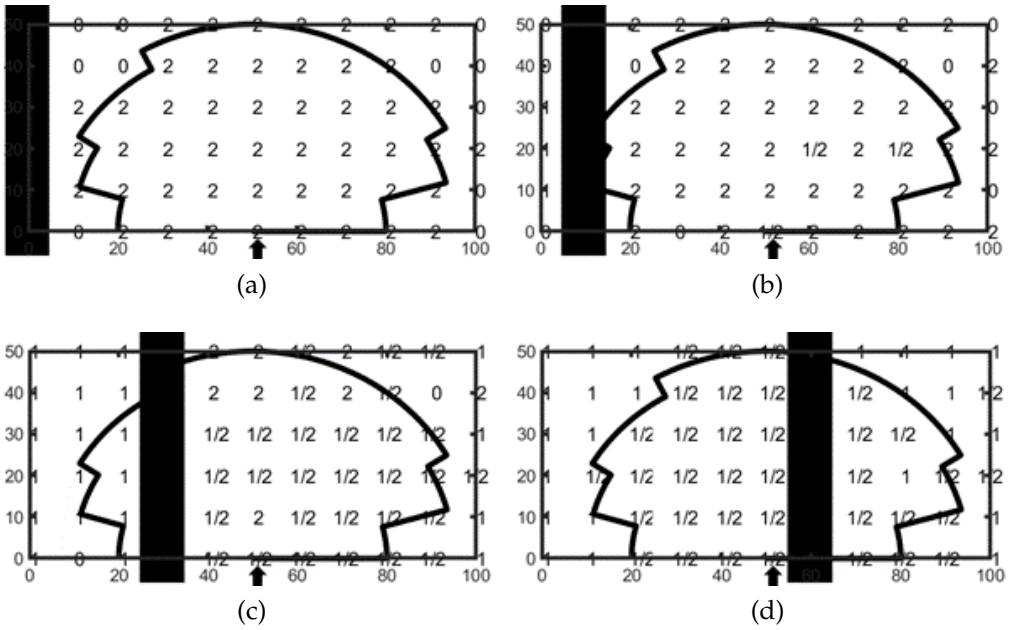

Figure 6.7: Results showing the tag detection area as a function of the 2 tags position. In particular, tag #1 is fixed on the black cell of each row, chosen as the reference position, while tag #2 is moved along all the other positions of the same row. The position of the reader is marked by the arrow.

the fixed tag #1.

Since the aim of this measurement procedure is to identify the areas in which MOI can occur, our attention must be focused on spots labeled as "1/2", representing the conditions in which a cross detection of multiple tags has been detected. To avoid the MOI incidence those combinations should be avoided.

As expected, in the case of tag #1 is out of the reader working range, only tag #2 is detected (see Figure 6.7a). In case of tag #1 is positioned close to the working area some MOI may occur (see Figure 6.7b), while in case of tag #1 is positioned inside the working range, a lot of MOIs are identified. As already evidenced in the previous analysis, tags positioned within a cone smaller than $\pm 45^{\circ}$ can be detected also if the reader-to-tag distance is greater than 30 cm.

Although few exceptions have been highlighted by the performed investigation, obtained results confirm the need to keep the inter-tag distance higher than 60 cm to avoid MOIs.

Asymmetries in the device behavior can be assumed to be dependent on the asymmetric irradiation diagram shown in Figure 6.5, which is due to intrinsic asymmetries of the device.

It must be underlined that these results are not related to the need of detecting objects handled by end-users, rather than with the opportunity to use the proposed technology to detect and recognize targets (services, landmarks, etc) next to end-users.

6.4 System Assessment in Real Scenarios

To validate the operating conditions defined during the system characterization, the system must be tested when it is used in a scenario simulating a homelike environment. In particular, two different scenarios are addressed: user handling objects and detecting tags next to the user.

6.4.1 Handling Tagged Objects

As already mentioned, one of the tasks to be assessed is the monitoring of the interaction between objects and user handling such objects. A typical scenario is a user standing in front of a table (working area), grabbing and using objects positioned on the table (water, drugs, food, etc.). In this case, the line of sight between tags and the antenna is guaranteed by a convenient positioning of the reader antenna on the user body and by avoiding shielding layers between tags and the reader.

The homelike environment has been simulated by considering a working surface (e.g. a table) on which two targets are positioned. The users have been asked to stand still in front of the table, with objects placed at a distance greater/equal of 50 cm from the user's hip (the RFID reader is worn on the right side of the user's hip while the objects are represented by two bottles of water), and to grasp and use them, one after another, 5 times each. For each use, the system output has been acquired and the following cases have been addressed: the system detects the handled

object (this case has been considered as a true positive TP), the system does not detect any object (a false negative FN) and the system detect the wrong object (a false positive FP). A schematization of the experimental setup is shown in Figure 6.8.

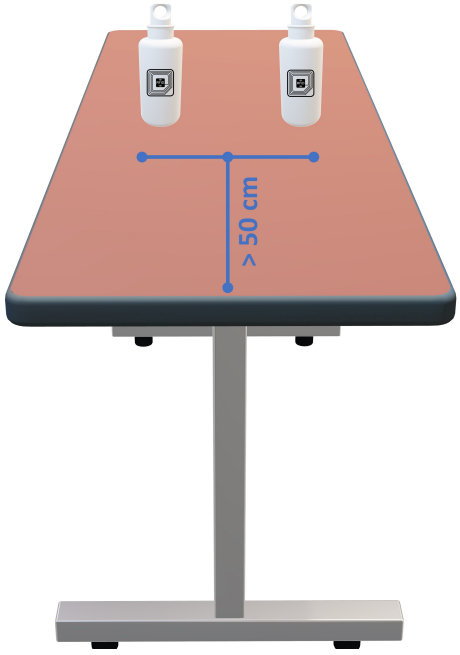

Figure 6.8: A schematization of the experimental setup which has been used for the assessment of the device in case of handled objects.

In particular, in order to assure that the system only detects the tag during the real user-target interaction and not while the user is approaching the table, tagged objects have been positioned at a minimum distance from the user line of action of 50 cm. Considering that the reader has been worn at the right side of the user's hip, objects have been positioned a distance greater than 45 cm from the table end. During the experiment users emulate typical actions associated with that specific object; as an example, if the object under investigation is a bottle, the action associate includes the opening of the bottle and the subsequent water pouring. Clearly, the device does not know if the user is really drinking or not, but is based on the idea that, if the user takes the bottle he intends to do it.

For this first assessment, 10 users (aged between 22 and 39, with different height and weight) were involved, all of whom have repeated the experiments 5 times per object. Users have been lightly instructed about how to mimic gestures typically performed by frail people, fulfilling the need of bringing the object within the system operating range (30 cm, $\pm 45°$). This phase is extremely important since, gestures normally computed by healthily and young people, may fall outside the reading area of the device.

The object detection is monitored through the Android application already introduced. Results for this experiment are shown in Figure 6.9.

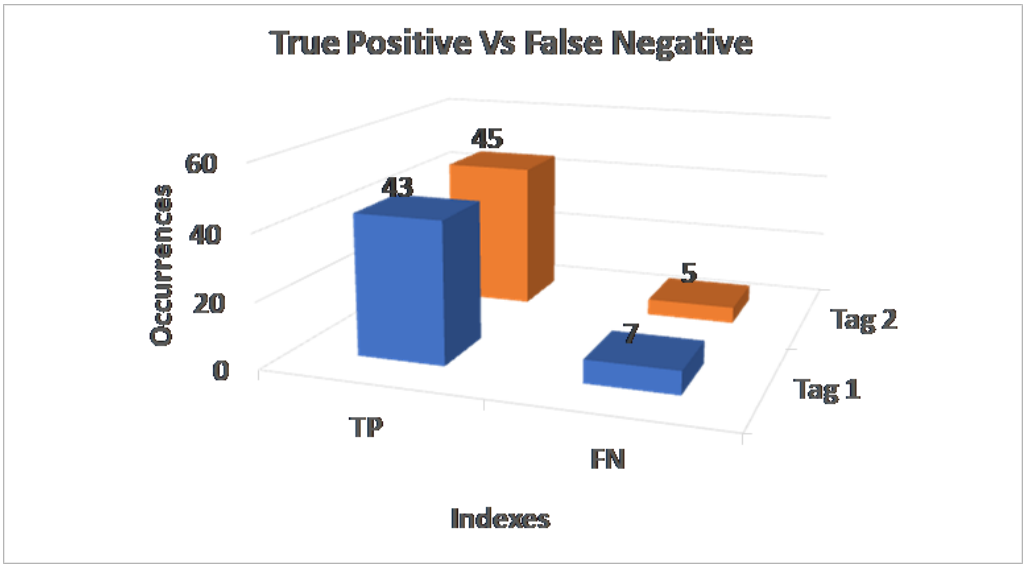

Figure 6.9: TP-FN behaviour in case of the experiment aiming at monitoring user handling of tagged objects. The number on top of each column represents the total number of occurrences for that specific index.

As first, as evidenced by Figure 6.9, no false positive (FP) and have been identified. This is explained considering that the experimental set-up has been realized according to rules defined in Section 6.3.1: placing the objects at a distance greater than 50 cm from the user assures their detection only during their use. Moreover, the low number of FN demonstrates that only a few times tags have not been detected during their use.

The above results confirm the reliability of the system, in case objects

to be handled are positioned by fulfilling constraints defined in Section 6.3.1.

6.4.2 Detecting Items Next to End-Users

The main goal of this assessment is not related to the need of detecting objects handled by end-users, rather with the opportunity to use the proposed technology to detect and recognize targets (services, landmarks, etc) next to end-users. That is why a second assessment has been conducted by analyzing the system capability to detect the correct item when two or more targets are positioned in the user surrounding area.

In order to mimic a possible scenario in which the aforementioned situation can occur, the following two possible scenarios have been considered:

- The user is exploring an area where appliances to be monitored can be close to each other;
- There's the need to monitor the user activity by detecting his/her transition to "target" placed throughout the environment.

Although different in appearance, both scenarios share the same problem: two or more tags can be possibly placed close to each other, increasing the probability to incur in MOI.

To address this issue, an experimental scenario has been prepared (Figure 6.10).

Tags have been placed on a wall with a fixed height (1 m from the ground) and with changing inter-tag distance (ΔT). The ΔT distances addressed are 60 cm, 50 cm, 40 cm. The experiments were conducted as follow:

- The device was positioned in the users' hip in such a way to direct the antenna toward the tag;
- Users, always starting from the same tag, follow a path (highlighted in the room's floor) keeping a constant distance of 40 cm from the wall (and hence from the tag) while keeping a slow pace;

Figure 6.10: A schematization of the scenario adopted for the sake of the second assessment.

- For each transition through a target an experimental supervisor was taking note of the following cases:
  - Tag read: considered as TP;
  - Tag not read: considered as a FN;
  - Tag correctly read and consecutive/previous tag read as well: considered both as a TP and a FP.

During the walk between two consecutive tags, an experimental supervisor was taking note of the occurrence of "any tag read" that has been considered as true negative (TN).

Users involved in these experiments are the same involved during the previous assessment. Each of them has repeated the experiment 5 times for each ΔT combination.

Since we are dealing with a binary classification, the following indexes has been used to assess the system performances:

- Sensitivity (S_e):

$$S_e = \frac{TP}{TP + FN} \tag{6.1}$$

- Specificity (S_p):

$$S_p = \frac{TN}{TN + FP} \tag{6.2}$$

Moreover, in order to also evaluate the incidence of the MOI in the system functionalities, the Specificity index has been normalized in the following way:

$$S_{p_N} = \frac{TN}{TN + FP}(1 - \frac{MOI}{TT}) \tag{6.3}$$

where TT stands for Total Trials.

Results concerning the aforementioned indexes are given from Figure 6.11 to Figure 6.12.

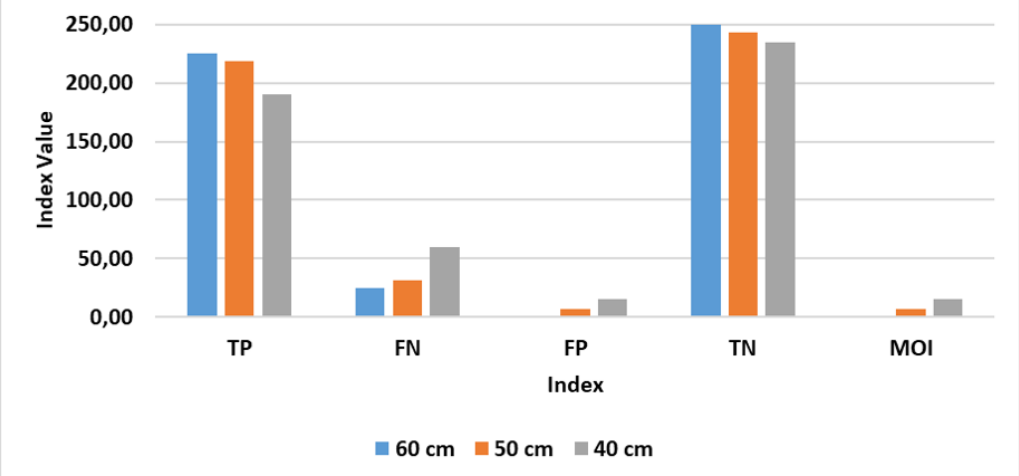

Figure 6.11: Raw indexes for each inter-tag distance addressed.

Figure 6.11 allows making an immediate comparison with the results discussed in Section 6.3.2. In particular, as the inter-tag distance is reduced, there is a clear increment in the FN, FP and MOI values, while

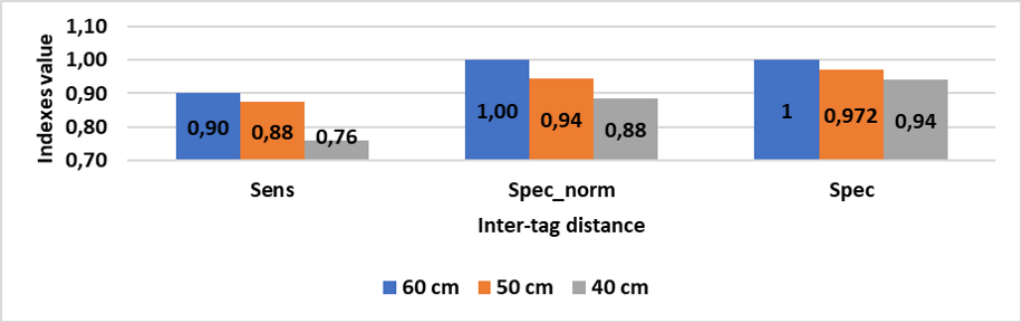

Figure 6.12: Sensitivity, Specificity and normalized Specificity for each considered ΔT.

the TP decreases. This can be interpreted as a general deterioration in the system capability to detect and recognize targets next to end-users. This trend is further confirmed by results shown in Figure 6.12, where a general deterioration of the system performances, as the inter-tag distance is reduced, can be noticed.

In conclusion, results coming from the assessment strategy make eligible the adoption and further assessment of this system in the NATIFLife living lab, also by involving real elderly users.

6.5 Conclusions

The population aging is leading to an exponential growth of serious health issues, including mobility and physical decline. Many solutions have been proposed for the sake of reducing the social effect of such phenomena, such as gait training, in case of falls, or reminder in case of nutrition and hydration. Those aspects are particularly important since a proper activity (in terms of an active lifestyle) and a correct nutrition/hydration can reduce the incidence of age-related traumas such as fall, postural instability, and, more in general, physical decline. In these scenarios, the use of technology improves the general outcome of the physical decline since they provide an objective estimation of user's habits, activity rates, or the use of tools/foods/equipment.

As a possible advance in this domain, an RFID based system, whose

goal is to monitor user's habits, such as the use of food/beverage/drugs, uses of equipment, exploitation of the indoor environment and the activity rate has been realized and assessed.

The advantages coming from the adoption of the proposed system relies on its low invasivity, flexibility, and intrinsic user identification feature.

For the scenario the solution is meant for, specific attention has been reserved for the optimization of the system characteristics, in terms of the physical dimension, power consumption, and reading range. Moreover, to avoid miss-identification, resulting in a miss-confidence of the solution, an assessment procedure has been conducted aiming at evaluating the system reliability when used in a scenario simulating a domestic area. Specificity, Sp, and Sensitivity, Se, indexes have proved the robustness and reliability of the solution.

Chapter 7

Conclusions and Final Remarks

The European population aging poses various challenges, especially in the health care scenario. This situation has been perceived by many as a threat to Europe's economy and competitiveness, in particular when it comes to the sustainability of the healthcare systems.

Therefore, the following questions arise: Who will take care of the current generation as we become older? What types of health and social organizations should we develop to preserve the quality of life of an aging population and sustain our health care systems over the medium and long term? To face this challenging situation, the EU Commission has launched several initiatives to promote active aging across Europe.

From a technical point of view, the greatest risks associated with a progressive increase of the population frailty, concern the onset of falls, often associated or preceded by postural instability, and the loss/reduction of autonomy. Often, these phenomena are further stressed by wrong habits in terms of nutrition and mobility.

These are then addressed problems within this PhD thesis.

In particular, the applications addressed by the following thesis are: detection and classification of falls, analysis and classification of postural instabilities, analysis and detection of user's habits. These three applications are intrinsically connected.

Concerning falls, an event-driven methodology, based on template matching techniques was proposed, analyzed, and validated where the adopted metrics and related classifiers, were selected to reduce the algo-

rithm computational complexity. One of the main objectives, common to all the presented activities, is the development of methodologies that can be easily integrated into low power microcontroller platforms. The results obtained in terms of classification between fall and non-fall events, as much as the classification among the specific falls, allow us to quantify the goodness of the proposed solution, also by comparing it with more complex methodologies present in the state of the art. Besides, a first exploratory implementation of some of the functionalities presented in the methodology was evaluated in collaboration with the company STMicroelectronics, demonstrating the feasibility of the integration.

In the context of postural instabilities, the use of inertial platforms has been validated against clinical solutions, such as force platforms and vision systems, through a careful analysis of results obtained by the comparison between the proposed solution and a reference system. Furthermore, in addition to the metrics qualifying the ability of the classifier to predict whether a given event belongs to the correct class, a reliability index has been defined and used to quantify the quality of the individual classification process (i.e. how much you need to trust that specific classification). The results obtained demonstrate the feasibility of using a low-cost inertial platform for the continuous analysis of postural conditions, even during normal daily operations.

A further proposal, in the context of instabilities, has been based on the use of the Wavelet transform. This particular mathematical transformation has been widely used in the literature for the analysis of the postural conditions of the subjects, with specific reference to the evaluation of posture control mechanisms. However, it should be specified that the results obtained from the analysis are rarely used to classify postural conditions. For this reason, the proposed methodology makes use of the Wavelet transform, in particular the discrete Wavelet transform, on which output features are calculated. A detailed analysis was made on the contribution made by each individual feature and, based on obtained results, it was possible to define the specifications of the needed classifier. In particular, a K-Nearest Neighbor classifier was employed. This choice was based on specific properties that make the classifier easily embeddable into microcontroller platforms. Also, in this case, obtained results, in terms of Sensitivity and Specificity, show the validity of the proposed

solution.

Finally, having shown how good habits in terms of nutrition and mobility can have a positive effect on a subject's conditions, a further application, concerning the development and characterization of a device for user' habits monitoring based on RFID technology, has been presented. In particular, the device was developed within an Interreg project (NATIFLife) which aimed at the development of an innovative framework of assistive devices that could improve elderly autonomy. The development of an integrated platform of assistive technology, which is open to the integration of traditional and innovative solutions, can produce an improvement of the life quality of the elderly and people with mobility impairments. In detail, the project aims at the assessment of the user habits, activity rate, nutrition and hydration, as well as the use of home appliances. The RFID system aims at integrating, in the NATIFLife platform, functionalities such as food/beverage monitoring as well as a unique identification of the user living the environment.

Conducted experiments were mainly aimed at the optimization of the system characteristics, in terms of physical dimension, power consumption, and reading range. Moreover, to avoid miss-identification, resulting in a miss-confidence of the solution, an assessment procedure has been conducted aiming at evaluating the system reliability when used in a scenario simulating a domestic area. Also, in this case, the adopted metrics have proved the robustness and reliability of the proposed solution.

Although not strictly related to the activity carried out during the PhD, two important aspects in the development of Assistive Technology have to do with the User-Centered Design (UCD) approach and the assessment by end-users. Both aspects are fundamental to increase acceptance by end-user and hence are mandatory before being actually adopted by real frail users. The activities presented in this thesis were mainly focused on the methodology development and, where real hardware has been used, this was neither optimized nor designed having in mind the end-users. Both aspects need to be further addressed in future works.

All the activities, therefore, have a single common goal: improving the living conditions of fragile subjects, increasing self-confidence and relative autonomy. Results obtained in all the presented applications, many of which have been already published in journals, allow us to conclude

that a major innovative contribution has been introduced through this thesis.

Bibliography

[1] EUROSTAT, "Population structure and ageing." https://ec.europa.eu/eurostat/statistics-explained/index.php/Population_structure_and_ageing, Last accessed on 2020-07-27.

[2] EUROSTAT, "Ageing europe - statistics on population developments." https://ec.europa.eu/eurostat/statistics-explained/index.php?title=Ageing_Europe_-_statistics_on_population_developments#Older_people_.E2.80.94_population_overview, Last accessed on 2020-07-27.

[3] M. P. Lawton and E. M. Brody, "Assessment of Older People: Self-Maintaining and Instrumental Activities of Daily Living1," *The Gerontologist*, vol. 9, pp. 179–186, 10 1969.

[4] S. Katz, A. B. Ford, R. W. Moskowitz, B. A. Jackson, and M. W. Jaffe, "Studies of Illness in the Aged: The Index of ADL: A Standardized Measure of Biological and Psychosocial Function," *JAMA*, vol. 185, pp. 914–919, 09 1963.

[5] E. T. E. P. H. Association, "Falls among older adults in the eu-28: Key facts from the available statistics." https://eupha.org/repository/sections/ipsp/Factsheet_falls_in_older_adults_in_EU.pdf, Last accessed on 2020-08-05.

[6] W. W. H. Organization, "Who mortality database." `https://apps.who.int/healthinfo/statistics/mortality/whodpms/`, Last accessed on 2020-08-05.

[7] "NATIFLife – Interreg Italia – Malta."

[8] K. Chaccour, R. Darazi, A. H. E. Hassani, and E. Andrès, "From fall detection to fall prevention: A generic classification of fall-related systems," *IEEE Sensors Journal*, vol. 17, pp. 812–822, Feb 2017.

[9] G. Rescio, A. Leone, and P. Siciliano, "Supervised Expert System for Wearable MEMS Accelerometer-Based Fall Detector," *J. Sensors*, vol. 2013, pp. 1–11, jul 2013.

[10] G. Panahandeh, N. Mohammadiha, A. Leijon, and P. Handel, "Chest-mounted inertial measurement unit for pedestrian motion classification using continuous hidden Markov model," in *2012 IEEE Int. Instrum. Meas. Technol. Conf. Proc.*, pp. 991–995, IEEE, may 2012.

[11] A. Leone, G. Rescio, A. Caroppo, and P. Siciliano, "A wearable emg-based system pre-fall detector," *Procedia Engineering*, vol. 120, pp. 455 – 458, 2015. Eurosensors 2015.

[12] G. Rescio, A. Leone, and P. Siciliano, "Support vector machine for tri-axial accelerometer-based fall detector," in *5th IEEE International Workshop on Advances in Sensors and Interfaces IWASI*, pp. 25–30, June 2013.

[13] J. Dunkel, R. Bruns, and S. Stipkovic, "Event-based smartphone sensor processing for ambient assisted living," in *2013 IEEE Elev. Int. Symp. Auton. Decentralized Syst.*, pp. 1–6, IEEE, mar 2013.

[14] C. Franco, A. Fleury, P. Y. Gumery, B. Diot, J. Demongeot, and N. Vuillerme, "ibalance-abf: A smartphone-based audio-biofeedback balance system," *IEEE Transactions on Biomedical Engineering*, vol. 60, pp. 211–215, Jan 2013.

[15] H. Ketabdar and M. Lyra, "System and methodology for using mobile phones in live remote monitoring of physical activities," in *2010 IEEE International Symposium on Technology and Society*, pp. 350–356, June 2010.

[16] C. Tacconi, S. Mellone, and L. Chiari, "Smartphone-based applications for investigating falls and mobility," in *2011 5th International Conference on Pervasive Computing Technologies for Healthcare (PervasiveHealth) and Workshops*, pp. 258–261, May 2011.

[17] Q. V. Vo, G. Lee, and D. Choi, "Fall Detection Based on Movement and Smart Phone Technology," in *2012 IEEE RIVF Int. Conf. Comput. Commun. Technol. Res. Innov. Vis. Futur.*, pp. 1–4, IEEE, feb 2012.

[18] B. Ando, S. Baglio, C. O. Lombardo, and V. Marletta, "A multisensor data-fusion approach for ADL and fall classification," *IEEE Trans. Instrum. Meas.*, vol. 65, no. 9, pp. 1960–1967, 2016.

[19] N. Otanasap, "Pre-impact fall detection based on wearable device using dynamic threshold model," in *2016 17th International Conference on Parallel and Distributed Computing, Applications and Technologies (PDCAT)*, pp. 362–365, Dec 2016.

[20] B. Cates, T. Sim, H. M. Heo, B. Kim, H. Kim, and J. H. Mun, "A novel detection model and its optimal features to classify falls from low- and high-acceleration activities of daily life using an insole sensor system," *Sensors*, vol. 18, no. 4, 2018.

[21] A. Sucerquia, J. D. López, and J. F. Vargas-Bonilla, "Real-life/real-time elderly fall detection with a triaxial accelerometer," *Sensors*, vol. 18, no. 4, 2018.

[22] R. Igual, C. Medrano, and I. Plaza, "Challenges, issues and trends in fall detection systems," *Biomed. Eng. Online*, vol. 12, p. 66, jul 2013.

[23] A. Shahzad and K. Kim, "Falldroid: An automated smart-phone-based fall detection system using multiple kernel learning," *IEEE Transactions on Industrial Informatics*, vol. 15, pp. 35–44, Jan 2019.

[24] Y. Hsu, K. Chen, J. Yang, and F. Jaw, "Smartphone-based fall detection algorithm using feature extraction," in *2016 9th International Congress on Image and Signal Processing, BioMedical Engineering and Informatics (CISP-BMEI)*, pp. 1535–1540, Oct 2016.

[25] C. L. Buzin Junior and A. G. Adami, "Sdqi - fall detection system for elderly," *IEEE Latin America Transactions*, vol. 16, pp. 1084–1090, April 2018.

[26] P. Turaga, R. Chellappa, V. S. Subrahmanian, and O. Udrea, "Machine recognition of human activities: A survey," *IEEE Transactions on Circuits and Systems for Video Technology*, vol. 18, pp. 1473–1488, Nov 2008.

[27] R. Messing, C. Pal, and H. Kautz, "Activity recognition using the velocity histories of tracked keypoints," in *2009 IEEE 12th International Conference on Computer Vision*, pp. 104–111, Sep. 2009.

[28] J. Lei, X. Ren, and D. Fox, "Fine-grained kitchen activity recognition using rgb-d," in *Proceedings of the 2012 ACM Conference on Ubiquitous Computing*, UbiComp '12, (New York, NY, USA), pp. 208–211, ACM, 2012.

[29] M. Rohrbach, S. Amin, M. Andriluka, and B. Schiele, "A database for fine grained activity detection of cooking activities," in *2012 IEEE Conference on Computer Vision and Pattern Recognition*, pp. 1194–1201, June 2012.

[30] M. A. As'ari and U. U. Sheikh, "Vision based assistive technology for people with dementia performing activities of daily living (adls) - an overview," *Proceedings of SPIE - The International Society for Optical Engineering*, vol. 8334, pp. 100–, 04 2012.

[31] F. Harrou, N. Zerrouki, Y. Sun, and A. Houacine, "Vision-based fall detection system for improving safety of elderly people," *IEEE Instrumentation Measurement Magazine*, vol. 20, pp. 49–55, December 2017.

[32] A. Núñez-Marcos, G. Azkune, and I. Arganda-Carreras, "Vision-Based Fall Detection with Convolutional Neural Networks," *Wirel. Commun. Mob. Comput.*, vol. 2017, pp. 1–16, dec 2017.

[33] A. Hein and T. Kirste, "A hybrid approach for recognizing adls and care activities using inertial sensors and rfid," in *Universal Access in Human-Computer Interaction. Intelligent and Ubiquitous Interaction Environments* (C. Stephanidis, ed.), (Berlin, Heidelberg), pp. 178–188, Springer Berlin Heidelberg, 2009.

[34] H. Li, A. Shrestha, F. Fioranelli, J. Le Kernec, H. Heidari, M. Pepa, E. Cippitelli, E. Gambi, and S. Spinsante, "Multisensor data fusion for human activities classification and fall detection," *Proc. IEEE Sensors*, vol. 2017-Decem, pp. 1–3, 2017.

[35] B. Andó, S. Baglio, C. O. Lombardo, and V. Marletta, "An Event Polarized Paradigm for ADL Detection in AAL Context," *IEEE Trans. Instrum. Meas.*, vol. 64, no. 7, pp. 1814–1825, 2015.

[36] D. Qiao, G. Pang, M. Kit, and D. Lam, "A new pcb-based low-cost accelerometer for human motion sensing," pp. 56 – 60, 10 2008.

[37] M. M. Magdy, N. A. Mansour, A. M. F. El-Bab, and S. F. Assal, "Human motion spectrum-based 2-dof energy harvesting device: Design methodology and experimental validation," *Procedia Engineering*, vol. 87, pp. 1218 – 1221, 2014. EUROSENSORS 2014, the 28th European Conference on Solid-State Transducers.

[38] H. Zeng and Y. Zhao, "Sensing movement: Microsensors for body motion measurement," *Sensors (Basel, Switzerland)*, vol. 11, pp. 638–60, 12 2011.

[39] N. Pannurat, S. Thiemjarus, and E. Nantajeewarawat, "Automatic fall monitoring: A review," *Sensors (Basel, Switzerland)*, vol. 14, pp. 12900–12936, 07 2014.

[40] A. Sucerquia, J. Lopez, and J. Vargas-Bonilla, "Sisfall: A fall and movement dataset," *Sensors*, vol. 17, p. 198, 01 2017.

[41] Feng Zhao, Qingming Huang, and Wen Gao, "Image matching by normalized cross-correlation," in *2006 IEEE International Conference on Acoustics Speech and Signal Processing Proceedings*, vol. 2, pp. II–II, 2006.

[42] J. Levin, U. Bertsch, H. Kretzschmar, and A. Giese, "Single particle analysis of manganese-induced prion protein aggregates," *Biochemical and Biophysical Research Communications*, vol. 329, no. 4, pp. 1200 – 1207, 2005.

[43] J. N. Sarvaiya, S. Patnaik, and S. Bombaywala, "Image registration by template matching using normalized cross-correlation," in *2009 International Conference on Advances in Computing, Control, and Telecommunication Technologies*, pp. 819–822, 2009.

[44] F. Hartge, T. Wetter, and W. E. Haefeli, "A similarity measure for case based reasoning modeling with temporal abstraction based on cross-correlation," *Computer Methods and Programs in Biomedicine*, vol. 81, no. 1, pp. 41 – 48, 2006.

[45] Jingdong Chen, Yiteng Huang, and J. Benesty, "Time delay estimation via multichannel cross-correlation [audio signal processing applications]," in *Proceedings. (ICASSP '05). IEEE International Conference on Acoustics, Speech, and Signal Processing, 2005.*, vol. 3, pp. iii/49–iii/52 Vol. 3, 2005.

[46] E. Nelson-Wong, S. Howarth, D. A. Winter, and J. P. Callaghan, "Application of autocorrelation and cross-correlation analyses in human movement and rehabilitation research," *Journal of Orthopaedic & Sports Physical Therapy*, vol. 39, no. 4, pp. 287–295, 2009. PMID: 19346626.

[47] T. M. Rath and R. Manmatha, "Word image matching using dynamic time warping," in *2003 IEEE Computer Society Conference on Computer Vision and Pattern Recognition, 2003. Proceedings.*, vol. 2, pp. II–II, 2003.

[48] G. Tomasi, F. van den Berg, and C. Andersson, "Correlation optimized warping and dynamic time warping as preprocessing meth-

ods for chromatographic data," *Journal of Chemometrics*, vol. 18, no. 5, pp. 231–241, 2004.

[49] H. Kaprykowsky and X. Rodet, "Globally optimal short-time dynamic time warping, application to score to audio alignment," in *2006 IEEE International Conference on Acoustics Speech and Signal Processing Proceedings*, vol. 5, pp. V–V, 2006.

[50] Y.-S. Jeong, M. K. Jeong, and O. A. Omitaomu, "Weighted dynamic time warping for time series classification," *Pattern Recognition*, vol. 44, no. 9, pp. 2231 – 2240, 2011. Computer Analysis of Images and Patterns.

[51] Jiangpeng Dai, Xiaole Bai, Zhimin Yang, Zhaohui Shen, and Dong Xuan, "Perfalld: A pervasive fall detection system using mobile phones," in *2010 8th IEEE International Conference on Pervasive Computing and Communications Workshops (PERCOM Workshops)*, pp. 292–297, March 2010.

[52] F. Wu, H. Zhao, Y. Zhao, and H. Zhong, "Development of a wearable-sensor-based fall detection system," *International Journal of Telemedicine and Applications*, vol. 2015, pp. 1–11, 02 2015.

[53] S. Abbate, M. Avvenuti, F. Bonatesta, G. Cola, P. Corsini, and A. Vecchio, "A smartphone-based fall detection system," *Pervasive and Mobile Computing*, vol. 8, no. 6, pp. 883 – 899, 2012. Special Issue on Pervasive Healthcare.

[54] D. Chen, W. Feng, Y. Zhang, X. Li, and T. Wang, "A wearable wireless fall detection system with accelerators," in *2011 IEEE International Conference on Robotics and Biomimetics*, pp. 2259–2263, 2011.

[55] S. Fang, Y. Liang, and K. Chiu, "Developing a mobile phone-based fall detection system on android platform," in *2012 Computing, Communications and Applications Conference*, pp. 143–146, 2012.

[56] T. Fawcett, "An introduction to ROC analysis," *Pattern Recognit. Lett.*, vol. 27, no. 8, pp. 861–874, 2006.

[57] G. Vavoulas, M. Pediaditis, C. Chatzaki, E. Spanakis, and M. Tsiknakis, "The mobifall dataset:: Fall detection and classification with a smartphone," *International Journal of Monitoring and Surveillance Technologies Research*, vol. 2, pp. 44–56, 07 2016.

[58] C. Medrano, R. Igual, I. Plaza, and M. Castro, "Detecting falls as novelties in acceleration patterns acquired with smartphones," *PLOS ONE*, vol. 9, pp. 1–9, 04 2014.

[59] K. Frank, M. J. Vera, P. Robertson, and T. Pfeifer, "Bayesian recognition of motion related activities with inertial sensors," pp. 445–446, 09 2010.

[60] T. Vilarinho, B. Farshchian, D. G. Bajer, O. H. Dahl, I. Egge, S. S. Hegdal, A. Lønes, J. N. Slettevold, and S. M. Weggersen, "A combined smartphone and smartwatch fall detection system," in *2015 IEEE International Conference on Computer and Information Technology; Ubiquitous Computing and Communications; Dependable, Autonomic and Secure Computing; Pervasive Intelligence and Computing*, pp. 1443–1448, 2015.

[61] A. Bruno, S. Baglio, R. Crispino, L. L'Episcopo, V. Marletta, M. Branciforte, and M. C. Virzi, "A smart inertial pattern for the SUMMIT IoT multi-platform," *Lecture Notes in Electrical Engineering*, vol. 544, pp. 1–11, 2018.

[62] M. W. Whittle, "Chapter 2 - normal gait," in *Gait Analysis (Fourth Edition)* (M. W. Whittle, ed.), pp. 47 – 100, Edinburgh: Butterworth-Heinemann, fourth edition ed., 2007.

[63] C.-H. Lee and T.-L. Sun, "Evaluation of postural stability based on a force plate and inertial sensor during static balance measurements," *Journal of Physiological Anthropology*, vol. 37, 12 2018.

[64] H. Chaudhry, B. Bukiet, Z. Ji, and T. Findley, "Measurement of balance in computer posturography: Comparison of methods—a brief review," *Journal of bodywork and movement therapies*, vol. 15, pp. 82–91, 01 2011.

[65] M. Patel, P. Fransson, D. Lush, and S. Gomez, "The effect of foam surface properties on postural stability assessment while standing," *Gait Posture*, vol. 28, no. 4, pp. 649 – 656, 2008.

[66] J. W. Błaszczyk, "The use of force-plate posturography in the assessment of postural instability," *Gait Posture*, vol. 44, pp. 1 – 6, 2016.

[67] G. Frykberg, B. Lindmark, H. Lanshammar, and J. Borg, "Correlation between clinical assessment and force plate measurement of postural control after stroke," *Journal of rehabilitation medicine : official journal of the UEMS European Board of Physical and Rehabilitation Medicine*, vol. 39, pp. 448–53, 07 2007.

[68] M. Rosenblum, G. Firsov, R. Kuuz, and B. Pompe, "Human postural control: Force plate experiments and modelling," in *Nonlinear Analysis of Physiological Data* (H. Kantz, J. Kurths, and G. Mayer-Kress, eds.), (Berlin, Heidelberg), pp. 283–306, Springer Berlin Heidelberg, 1998.

[69] E. S. Sazonov, G. Fulk, J. Hill, Y. Schutz, and R. Browning, "Monitoring of posture allocations and activities by a shoe-based wearable sensor," *IEEE Transactions on Biomedical Engineering*, vol. 58, no. 4, pp. 983–990, 2011.

[70] P. Paulick, H. Djalilian, and M. Bachman, "Stabilitysole: Embedded sensor insole for balance and gait monitoring," in *Digital Human Modeling* (V. G. Duffy, ed.), (Berlin, Heidelberg), pp. 171–177, Springer Berlin Heidelberg, 2011.

[71] S. Crea, M. Donati, S. De Rossi, C. Oddo, and N. Vitiello, "A wireless flexible sensorized insole for gait analysis," *Sensors*, vol. 14, p. 1073–1093, Jan 2014.

[72] J. A. Bauer, J. H. Cauraugh, and M. D. Tillman, "An insole pressure measurement system: Repeatability of postural data," *Foot & Ankle International*, vol. 21, no. 3, pp. 221–226, 2000. PMID: 10739153.

[73] X. Hu, J. Zhao, D. Peng, Z. Sun, and X. Qu, "Estimation of foot plantar center of pressure trajectories with low-cost instrumented insoles using an individual-specific nonlinear model," *Sensors*, vol. 18, p. 421, Feb 2018.

[74] ReTiSense, "Sensorized insole." `https://retisense.com/`, Last accessed on 2020-08-28.

[75] SENSOR PRODUCTS INC., "Sensorized insole." `https://www.sensorprod.com/dynamic/foot-insole.php`, Last accessed on 2020-08-28.

[76] FlexinFit, "Sensorized insole." `https://www.sensormedica.com/it/prodotti/hardware-it/sensorized-insole`, Last accessed on 2020-08-28.

[77] Moticon, "Sensorized insole." `https://www.moticon.de/`, Last accessed on 2020-08-28.

[78] G. Tierney, H. Joodaki, T. Krosshaug, J. Forman, J. Crandall, and C. Simms, "The kinematics of head impacts in contact sport: An initial assessment of the potential of model based image matching," 08 2016.

[79] J. Gill, S. Garcia, L. Ting, M. Wu, and H. Chiel, "neurotic: Neuroscience tool for interactive characterization," *eneuro*, vol. 7, pp. ENEURO.0085–20.2020, 04 2020.

[80] Y. Nagasaka, K. Shimoda, and N. Fujii, "Multidimensional recording (mdr) and data sharing: An ecological open research and educational platform for neuroscience," *PLOS ONE*, vol. 6, pp. 1–7, 07 2011.

[81] Insider, "Motion capture in action." `https://www.insider.com/the-evolution-of-how-marvel-animated-iron-mans-suit-2020-7`, Last accessed on 2020-08-28.

[82] I. Olatunji, "Human activity recognition for mobile robot," *Journal of Physics: Conference Series*, vol. 1069, 01 2018.

[83] E. L. Johnsen, P. H. Mogensen, N. A. Sunde, and K. Østergaard, "Improved asymmetry of gait in parkinson's disease with dbs: Gait and postural instability in parkinson's disease treated with bilateral deep brain stimulation in the subthalamic nucleus," *Movement Disorders*, vol. 24, no. 4, pp. 588–595, 2009.

[84] E. L. Stegemöller, T. A. Buckley, C. Pitsikoulis, E. Barthelemy, R. Roemmich, and C. J. Hass, "Postural instability and gait impairment during obstacle crossing in parkinson's disease," *Archives of Physical Medicine and Rehabilitation*, vol. 93, no. 4, pp. 703 – 709, 2012.

[85] C. Buckley, L. Alcock, R. McArdle, R. Z. U. Rehman, S. Del Din, C. Mazzà, A. J. Yarnall, and L. Rochester, "The role of movement analysis in diagnosing and monitoring neurodegenerative conditions: Insights from gait and postural control," *Brain Sciences*, vol. 9, p. 34, Feb 2019.

[86] J. M. Wood, P. F. Lacherez, A. A. Black, M. H. Cole, M. Y. Boon, and G. K. Kerr, "Postural Stability and Gait among Older Adults with Age-Related Maculopathy," *Investigative Ophthalmology Visual Science*, vol. 50, pp. 482–487, 01 2009.

[87] C. Godinho, J. Domingos, G. Cunha, A. Santos, R. Fernandes, D. Abreu, N. Gonçalves, H. Matthews, T. Isaacs, J. Duffen, A. Al-Jawad, F. Larsen, J. A. Serrano, P. Weber, A. Thoms, S. Sollinger, H. Graessner, W. Maetzler, and J. Ferreira, "A systematic review of the characteristics and validity of monitoring technologies to assess parkinson's disease," *Journal of NeuroEngineering and Rehabilitation*, vol. 13, 12 2016.

[88] A. Ferrari, M. G. Benedetti, E. Pavan, C. Frigo, D. Bettinelli, M. Rabuffetti, P. Crenna, and A. Leardini, "Quantitative comparison of five current protocols in gait analysis," *Gait Posture*, vol. 28, no. 2, pp. 207 – 216, 2008.

[89] J. Howcroft, J. Kofman, and E. Lemaire, "Review of fall risk assessment in geriatric populations using inertial sensors," *Journal of neuroengineering and rehabilitation*, vol. 10, p. 91, 08 2013.

[90] T. M. Santos, M. F. Barroso, R. A. Ricco, E. G. Nepomuceno, Érika L.F.C. Alvarenga, Álvaro C.O. Penoni, and A. F. Santos, "A low-cost wireless system of inertial sensors to postural analysis during human movement," *Measurement*, vol. 148, p. 106933, 2019.

[91] M. Gago, V. Fernandes, J. Ferreira, H. Silva, L. Rocha, E. Bicho, and N. Sousa, "Postural stability analysis with inertial measurement units in alzheimer's disease," *Dementia and geriatric cognitive disorders extra*, vol. 4, pp. 22–30, 01 2014.

[92] J. Liu, X. Zhang, and T. E. Lockhart, "Fall risk assessments based on postural and dynamic stability using inertial measurement unit," *Safety and Health at Work*, vol. 3, no. 3, pp. 192 – 198, 2012.

[93] S. Bonnet, P. Couturier, F. Favre-Reguillon, and R. Guillemaud, "Evaluation of postural stability by means of a single inertial sensor," in *The 26th Annual International Conference of the IEEE Engineering in Medicine and Biology Society*, vol. 1, pp. 2275–2278, 2004.

[94] C. Doherty, L. Zhao, J. Ryan, Y. Komaba, A. Inomata, and B. Caulfield, "Quantification of postural control deficits in patients with recent concussion: An inertial-sensor based approach," *Clinical Biomechanics*, vol. 42, pp. 79 – 84, 2017.

[95] C. Neville, C. Ludlow, and B. Rieger, "Measuring postural stability with an inertial sensor: Validity and sensitivity," *Medical Devices: Evidence and Research*, vol. 8, p. 447, 11 2015.

[96] L. Rocchi, L. Palmerini, A. Weiss, T. Herman, and J. Hausdorff, "Balance testing with inertial sensors in patients with parkinson's disease: Assessment of motor subtypes," *IEEE transactions on neural systems and rehabilitation engineering : a publication of the IEEE Engineering in Medicine and Biology Society*, vol. 22, 12 2013.

[97] H. Mjøsund, E. Boyle, P. Kjaer, R. Mieritz, T. Skallgård, and P. Kent, "Clinically acceptable agreement between the vimove wireless motion sensor system and the vicon motion capture system when measuring lumbar region inclination motion in the sagittal and coronal planes," *BMC Musculoskeletal Disorders*, vol. 18, 12 2017.

[98] W. Y. Wong and M. S. Wong, "Trunk posture monitoring with inertial sensors," *European spine journal : official publication of the European Spine Society, the European Spinal Deformity Society, and the European Section of the Cervical Spine Research Society*, vol. 17, pp. 743–53, 05 2008.

[99] D. Dinu, M. Fayolas, M. Jacquet, E. Leguy, J. Slavinski, and N. Houel, "Accuracy of postural human-motion tracking using miniature inertial sensors," *Procedia Engineering*, vol. 147, pp. 655 – 658, 2016. The Engineering of SPORT 11.

[100] L. K. Philpott, S. Weaver, D. Gordon, P. P. Conway, and A. A. West, "Assessing wireless inertia measurement units for monitoring athletics sprint performance," in *SENSORS, 2014 IEEE*, pp. 2199–2202, 2014.

[101] D. L. C. Collins JJ, "Open-loop and closed-loop control of posture: a random-walk analysis of center-of-pressure trajectories," *Experimental Brain Research*, vol. 20, pp. 308–318, 1993.

[102] J. Norris, A. Marsh, I. Smith, R. Kohut, and M. Miller, "Ability of static and statistical mechanics posturographic measures to distinguish between age and fall risk," *Journal of biomechanics*, vol. 38, pp. 1263–72, 07 2005.

[103] T. Vieira, L. Oliveira, and J. Nadal, "Estimation procedures affect the center of pressure frequency analysis," *Brazilian journal of medical and biological research = Revista brasileira de pesquisas médicas e biológicas / Sociedade Brasileira de Biofísica ... [et al.]*, vol. 42, pp. 665–73, 08 2009.

[104] T. Sim, H. Yoo, D. Lee, S.-W. Suh, J.-H. Yang, H. Kim, and J. Mun, "Analysis of sensory system aspects of postural stability during quiet standing in adolescent idiopathic scoliosis patients," *Journal of NeuroEngineering and Rehabilitation*, vol. 15, 12 2018.

[105] N. Singh, H. Snoussi, D. Hewson, and J. Duchêne, "Wavelet transform analysis of the power spectrum of centre of pressure signals

to detect the critical point interval of postural control," vol. 52, pp. 235–244, 01 2010.

[106] J. Fiołka, "Postural stability analysis : A wavelet — based approach," in *ICSES 2010 International Conference on Signals and Electronic Circuits*, pp. 101–104, 2010.

[107] T. Lockhart, R. Songra, J. Zhang, and X. Wu, "Wavelet based automated postural event detection and activity classification with single imu," *Biomedical sciences instrumentation*, vol. 49, pp. 224–233, 04 2013.

[108] J. M. H. H. N. Z. A. R. C. K. R. T. A. S. James R. Chagdes, Shirley Rietdyk, "Multiple timescales in postural dynamics associated with vision and a secondary task are revealed by wavelet analysis.," *Exp Brain Res.*, vol. 197, pp. 297–310, 03 2009.

[109] N. Richer and Y. Lajoie, "Automaticity of postural control while dual-tasking revealed in young and older adults," *Experimental Aging Research*, vol. 46, pp. 1–21, 11 2019.

[110] "A really friendly guide to wavelets." `https://www.cs.unm.edu/~williams/cs530/arfgtw.pdf`, Last accessed on 2020-08-16.

[111] D. T.L. and A. Yamamoto, "Wavelet analysis: Theory and applications." `https://www.hpl.hp.com/hpjournal/94dec/dec94a6a.pdf`, Last accessed on 2020-08-16.

[112] L. Chun-Lin, "A tutorial of the wavelet transform." `http://people.duke.edu/~hpgavin/SystemID/References/Liu-WaveletTransform-2010.pdf`, Last accessed on 2020-08-16.

[113] M. Ghislieri, L. Gastaldi, S. Pastorelli, S. Tadano, and V. Agostini, "Wearable inertial sensors to assess standing balance: A systematic review," *Sensors*, vol. 19, p. 4075, 09 2019.

[114] D. Schoene, S. Wu, A. S. Mikolaizak, J. Menant, S. Smith, K. Delbaere, and S. Lord, "Discriminative ability and predictive validity of

the timed up and go test in identifying older people who fall: Systematic review and meta-analysis," *Journal of the American Geriatrics Society*, vol. 61, 01 2013.

[115] R. Munhoz, J.-Y. Li, M. Kurtinecz, P. Piboolnurak, A. Constantino, S. Fahn, and A. Lang, "Evaluation of the pull test technique in assessing postural instability in parkinon's disease," *Neurology*, vol. 62, pp. 125–7, 02 2004.

[116] H. Cohen, A. Mulavara, B. Peters, H. Sangi-Haghpeykar, D. Kung, D. Mosier, and J. Bloomberg, "Sharpening the tandem walking test for screening peripheral neuropathy," *Southern medical journal*, vol. 106, pp. 565–569, 10 2013.

[117] A. Ruhe, R. Fejer, and B. Walker, "Center of pressure excursion as a measure of balance performance in patients with non-specific low back pain compared to healthy controls: A systematic review of the literature," *European spine journal : official publication of the European Spine Society, the European Spinal Deformity Society, and the European Section of the Cervical Spine Research Society*, vol. 20, pp. 358–68, 03 2011.

[118] H. Amoud, M. Abadi, D. Hewson, V. Michel-Pellegrino, M. Doussot, and J. Duchêne, "Fractal time series analysis of postural stability in elderly and control subjects," *Journal of NeuroEngineering and Rehabilitation*, vol. 4, pp. 12 – 12, 2006.

[119] G. C. Gauchard, C. Jeandel, A. Tessier, and P. P. Perrin, "Beneficial effect of proprioceptive physical activities on balance control in elderly human subjects," *Neuroscience Letters*, vol. 273, no. 2, pp. 81 – 84, 1999.

[120] P. Perrin, D. Deviterne, F. Hugel, and C. Perrot, "Judo, better than dance, develops sensorimotor adaptabilities involved in balance control," *Gait Posture*, vol. 15, no. 2, pp. 187 – 194, 2002.

[121] C. Carello, M. T. Turvey, and P. N. Kugler, "The informational support for upright stance," *Behavioral and Brain Sciences*, vol. 8, no. 1, p. 151–152, 1985.

[122] O. Huxhold, S.-C. Li, F. Schmiedek, and U. Lindenberger, "Dual-tasking postural control: Aging and the effects of cognitive demand in conjunction with focus of attention," *Brain Research Bulletin*, vol. 69, no. 3, pp. 294 – 305, 2006.

[123] R. Emmerik and E. van Wegen, "On the functional aspects of variability in postural control," *Exercise and sport sciences reviews*, vol. 30, pp. 177–83, 11 2002.

[124] S. Donker, M. Roerdink, A. Greven, and P. Beek, "Regularity of center-of-pressure trajectories depends on the amount of attention invested in postural control," *Experimental brain research. Experimentelle Hirnforschung. Expérimentation cérébrale*, vol. 181, pp. 1–11, 07 2007.

[125] L. Ladislao and S. Fioretti, "Nonlinear analysis of posturographic data," *Medical biological engineering computing*, vol. 45, pp. 679–88, 08 2007.

[126] M. Roerdink, M. Haart, A. Daffertshofer, S. Donker, A. Geurts, and P. Beek, "Dynamical structure of center-of-pressure trajectories in patients recovering from stroke," *Experimental brain research. Experimentelle Hirnforschung. Expérimentation cérébrale*, vol. 174, pp. 256–69, 10 2006.

[127] J. Haddad, R. Emmerik, J. Wheat, and J. Hamill, "Developmental changes in the dynamical structure of postural sway during a precision fitting task," *Experimental brain research. Experimentelle Hirnforschung. Expérimentation cérébrale*, vol. 190, pp. 431–41, 10 2008.

[128] V. H. Rodriguez, C. Medrano, and I. Plaza, "A real-time qrs complex detector based on discrete wavelet transform and adaptive threshold as standalone application on arm microcontrollers," in *2018 International Conference on Biomedical Engineering and Applications (ICBEA)*, pp. 1–6, 2018.

[129] R. Stojanovic, S. Knezevic, D. Karadaglic, and G. Devedzic, "Optimization and implementation of the wavelet based algorithms for

embedded biomedical signal processing," *Computer Science and Information Systems*, vol. 10, pp. 503–523, 01 2013.

[130] V. Rodriguez, C. Medrano, and I. Plaza, "Embedded system based on an arm microcontroller to analyze heart rate variability in real time using wavelets," *Wireless Communications and Mobile Computing*, vol. 2018, pp. 1–14, 10 2018.

[131] L. E. Peterson, "K-nearest neighbor," *Scholarpedia*, vol. 4, no. 2, p. 1883, 2009. revision #137311.

[132] R. Gary and J. Fleury, "Nutritional status: Key to preventing functional decline in hospitalized older adults," *Topics in Geriatric Rehabilitation*, vol. 17, pp. 40–71, 03 2002.

[133] A. Zisberg, E. Shadmi, N. Gur-Yaish, O. Tonkikh, and G. Sinoff, "Hospital-associated functional decline: The role of hospitalization processes beyond individual risk factors," *Journal of the American Geriatrics Society*, vol. 63, no. 1, pp. 55–62, 2015.

[134] M.-N. Vercambre, M.-C. Boutron-Ruault, K. Ritchie, F. Clavel-Chapelon, and C. Berr, "Long-term association of food and nutrient intakes with cognitive and functional decline: a 13-year follow-up study of elderly french women," *British Journal of Nutrition*, vol. 102, no. 3, p. 419–427, 2009.

[135] A. N. Galanos, C. F. Pieper, J. C. Cornoni-Huntley, C. W. Bales, and G. G. Fillenbaum, "Nutrition and function: Is there a relationship between body mass index and the functional capabilities of community-dwelling elderly?," *Journal of the American Geriatrics Society*, vol. 42, no. 4, pp. 368–373, 1994.

[136] S. Lafrenière, N. Folch, S. Dubois, L. Bédard, and F. Ducharme, "Strategies used by older patients to prevent functional decline during hospitalization," *Clinical Nursing Research*, vol. 26, no. 1, pp. 6–26, 2017. PMID: 26324514.

[137] "Nutrition & Dehydration for people with Dementia, Nestle | HelloCare."

[138] "Supporting an Ageing Population - The IET."

[139] E. Fabbri, M. Zoli, M. Gonzalez-Freire, M. E. Salive, S. A. Studenski, and L. Ferrucci, "Aging and Multimorbidity: New Tasks, Priorities, and Frontiers for Integrated Gerontological and Clinical Research," aug 2015.

[140] B. Andò, S. Baglio, S. La Malfa, and V. Marletta, "A sensing architecture for mutual user-environment awareness case of study: A mobility aid for the visually impaired," *IEEE Sensors Journal*, vol. 11, pp. 634–640, March 2011.

[141] "Obli Encouraging and Monitoring Fluid Intake -."

[142] A. M. Kassim, H. I. Jaafar, M. A. Azam, N. Abas, and T. Yasuno, "Design and development of navigation system by using RFID technology," in *2013 IEEE 3rd Int. Conf. Syst. Eng. Technol.*, pp. 258–262, IEEE, aug 2013.

[143] L. Ni, Yunhao Liu, Yiu Cho Lau, and A. Patil, "LANDMARC: indoor location sensing using active RFID," in *Proc. First IEEE Int. Conf. Pervasive Comput. Commun. 2003. (PerCom 2003).*, pp. 407–415, IEEE Comput. Soc.

[144] B. Andò, S. Baglio, V. Marletta, R. Crispino, and A. Pistorio, "A measurement strategy to assess the optimal design of an rfid-based navigation aid," *IEEE Transactions on Instrumentation and Measurement*, pp. 1–7, 2018.

[145] J. Barman, G. Uswatte, T. Ghaffari, B. Sokal, E. Byrom, E. Trinh, M. Brewer, C. Varghese, and N. Sarkar, "Sensor-enabled rfid system for monitoring arm activity: Reliability and validity," *IEEE Transactions on Neural Systems and Rehabilitation Engineering*, vol. 20, pp. 771–777, Nov 2012.

[146] S. S. Rao, E. G. Rajan, and K. Lalkishore, "Human activity tracking using rfid tags," 2009.

[147] "Sensor CDT spin-out company to disrupt assisted living technology market — Sensor CDT."